F3

Faculty of Electrical Engineering

Department of Electric Drives and Traction (13114)

Bachelor's Thesis

Synchronous Reluctance Motor and Its Efficiency

Petr Tlamsa

Study program: Electrical Engineering, Power Engineering and Management

Specialization: Applied Electrical Engineering

May 2024

Supervisor: doc. Ing. Jan Bauer, Ph.D.

Consultant: Ing. Martin Labonek

BACHELOR‘S THESIS ASSIGNMENT

I. Personal and study details

Student's name: **Tlamsa Petr** Personal ID number: **499039**

Faculty / Institute: **Faculty of Electrical Engineering**

Department / Institute: **Department of Electric Drives and Traction**

Study program: **Electrical Engineering, Power Engineering and Management**

Specialisation: **Applied Electrical Engineering**

II. Bachelor’s thesis details

Bachelor’s thesis title in English:

Synchronous Reluctance Motor and Its Efficiency

Bachelor’s thesis title in Czech:

Synchronní reluktanční motor a jeho účinnost

Guidelines:

1) Conduct a research on types of synchronous reluctance motors.
2) Compare qualitative parameters of synchronous reluctance motors and induction motors.
3) Perform a measurement of the efficiency map of a drive system with a synchronous reluctance motor.
4) Compare the measured data with the data available in the SINAMICS S120 drive.
5) Analyze options available for the implementation of closed-loop torque control into the drive system using SINAMICS S120 drive.

Bibliography / sources:

[1] V. Hrabovcová, L. Janoušek, P. Rafajdus, M. Ličko, Moderné elektrické stroje, Žilinská univerzita, 2001. ISBN 80-7100-809-5.
[2] Ozcelik NG, Dogru UE, Imeryuz M, Ergene LT, Synchronous Reluctance Motor vs. Induction Motor at Low-Power Industrial
Applications: Design and Comparison, Energies, 2019.
[3] Siemens Catalog D 21.4: SINAMICS S120 and SIMOTICS, Siemens, 2017.
[4] Siemens Catalog D 81.1: SIMOTICS GP, SD, XP, DP Low-Voltage Motors – February 2022, Siemens, 2022.

Name and workplace of bachelor’s thesis supervisor:

doc. Ing. Jan Bauer, Ph.D. Department of Electric Drives and Traction FEE

Name and workplace of second bachelor’s thesis supervisor or consultant:

Date of bachelor’s thesis assignment: **02.05.2024** Deadline for bachelor thesis submission: **24.05.2024**

Assignment valid until: **15.02.2026**

doc. Ing. Jan Bauer, Ph.D. Supervisor’s signature	Head of department’s signature	prof. Mgr. Petr Páta, Ph.D. Dean’s signature

III. Assignment receipt

The student acknowledges that the bachelor’s thesis is an individual work. The student must produce his thesis without the assistance of others, with the exception of provided consultations. Within the bachelor’s thesis, the author must state the names of consultants and include a list of references.

.	
Date of assignment receipt	Student’s signature

Acknowledgements / Declaration

First of all, my sincere thanks to my thesis supervisor, doc. Ing. Jan Bauer, Ph.D., for allowing me to work on a topic that I find interesting and exciting, and for helping me with the formulation of the custom thesis assignment. I also thank him for his valuable advice, patience and guidance throughout the completion of the thesis, which often helped me to head in the right direction, as well as for the time he dedicated to me in general.

Second, I would like to thank Ing. Martin Labonek along with all of my colleagues from Innomotics s.r.o., for all the knowledge and skills they have passed onto me so far, their advice, patience and for accommodating adjustments to my work schedule.

Third, I express my thanks to RNDr. Petr Olšák for helping me with TEX.

And last but not least, I would like to express my gratitude to my family and friends for their understanding and support.

I hereby declare that I have independently authored the presented work and have referenced all the utilized information sources in accordance with The Methodological Directive No. 1/2009 on Compliance with Ethical Principles in the Preparation of University Final Theses.

Prague, 5th May, 2024

.....

Abstract / Abstrakt

This bachelor's thesis comprehensively addresses the topic of Synchronous Reluctance Motor (SynRM), covering its construction, working principle, mathematical model, Field-Oriented Control (FOC) method, qualitative parameters, applications and future prospects.

Due to SynRM being often mentioned nowadays, thanks to its higher efficiency, as a potential successor of generally most frequently used electric motor – Induction Motor (IM), an outline of this issue and its potential future development is going to be provided.

Furthermore, a measurement of the efficiency map of a SynRM drive system built on Siemens products is going to be performed at the faculty's laboratory workplace.

Lastly, options available for realization of closed-loop torque control using the drive system's SINAMICS S120 drive are going to be analyzed.

Keywords: Synchronous Reluctance Motor, SynRM, Vector Control, FOC, efficiency, sustainability, Induction Motor, IM, Asynchronous Motor, AM, ASM, Siemens, SINAMICS S120, S120, TIA Portal, TIA.

Tato bakalářská práce komplexně pojednává o synchronním reluktančním motoru (SynRM) z pohledu jeho konstrukce, principu funkce, matematického modelu, metody řízení Field-Oriented Control (FOC), kvalitativních parametrů, aplikací, ve kterých se využívá a vyhlídek do budoucna.

Vzhledem k tomu, že se o SynRM díky jeho vyšší účinnosti dnes často hovoří jako o potenciálním nástupci dnes obecně nejpoužívanějšího elektromotoru – asynchronního motoru (AM), bude uveden nástin této problematiky a její potenciální budoucí vývoj.

Dále bude na laboratorním pracovišti fakulty provedeno měření účinnostní mapy pohonu se SynRM vystavěného na produktech firmy Siemens.

A nakonec budou analyzovány možnosti realizace uzavřené momentové smyčky tohoto pohonu pomocí jeho měniče SINAMICS S120.

Klíčová slova: Synchronní reluktanční motor, SynRM, vektorové řízení, FOC, účinnost, udržitelnost, asynchronní motor, AM, ASM, Siemens, SINAMICS S120, S120, TIA Portal, TIA.

Překlad titulu: Synchronní reluktanční motor a jeho účinnost

Contents /

Figures / Tables

Introduction

Let us begin by defining which electric machines are considered as Reluctance Machines (RM). The following fall into the category:

- Stepper motor,
- Switched Reluctance Machine (SRM),
- Synchronous Reluctance Machine (SynRM).

The term 'RM' stems from the fact that these machines function based on magnetic reluctance (or simply reluctance), which is measured in the SI unit of H^{-1}. Equivalently, it can be said that they function based on magnetic permeance (or simply permeance), which is just the reciprocal of reluctance and is measured in the SI unit of H. All RM are synchronous machines [1].

In this thesis, only SynRM are going to be discussed, providing a comprehensive description and analysis from multiple standpoints. In the literature, other terms referring to this type of motor can be encountered, such as:

- Reluctance Synchronous Machine (RSM),
- Synchronous Reluctance Machine (SRM).

However, 'SRM' is particularly misleading when referring to SynRM, as this abbreviation should be reserved for Switched Reluctance Machines only. Nevertheless, SynRM is the term most commonly used in literature [2], and it is the one that is going to be used in this thesis.
Furthermore, from now on, all machines that will be mentioned in the thesis will be considered only in motor mode, unless stated otherwise. Thus, the abbreviation 'SynRM' will now be understood as 'Synchronous Reluctance Motor'.
While SynRM can also be used in generator mode, this is not going to be discussed in the thesis due to its complex working principle and rarity of usage [3].
Other abbreviations reflecting the particular type of SynRM and its features can be added in front of the 'SynRM' abbreviation, which is going to be shown later in the thesis.

The history of SynRM dates back to 1923 when J. K. Kostko published a paper establishing the fundamental theory for this type of motor for the first time ever [4].
More than 100 years have now passed during which various studies regarding optimal design were conducted, and during which SynRM was repeatedly almost forgotten and then brought back into the scientists' and commercial sphere's scope again.
Nowadays, with the huge help of semiconductor technology experiencing rapid advancement in the second half of the 20th century and with the help of other favorable aspects, SynRM stands among the elite of the electric motor market. Its most attractive feature is its high efficiency, a very positive and important attribute for a motor to have in today's world, where ecodesign and CO_2 emissions reduction are constantly emphasized.

For this reason, SynRM is often considered as a possible successor to today's most used type of electric motor – Induction Motor (IM), also sometimes called Asynchronous Motor (AM, ASM) [5], which was first constructed by Galileo Ferraris in 1885, followed by Nikola Tesla in 1887 [6].
This is why a demonstrative measurement of the efficiency of a SynRM drive system was incorporated into the thesis. The measurement is going to take place at a workplace located in the faculty's laboratory T2:H1-26.

The last topic to be addressed in the thesis is going to also focus on the workplace and discuss options available for the realization of closed-loop torque control using the workplace's SINAMICS S120 drive. This topic is an extension to the bachelor's thesis of my colleague John Francis Horabin from May 2023, who built the workplace using available Siemens equipment [7].

Finally, after reading this thesis, one should have a basic understanding of SynRM and its implementation in today's world. However, it is assumed that the reader possesses a basic knowledge of principles from electrical engineering, as the thesis builds upon them. Additionally, one should refer to the cited literature for a deeper understanding of any of the discussed topics.

Chapter 1
Construction

A modern SynRM with no modifications has a simple structure and its manufacturing does not require many different materials, making its production relatively easy. SynRM boasts numerous advantages, such as high efficiency, low thermal losses, high thermal endurance, low moment of inertia, and being a rare-earth-free product (applies always, except for only one case described in *subchapter 1.3.2*).
However, it also possesses many disadvantages, namely low power factor, relatively high torque ripple, and lower mechanical stability. Mechanical stability is particularly problematic at high speeds (over 10 000 rpm), where centrifugal forces exert huge pressures on the rotor structure. All these issues stem from the construction of the motor [8], [9].
The design procedure of SynRM and many of its design aspects are not going to be delved into in detail, as it is not the objective of this thesis. Moghaddam's master's thesis [2] thoroughly covers this topic. For now, it is sufficient to know that the **Finite Element Method (FEM)**, which involves numerical analysis of magnetic fluxes flowing through the motor and also numerical analysis of mechanical strain of the motor is used [5] and that the number of rotor poles is chosen to be the same as the number of stator poles [1], [10].

1.1 Stator

SynRM uses the same stator as the IM [11]. It is made of electrical steel sheets designed in a tooth-slot geometry (see *Figure 1.1*). This geometry is achieved by punching the steel sheets using a punching tool [12]. These sheets are then stacked on top of each other and electromagnetically isolated from each other [13], before being compressed together to form a solid stack.
The stator winding is then distributed into the slots along the inner circumference of the stator. In most cases, it is a 3-phase winding and although multiphase SynRM do exist, they are not going to be considered in this thesis [14]. The winding is distributed sinusoidally, which, together with appropriate powering, ensures the creation of a rotating circular magnetic field in the air gap, which means that the waveform of magnetic induction in the air gap will be almost sinusoidal ('almost', as in reality there is no ideal motor) [13]. In most cases, the stator of a SynRM is non-skewed [15].

Real parts of a stator of a SynRM can bee seen in the figure below:

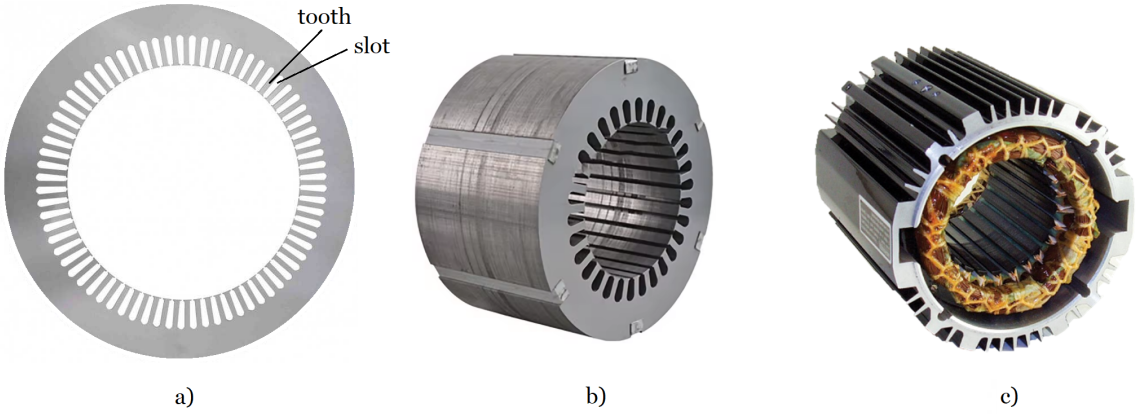

Figure 1.1: A stator of a SynRM – a) a sheet, b) a stack, c) the stack wound and fitted into housing [16], [17], [18] (edited).

All this means that SynRM stators can be produced in the same, already existing assembly lines where IM are produced, which makes mass production of SynRM significantly easier [12].

1.2 Rotor

The rotor of a SynRM, in the vast majority of cases (as is going to be shown later), consists of only electrical steel sheets that are electromagnetically isolated from each other and put together in the same manner as described for the stator. The only difference is, of course, that the geometry of the sheets will be different for the rotor compared with the stator. Other than that, there is neither winding nor any cage, which implies that, in terms of construction, they differ from IM only in their rotors [15].

The design of the rotor is crucial for SynRM, as it determines its resulting behavior and qualitative parameters (such as output torque, torque ripple, efficiency, power factor, etc.). Therefore, before designing the rotor, one should determine which of its advantages should be emphasized the most and which of its disadvantages should be minimized regarding this type of motor [19].

For further analysis, the concept of the d and q axes will now be introduced, demonstrated using a ‘universal’ rotor sheet of a SynRM:

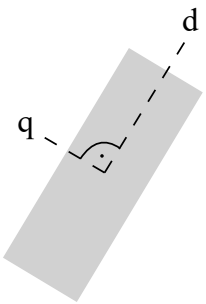

Figure 1.2: A ‘universal’ rotor sheet of a SynRM [3].

In the direction of the **d-axis (direct)**, the material's reluctance is the lowest (permeance is the highest, respectively). It can be also said that in the direction of the d-axis, the material's inductance L_d (reactance X_d respectively) is the highest.
Conversely, in the direction of the **q-axis (quadrature)**, the material's reluctance is the highest (permeance is the lowest, respectively). And similarly, it can be also said that in the direction of the q-axis, the material's inductance L_q (reactance X_q respectively) is the lowest [13].
The term **'ideal rotor of a SynRM'** is defined as a theoretical model, in which the rotor would have an ideal magnetically anisotropic strucuture. This implies that $L_\mathrm{d} \to \infty$ and $L_\mathrm{q} \to 0$, resulting in zero reluctance in the direction along the magnetic field lines (the d-axis) and infinite reluctance in the direction across them (the q-axis) [19].

Thus, in practice, an essential parameter for the design of SynRM rotors is the so-called **saliency ratio**, denoted by ξ. It is defined as:

$$\xi = \frac{L_\mathrm{d}}{L_\mathrm{q}}. \tag{1.1}$$

It can also be defined the same way but using X_d and X_q. Almost all qualitative parameters of SynRM are affected by this ratio. The higher it is, the better the parameters usually are and the more the unwanted phenomena are usually suppressed. Therefore, the main goal is almost always to achieve the highest possible L_d and the lowest possible L_q, thus maximizing ξ.
Furthermore, the higher ξ is, the better (by a large margin) the performance in **field-weakening (FW)** range of all SynRM, with the exception of some of its rotor-modified versions [20]. On the other hand, increasing ξ makes the rotor construction more complicated, as well as the manufacturing process, resulting in a drastic increase in the price of the motor [8].

For further enhancement of qualitative parameters or to suppress unwanted phenomena, modifications are available, mainly for the rotor. The modifications are going to be presented in *subchapter 1.3* [15].

The rotor of a SynRM can be generally considered as cylindrical pole (with exceptions for salient pole rotors and other sporadic designs) [1].

In the following subchapters, a possible classification of SynRM rotors are going to be presented according to the literature referenced in *subchapter 1.2*.
However, the presented clusters do not necessarily exclude one another. This means that the final rotor design can possibly be a mixture of different presented designs, though it is not common [15].

1.2.1 Salient pole rotors

A salient pole rotor is the simplest design of a SynRM rotor. Quasi-square-shaped cutouts oriented in the direction of the q-axis are made of the original uncut electrical steel sheets with no geometry. This results in a mechanically stable and robust design that requires low technological effort in terms of manufacturing [8].

The outcome is depicted in the figure below:

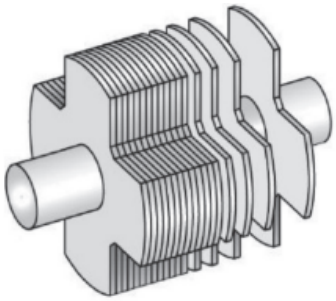

Figure 1.3: A sketch of a salient pole rotor indicating stacking of the sheets [8] (edited).

The cutouts can, of course, also be shapes other than quasi-square. Moreover, they can occur more frequently, resulting in the rotor having higher number of poles [8], [19].
On the other hand, this design has relatively low ξ (which cannot be expected to exceed 3 – with the common span being 2-3 [19]), because widening the interpolar cutout to decrease L_q would simultaneously decrease L_d due to a narrower pole arc.
Hence, such rotors are considered to have weak performance in terms of qualitative parameters (such as output torque, efficiency, power factor etc.) to make them competitive compared with other types of rotors, especially modern TLA and ALA designs, which are going to be discussed later. Therefore, they are not generally preferred [11], [12], [21], [22] and will not be discussed in further detail in this thesis.

1.2.2 Segmented rotors (Magneto-isolated pole rotors)

A Segmented rotor, also known as a Magneto-isolated pole rotor, is another infrequently used SynRM rotor design that is only rarely seen [12]. In this design, multiple stacks are formed from electrical steel sheets, with each stack making up one rotor pole (or one segment). These stacks are designed to leave a small air gap between them when mounted on the rotor core, creating reluctance in the q-axis. The entire structure is then mounted on the shaft [23].

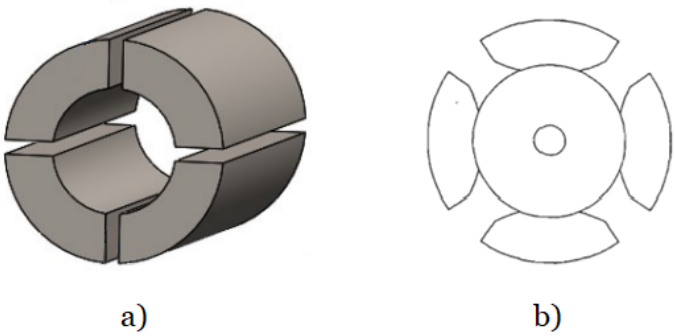

Figure 1.4: A segmented (Magneto-isolated pole) rotor – a) only the poles, b) an entire rotor [5], [12] (edited).

Segmented rotors are claimed to have better ξ than salient pole rotors, therefore SynRM with segmented rotors reportedly exhibit higher output torque, efficiency and power factor than SynRM with salient pole rotors [24].
Despite this, due to the forementioned rarity of this rotor design, it will not be discussed in further detail in this thesis.

1.2.3 Modern barrier rotors

Nowadays, the state of the art SynRM rotors, most commonly used and manufactured, are the so-called barrier rotors. Their name stems from the fact that in most cases, they introduce **air barriers** (also called **flux barriers, magnetic barriers**) in the direction of their q-axis, to create reluctance (for decreasing L_q respectively).

When designing a barrier rotor, its resulting electromagnetic and mechanical properties are determined by the design of the barriers.
The main aspects to consider in the design process of the barriers are their:

- shape,
- width,
- number per sheet [2].

Shapes composed of rectangular cutouts are used, as well as more circular, or combined [14]. Regarding the width, the so-called **insulation ratio** is used to gauge the proportions. Therefore, in this instance, width is considered in the 'from the center of the shaft outwards' sense. The insulation ratio is defined as:

$$K_w = \frac{w_{bar}}{w_{car}}, \tag{1.2}$$

where w_{bar} is the total width of all the flux barriers and w_{car} is the total width of all the flux carriers (also called flux guides – electrical steel segments in the q-axis direction left after introducing the flux barriers into the rotor). The radius of the rotor is then obtained after adding $w_{bar}+w_{car}$. The upper limit of K_w is constrained by the saturation of the iron segments, since ξ starts to decrease. K_w is an important design parameter that directly influences ξ, as well as the output torque and other qualitative parameters, and is helpful when comparing different rotor geometries [14], [25].

The number of barriers per sheet has the most substantial effect on the qualitative parameters of the motor out of all of the barrier parameters [21] and is chosen depending on the number of rotor poles and stator slots.
In theory, to maximize ξ, the number of barriers per sheet should be as high as possible. However, a substantial volume of the rotor material is then removed, which endangers the mechanical stability of the rotor structure. Therefore, an optimal trade-off between electromagnetical, mechanical (including the weight of the rotor, and thus its moment of inertia on whose magnitude the weight takes part) and thermal properties of the rotor is always sought [2], [9]. For further reference, this principle will be referred to as **'the trade-off rule'**.
In practice, 4 is the optimal recommended number of barriers per sheet. A higher number would make the rotor technology too complicated, and beyond the optimal number, the improvement in qualitative parameters would become less and less significant [22]. Conversely, a lower number would result in excessively high torque ripple [8].

Besides barrier parameters, **the optimal number of rotor poles** is also important when designing this type of rotor. A low number, that is 2, would lead to the desired low L_q, but on the other hand, also to a higher torque ripple. Conversely, when the number of rotor poles is high, that is 8 or more, it is difficult to create more than one barrier per pole, which leads to a reduction in ξ.
Thus, majority of barrier rotors is manufactured as 4-pole. 6-pole designs are also used [10].

Barrier rotors report by far the best results among all SynRM rotors in terms of ξ and subsequent qualitative parameters, which justifies why barrier rotors are currently the most widespread, as mentioned earlier [9], [19], [24].

Despite this being true, they also possess some significant weaknesses, and there is definitely room for improvement, which is currently ongoing in the Research and Development (R&D) sphere.
Their biggest weakness is their low mechanical stability and integrity, especially at high speeds. Therefore, a lot of the R&D efforts is invested in researching options for strengthening the mechanical construction, with respect to the forementioned trade-off rule. Some of these options are going to be presented later in this thesis [9].

When comparing barrier rotors to a rotor of an IM, the structure of the latter is much more solid, with no air introduced to its insides, resulting in much higher mechanical stability and reduced sensitivity to mechanical stress [14].

Two main designs of barrier rotors (and of SynRM rotors in general) on which the majority of the commercial and R&D sphere is currently focused [12] are now going to be introduced.

1.2.3.1 Axially Laminated Anisotropy (ALA)

This type of barrier rotor is composed of a combination of suitably shaped electrical steel sheets and barriers that subsequently copy the shape of the sheets and electromagnetically isolate them from each other. The barrier material can be air, but it is often some other electromagnetically insulating material (referred to as passive material), such as epoxy [5], [12].
The term 'suitably shaped' refers to the shaping of the sheets to precisely replicate the natural flow of magnetic field lines in a solid rotor:

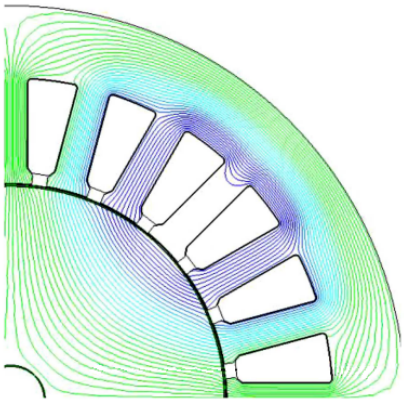

Figure 1.5: The natural flow of magnetic field lines in a solid rotor [26] (edited).

This will ensure that the design will come close to fulfulling the definition of ideal rotor of a SynRM (though this only applies if the influence of stator slotting is omitted and simultaneously, $p_\mathrm{p} = 2$, where p_p is the number of pole pairs) [19], [27].

Continuing with the design, the sheets and barriers are then put together axially (meaning lengthwise with respect to the horizontal axis of the shaft) in a 'sheet-barrier-sheet-barrier' manner [5], [12]. This creates a stack, with the number of stacks equaling the number of rotor poles, which is almost always 4. Each sheet and barrier within a particular stack (that are all made the same) has its own unique shape [5], [21].

Increasing the number of sheet + barrier combinations above 10 has only a minimal effect on further enhancements of the motor's properties [19].
The stacks are then affixed to the inner part of the rotor using pole holders and screws. The inner part of the rotor is made of electromagnetically insulating material [19]. The screws are also made of electromagnetically insulating material to prevent an increase in L_q. The entire structure is then mounted on the shaft [21], as shown in the figure below:

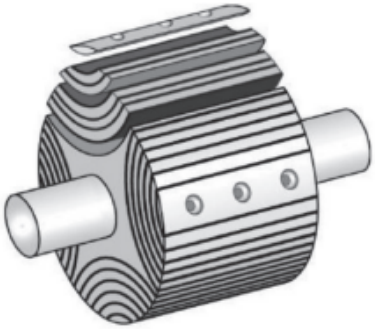

Figure 1.6: A sketch of an ALA rotor indicating the stacking of the sheets and barriers [8] (edited).

The most lucrative feature of the design is that the number of flux barriers can be drastically increased, leading to very high values of ξ. A SynRM that possess this type of rotor is called an **Axially Laminated Anisotropy Synchronous Reluctance Motor (ALA-SynRM)** [12].
However, these are also not going be discussed in much detail in this thesis.

1.2.3.2 Transversely (Radially) Laminated Anisotropy (TLA)

Similarly to ALA rotors, TLA rotors are made of electrical steel sheets that are electromagnetically isolated from each other. However, the sheets of TLA rotors are shaped 'conventionally', meaning they are round.
Unlike in ALA rotors, the sheets of TLA rotors are then put together transversely (radially respectively) with respect to the horizontal axis of the shaft. After compressing the sheets together, a stack is created. This stack is then mounted on the shaft [22].
The entire structure is depicted in the figure below:

Figure 1.7: A TLA rotor – a) a sketch indicating the stacking of the sheets, b) in reality [8], [28] (edited).

The air barries are, of course, introduced into the sheets before the stack assembly. For this purpose, there are two most widely used methods:

- punching,
- laser cutting.

In the punching method, a punching tool is used. Moreover, if the SynRM is mass-produced using this method, the entire SynRM (including its stator) can be produced the same way in the same (already existing) assembly line as an IM. The only differences lie in changing the punching tool for the rotor geometry and, in most cases, not creating the squirrel cage (as is going to be explained later).
There are also other methods, but they are often only used in prototype manufacturing [22].

Both methods leave thin steel **bridges** (or **ribs**, but the term 'bridges' will be used throughout the thesis) in the q-axis, connecting the flux carriers within each rotor pole. This serves to improve the mechanical stability and mechanical strength of the rotor [10], [12], [22], [29]. For a better illustration, a sketch of a TLA rotor sheet is depicted in the following figure:

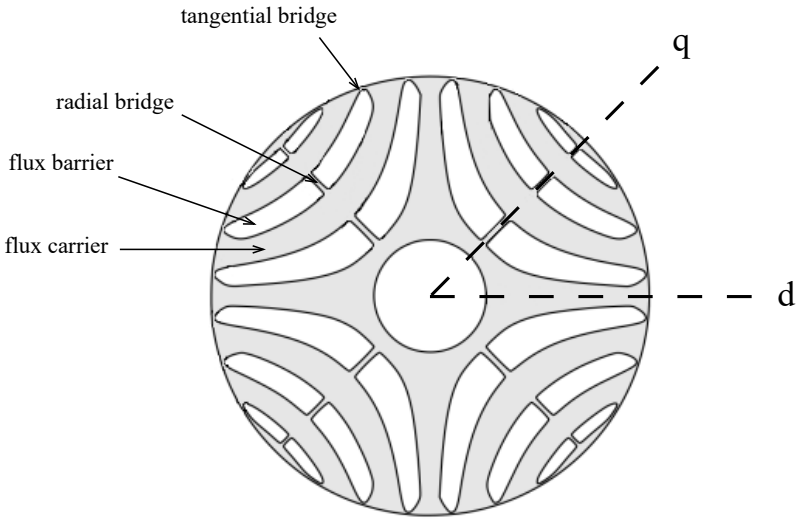

Figure 1.8: A sketch of a TLA rotor sheet [30] (edited).

As seen in the figure above, the bridges are classified as:

- **tangential** (or **end bridges**),
- **radial** [10], [29].

Radial bridges can be present in all of the barriers, only in some them, or in none at all. Their presence depends on how high the magnitude of mechanical stress exerted on the flux carriers is, which can be analyzed using FEM [5].

Generally, a bridge should be > 1 mm wide, or problems with manufacturing will occur [11], [14].

There are also other methods for making TLA rotor structure more mechanically stable and supported [9], which are going to be discussed in *subchapter 1.3*.
Applying the trade-off rule, by incorporating the bridges into the design, L_q increases, leading to worsened electromagnetic properties of the rotor [10], [11].

The increased L_q causes two following nonlinearities of TLA rotors:

- an increase in **magnetic saturation limit in the q-axis**,
- an increase in **cross-coupling**.

Cross-coupling is a relatively strong nonlinearity that can be defined as the coupling between magnetic flux linkages of the d and q axes, which occurs because the axes 'share' the same rotor sheet which is, moreover, not interrupted on its edges. Conversely, this phenomenon is almost non-existent in ALA rotors [10], [11].
Both nonlinearities lead to another set of undesirable consqeuences [14] and become more significant as the width of the bridges increases [11]. In practice, their main impact is on the mathematical modeling of the motor and on the precise control of the motor, which both become significantly more complicated. The latter may also become less efficient.
Thus, the objective is to find an optimal width of the bridges that ensures an early and deep saturation of the bridges, causing them to start appearing as mangetically non-conductive, while maintaining sufficient mechanical stability and integrity of the rotor structure [10].

The design of TLA rotors is, from the geometrical standpoint, a difficult task, and the optimal geometry is still under study, as there are plenty of input parameters [5]. The main ones are:

- the number of poles (or the number of pole pairs p_p),
- the number of stator slots,
- the width of air gap δ between the stator and the rotor,
- the number of flux carriers,
- the number of flux barriers [12],
- the width of the flux barriers,
- the shape of the flux barriers [5],
- K_w [12],
- the number of tangential and radial bridges [5],
- the width of the tangential and the radial bridges [12],
- the flux barrier alignment with the stator teeth [5].

For example, the number of flux barriers and the number of tangential and radial bridges vary according to the number of stator slots and the overall level of optimization of the rotor [5]. A change in any of the parameters listed above can significantly affect the properties of the motor, such as ξ, power and torque density, torque ripple, power factor, and others.
Moreover, the change cannot be selectively aimed with the intention of affecting only the property that is in the scope, as the change will always affect other properties as well [5].

Eventually, a SynRM that possess this type of rotor is called a **Transversely Laminated Anisotropy Synchronous Reluctance Motor (TLA-SynRM)** [12]. This is the type of a SynRM rotor that is in the main scope of this thesis. Henceforth, in all subsequent parts of this thesis, it will be automatically assumed that when describing a SynRM, its rotor is TLA and with no modifications, unless stated otherwise. The reasons for this assumption are going to be presented in the following subchapter.

1.2.3.3 ALA vs. TLA

The comparison is going to commence with a brief tabular evaluation of the properties of ALA and TLA rotors, assigning a score to each of the properties, based on the design of the rotor:

Property	ALA	TLA
ξ	[12], [27]	[12], [27]
Torque ripple	[5], [11], [27]	[5], [11], [27]
Iron losses	[5], [11], [22], [27]	[5], [11], [22], [27]
Efficiency	[11]	[11]
Mechanical stability and strength	[5], [11], [29]	[5], [11], [29]
Skewing feasibility	[11], [20], [21]	[11], [20], [21], [22]
Series production suitability	[11], [21]	[11], [21]
KEY		
EXCELLENT		
GOOD		
SATISFACTORY		
BAD		

Table 1.1: A comparison of properties of ALA and TLA rotors.

Further comments on majority of the properties listed in the table above are now going to be given.

ξ

Values for ALA are the highest out of all SynRM rotors, that is over up to 20 [27], while values for TLA are usually 10-12 [12].

Torque ripple

As both ALA and TLA face problems with this phenomenon, stator skewing in case of ALA-SynRM and rotor skewing in case of TLA-SynRM is a necessity [20].

Iron losses

Assuming the same electrical steel is used for both ALA and TLA, the increased iron losses in ALA compared with TLA can be explained by the relatively high eddy current losses in ALA.
This is due to the fact that ALA rotors are put together axially, whereas TLA rotors are put together transversely. As a result, eddy currents have much more surface area to which they can induce in ALA design, rather than in TLA design [5], [27].

Mechanical stability and strength

For both designs, this is definitely their biggest weakness and both designs are inherently less mechanically stable compared with a rotor of an IM.

In terms of high speed aplications, ALA cannot be used, because mechanical stress exterted on the rotor structure generally rises with the speed of the rotor, and due to ALA being assembled from multiple parts that are screwed together (meaning there are no solid sheets), the whole structure could potentially break down [5], [11], [29].
TLA can be used in high speed aplications, though its performance is will not be optimal [9]. Besides that, higher number of wider bridges would be needed, which would lead to many undesirable consequences [10].

Skewing feasibility

The design of ALA rotor inherently makes its skewing very difficult, thus leaving skewing of the stator stack as the only option. For TLA rotors, skewing can be done without any problems [21].

Series production suitability

Due to its unique construction, manufacturing and assembly of ALA-SynRM rotor is much more technologically complex than of TLA-SynRM and by introducing more barriers into the ALA rotor, the complexity further rises [3], [5], [11], [12], [22], [29].
The complexity lies mainly in the following:

- different design and size of every laminate segment must be made,
- inter-segment insulation thickness has to vary inbetween layers,
- rotor circumference needs to be machined after laminate mounting,
- only stator stack skewing is feasible.

The additional machining could lead to a change in the material properties and an increase in iron losses. For the skewing, the vast majority of SynRM stators are mass-produced as non-skewed, since they use same stator as IM. Moreover, if the stator skewing was performed, it would become very challenging if the skewed stator now had to be wound by a winding machine [20], [21].
In practice, the mentioned arguments give a reason for ALA-SynRM manufacturing and assembly costs to be higher than for TLA-SynRM, whose construction is more suitable for series production [21], can be manufactured in already existing assembly lines for IM (thus the construction of new assembly lines is spared) [3], [5], [11], [12], [22], [29] and their production itself is relatively cheap [25].

Based on all the information presented so far, including the data in *Table 1.1* along with the accompanying comments, it is evident why TLA is the most prevalent type of SynRM rotor and why the majority of attention from R&D and commercial companies involved with SynRM is focused on it today [2], [12]. In recent years, there has been an effort to optimize TLA, as it is believed to be the most promising rotor design of SynRM [5].

1.2.3.4 TLA-derived

Optimized TLA designs

There are constant efforts to optimize the rotor according to the trade-off rule. For example, the following sheet design for a 6-pole motor was proposed using an optimization algorithm:

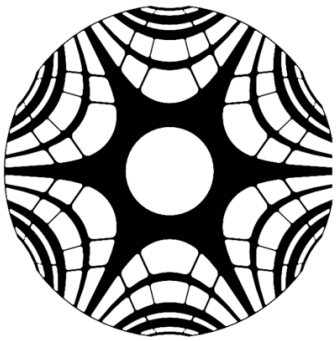

Figure 1.9: An optimized design of TLA rotor sheet (6-pole) [10].

While the design contains more bridges to ensure better mechanical properties, they are made as thin as possible to facilitate reaching their magnetic saturation.
According to reports, the design meets the requirements for the mechanical stability of the rotor while achieving excellent electromagnetic properties [10].

Dovetail rotor

Dovetail rotors are a branch of TLA rotors with a specific design, where its poles are divided into segments that are dovetail-shaped, and these segments fit into each other, being mutually fixated using an electromagnetically non-conductive supporting material [5], [22], as can be seen in the figure below:

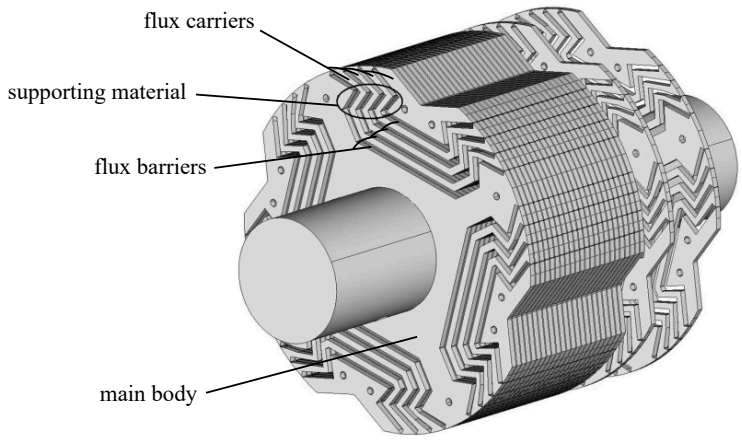

Figure 1.10: A sketch of a dovetail TLA rotor design [29], [31] (edited).

As a result, the design does not require and thus does not have bridges. The dovetail design ensures significantly higher mechanical strength compared with 'conventional' TLA, enabling operation at higher speeds [5], [22], [31], [32].

However, higher mechanical strength would in 'conventional' TLA typically lead to deterioration in electromagnetic properties, which may not necessarily be the case with the dovetail design [31].
Though, it is generally argued that dovetail, although not having bridges that cause the forementioned deterioration in electromagnetic properties, pays for its higher mechanical strength by higher torque ripple, slightly lower efficiency and power factor compared with 'conventional' TLA [5], [29].

1.2.4 Rotors for torque ripple reduction

A suitable rotor construction is one of the solutions that can be used for reducing the relatively high torque ripple that SynRM generally suffers from. Today, such constructions are being studied, and there are many of them.
In the following two subchapters the main two of them, which are based on optimal adjustment of asymmetrically arranged flux barrier shapes are going to be presented [5], [32].

1.2.4.1 Romeo and Juliet (R&J)

This design still belongs into TLA category, only with the difference that compared with the 'conventional' TLA, the stack consists of two types of sheets – Romeo and Juliet (R&J), with Romeo (R) type of sheet having different barrier shape than Juliet (J) type of sheet, as can be seen in the figure below:

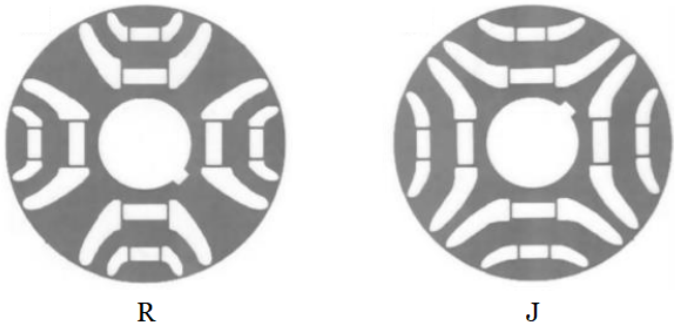

Figure 1.11: R and J rotor sheets in reality [32] (edited).

The sheets are then put and compressed together in R-J-R-J manner to create the final stack. This alternating manner of composing the stack causes higher harmonics of torque produced by R sheets to offset each other with higher harmonics of torque produced by J sheets.
The content of higher harmonics in the resulting SynRM torque waveform is thus going to be significantly reduced, resulting in a substantial decrease in torque ripple [5], [32].

1.2.4.2 Machaon

Machaon is just another level of development of R&J, which combines these sheets into one. Thus, all the sheets in the stack are uniform, while the principle of torque ripple reduction remains the same.

Figure 1.12: Machaon rotor sheet in reality [32].

The name of the design was derived from the characteristic appearance of the swallowtail butterfly – in Latin: *Papilio machaon*, which has two large and two small wings, as the similarity can be seen in *Figure 1.12* [5], [32].

1.3 Modifications

Modifications are performed in order for the motor to be capable of something it was not capable of before or for the purpose of improving some of its properties (torque ripple reduction, power factor improvement etc.). Modifications can be divided into:

- stator modifications,
- rotor modifications,

where rotor modifications make up the absolute majority of all the modifications available. Apart from *subchapter 1.3.1*, these rotor modifications are going to concern TLA rotors exclusively. The motor may also incorporate multiple of stator/rotor modifications simultaneously, if the combination is sensible and feasible [15].

1.3.1 Squirrel cage (Starting cage)

Inserting a squirrel cage (also known as **starting cage**) into the rotor enables asynchronous starting, thus a **frequency converter (or VFD – Variable Frequency Drive/VSD – Variable Speed Drive)** is then not needed for the starting. However, since such SynRM are designed for operation on a constant voltage and frequency power grid (generally for motors, the term **DOL – Direct On Line** is frequently used for this type of operation and for starting motors connecting them directly to the power grid [15]), the operation of the motor is then going to be limited to a single operating speed determined by this frequency [3].
Nowadays, this modification is merely a historical relic from the times when VFD did not yet exist, therefore now in practice, this modification is almost non-existent.

Additionally, the modification has many disadvantages, such as worse resulting rotor properties (e.g. $\xi = 2 \div 3$ [3]), minimal prospects in the contemporary world, and others [5]. Moreover, for ALA, due to the nature of this rotor design, inserting the cage would be very difficult, although being done in the times when VFD did not yet exist [19].
A SynRM with this type of modification is called a **Line Start Synchronous Reluctance Motor (LS-SynRM)** [15].
However, due to the evident reasons, this modification is not going to be further discussed in this thesis.

1.3.2 Permanent magnets (PM)

Through a suitable addition of PM into the air barriers of TLA rotor, synchronous torque is added to the motor's overall torque, which has so far consisted only of reluctance torque. The addition can improve the power and torque density, efficiency and power factor of the given SynRM [33], which would not be achieved with other rotor modifications either at all or to such an extent.
This synchronous torque component also assists the SynRM during starting when it is necessary to overcome the rotor's stiction and, in general, enhances its dynamics, especially at low speeds [34].

However, the idea of introducing PM is based on the assumption that, with sufficient accuracy, the following applies:

$$\mu_{\mathrm{r,PM}} \approx \mu_{\mathrm{r,air}}, \tag{1.3}$$

where $\mu_{\mathrm{r,PM}}$ is the relative permeability of the PM and $\mu_{\mathrm{r,air}}$ is the relative permeability of air. In other words, the assumption is, that the PM behave more or less like air barriers. If PM were to have a greater relative permeability than air, their introduction would also mean an increase in L_{q}, which is generally aimed to avoid [33].

It is also possible to encounter the abbreviation **IPM (Internal Permanent Magnets)**, which only indicates that the permanent magnets are housed inside the rotor (therefore Internal), rather than on its surface. However, in this thesis, except where context necessitates it, the abbreviation PM will be adhered to, as the area of their placement has already been specified, thus eliminating further dispute.

The design of SynRM with PM for optimum reluctance and synchronous torque components is generally a complex task, since rotor dimensioning for one torque component limits the possibility to optimize the other torque component [25].

Furthermore, the addition of PM should be included in the motor design from the outset, as adding them later to an already manufactured motor could have the opposite effect on some of its qualitative parameters, contrary to what is wanted from the addition of PM [35].

It is also necessary to consider that after adding PM, there may be an attraction of metallic impurities (most commonly in the form of metal dust), which can clog the motor and even with periodic maintenance, it may lead to a reduction in the motor's lifespan and, in severe cases, even to its destruction [3].

If the addition of PM caused the reluctance torque component of the overall torque to be smaller than the synchronous torque component of the overall torque formed by the PM, logically speaking, the motor should be rather called **Interior Permanent Magnet Synchronous Motor (IPMSM)**. That is a synchronous motor with PM placed inside the rotor, where, if present, the reluctance torque component plays only a supplementary role [25].

There are multiple aspects to consider regarding PM that play a role in affecting the resulting properties of the given SynRM. That is their:

- material,
- shape, dimensions, quantity,
- arrangement,
- occupation of barrier layers [5].

Each of the aspects is now going to be analyzed.

Material

Currently available PM suitable for the addition are made from:

- rare-earth metals,
  - neodymium (NdFeB alloys),
  - samarium (SmCo alloys),
- hard ferrites,
- AlNiCo alloys [33].

The material used will then determine the resulting properties of the PM, which are primarily judged by their magnetic energy density (simply put, the 'strength' of the PM), maximum and minimum operating temperature, and corrosion resistance. Projected on a given SynRM, then for example, higher magnetic energy density causes, besides other, higher power factor [20], [33].

For the purpose of adding PM into air barriers of TLA rotor, PM from rare-earth metals are the most commonly used. Though if used, then obviously, the given SynRM is no longer going to be a rare-earth free product, which has already been encountered in *chapter 1*.
In the case of neodymium (Nd), iron (Fe), and boron (B), they are added to form an alloy NdFeB, from which the PM is then made, thus this type of PM will be referred to by the name of the alloy. Out of all rare-earth PM, NdFeB are the ones that are preferred and used the most due to the fact that their magnetic energy density is the highest out of all of the commercially used PM, thus a reduction in the motor's volume can be achieved. On the other hand, they are expensive, prone to market fluctuations [36] and can demagnetize at higher temperatures (from 150 °C). Moreover, if a performance across the entire FW range of a SynRM containing NdFeB should be evaluated, it would be rated as 'satisfactory' [20].
Similarly, in the case of samarium (Sm), cobalt (Co) is added to form an alloy SmCo, from which the PM is then made, thus this type of PM is also going to be referred to by the name of the alloy. Conversely, SmCo can withstand higher temperatures and more corrosive environments than NdFeB – however, its magnetic energy density is not as high as of NdFeB and also are even more expensive. Therefore, in the category of rare-earth PM, they are less used than NdFeB.

PM from hard ferrites, which are ceramic compounds derived from iron oxides, generally have worse properties than rare-earth PM. There is also a risk of demagnetization at low temperatures (from –40 °C) [20]. On the other hand, their price is lower than of rare-earth PM.

AlNiCo alloys (Al – aluminium, Ni – nickel) are used the least out of all the mentioned options [5], [33].

The selection of the material will also highly depend on the nature of the application in which the motor is to be used, the operating environment that is associated with the application, and last but not least, the price of the resulting PM [5], [33].

Shape, dimensions, quantity

This aspect is highly limited by the number of barrier layers per pole and by the barrier geometry [33], as it is, for example, not feasible to insert rectangular PM inside circular barriers [36].
A coefficient α is introduced:

$$\alpha = \frac{M_1}{B_1} = \ldots = \frac{M_n}{B_n} = const., \tag{1.4}$$

where M is the width of the PM (meaning the longest side of the rectangle representing the given PM in a cross-sectional drawing of the rotor), B is the width of the barrier (in the same sense) and n is the order of the barrier layer, counted from the center of the rotor sheet onwards to its edge.
Thus, the width of the PM is going to be gradually decreasing towards the outermost barrier layer [37], which is shown in the figure below:

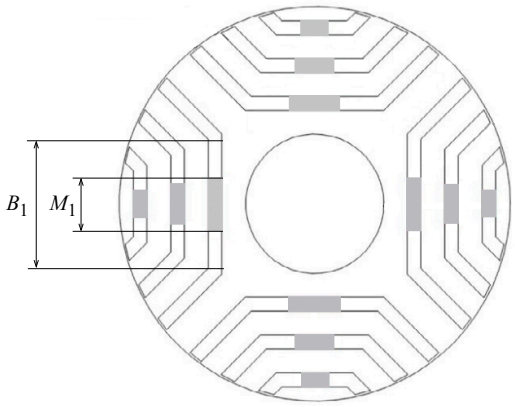

Figure 1.13: A sketch of PM inserted into a TLA rotor [37] (edited).

Depending on the number of barrier layers per pole of the motor, there is always an α, which is optimal for the motor in terms of factors such as torque per unit volume of the PM, use ratio of the PM, torque ripple, and overall performance. For example, through analysis it has been concluded that for a rotor with 3 layers of barriers per pole, $\alpha = 0.4$ is the optimal value [37].

Arrangement

It is always necessary to ensure symmetry of the arrangement and to avoid having more mass in one part of the rotor than in another, which would have many unacceptable consequences [35]. The distance of the PM from the shaft also plays a role. For example, the further away from the shaft the PM are placed, the lower is their influence on overall torque of the motor [5], [35].

Essentially, there are 3 different arrangement patterns for the PM in which they can be inserted into the rotor of a SynRM. The motor is then called based on the pattern it possesses [38]. Description of the patterns, along with figures (for only the first barrier layer occupied), is now going to be provided.

1.3.2.1 PMa-SynRM

PM are inserted only into q-axes in this pattern, which is shown in the figure below:

Figure 1.14: PM inserted into q-axes [38] (edited).

The magnetic flux linkage of the PM then acts against the magnetic flux linkage in q-axis caused by the stator current, while also contributing to the saturation of tangential and radial bridges, which both leads to a reduction in L_q.

The magnetic flux linkage of the PM also intervenes into the d-axis, where it, conversely, adds up with the stator magnetic flux linkage, thus increasing the overall magnetic flux in the motor. However, the influence in the d-axis is not as crucial here, and therefore it is often neglected. This pattern is the most basic and also the most frequent out of the 3. A SynRM that possesses this pattern is called a **Permanent Magnet assisted Synchronous Reluctance Motor (PMa-SynRM)** [35], [38].

1.3.2.2 FI-PMa-SynRM

PM are inserted only into d-axes in this pattern, which is shown in the figure below:

Figure 1.15: PM inserted into d-axes [38] (edited).

The magnetic flux linkage of the PM primarily complements the stator magnetic flux linkage, thus increasing L_d.
The effect of the magnetic flux linkage of the PM on the q-axis is neglected.
This pattern is less frequent than PMa-SynRM. A SynRM that possesses this pattern is called a **Flux Intensifying Permanent Magnet assisted Synchronous Reluctance Motor (FI-PMa-SynRM)** (also known as **Permanent Magnet excited Synchronous Reluctance Motor (PMe-SynRM)**) [35], [38].

1.3.2.3 PMa-SynRM + FI-PMa-SynRM

PM are inserted into both d and q axes in this pattern, which is shown in the figure below:

Figure 1.16: PM inserted into both d and q axes [38] (edited),

and it combines the features of both of the previous patterns into one [35], [38].

For the rest of the thesis, the term PMa-SynRM will be used generally for any SynRM that contains PM in its rotor.

Occupation of barrier layers

PM may or may not be present in each of the barrier layers. If more of them are occupied, then for example, power factor of the motor will improve even further.
On the other hand, the moment of inertia of the rotor as well as the price of the motor will increase, therefore it is necessary to find a compromise [5], [35].

Generally, the influence of the addition of PM on torque ripple is still not well understood. However, it is suggested that with the occupation of more barrier layers per pole, it should decrease. In the case of only partial layer occupancy, its magnitude will heavily depend on which layers with respect to the distance from the center of the rotor sheet were occupied [35], [38] Generally, during the operation of PMa-SynRM, it is necessary to ensure that they are not excessively overloaded, as this could lead to irreversible demagnetization of the PM used [5]. LS-SynRM can also contain PM – in such case, the abbreviation of its name will be **LS-PMa-SynRM** [15].

1.3.3 Skewing

Stator as well as rotor skewing can be performed on a SynRM. However, only one of them is usually done [20].

1.3.3.1 Stator skewing

In this modification, skewing of the stator stack is done, which can be seen in the figure below:

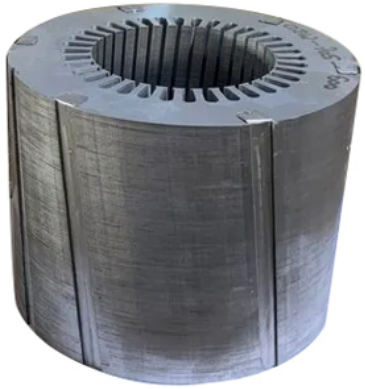

Figure 1.17: A skewed stator stack of a SynRM [39].

Generally for SynRM, stator skewing is much less common than rotor skewing, as it is performed only in cases where rotor skewing is technologically very poorly feasible (e.g. in case of ALA rotor) or completely impossible [20].

1.3.3.2 Rotor skewing

When rotor skewing is performed on a SynRM, the rotor stack is typically skewed by the size of a stator tooth [5]. Rotor skewing is depicted in the figure below:

Figure 1.18: A sketch of a skewed TLA rotor [40] (edited).

Thanks to rotor skewing, a reduction of the content of higher harmonics in the torque waveform caused by the rotor construction will be achieved [5], which leads to a significant reduction in torque ripple [21], though it is not sufficient to smooth out the torque completely [32].
Rotor skewing is primarly meant for TLA rotors. For ALA rotors, it appears to be very difficult to implement [27].
If it is a PMa-SynRM, only step skewing is possible. The rotor is then imaginarily split into two or more parts, and each of them is skewed with respect to the others [32].

1.3.4 Axially-sinusoidal cut-offs

In the rotor stack, the so-called cut-offs are created, meaning that some of the rotor material is selectively removed from the stack (using a laser, for example). The cut-offs are created in a so-called axial-sinusoidal shape, and each sheet then has its own unique shape compared with others [41], which can be seen in the figure below:

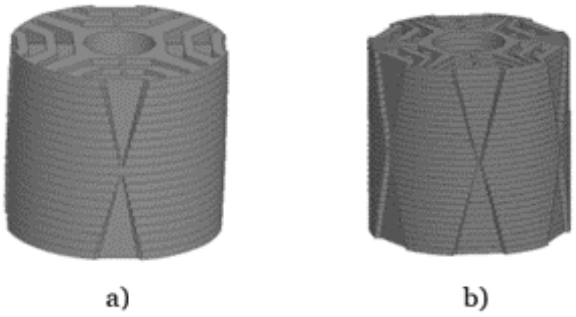

Figure 1.19: TLA rotors with axially-sinusoidal cut-offs – a) 4-pole, b) 6-pole [41], [42] (edited).

This modification leads to a reduction in the motor's torque ripple [41].

1.3.5 Epoxy resin

In practice, it is possible to completely omit the bridges of the TLA rotor and fill the air barriers with epoxy resin, which has similarly suitable electromagnetically insulating properties [5], [9]. As a result, the rotor exhibits significantly better electromagnetic and primarily mechanical properties than it would with bridges [5], [9]. On the other hand, thermal properties of the rotor will worsen, the rotor will become a little heavier and thus its moment of inertia will also increase, which is generally not wanted [5]. However, this modification is still more in the developmental stage, thus it is not commonly seen in today's practice [9].

1.3.6 Retaining sleeve

Retaining sleeve is a constructional addition primarily to TLA rotors in the form of a rotor sleeve, which has a hollow cylindrical shape and is made of carbon fibers or of electrically conductive, yet non-magnetic material (Inconel alloys for example). The main task of the sleeve is to improve the mechanical properties of the rotor. The sleeve is depicted in the following cross-section of a TLA-SynRM, highlighted in orange:

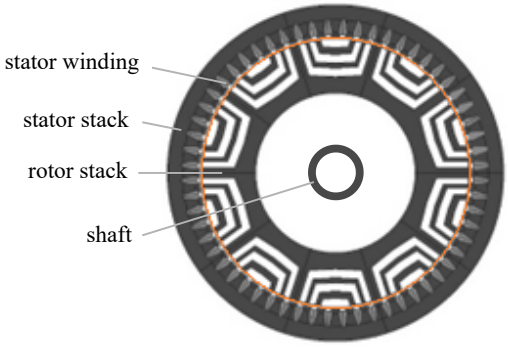

Figure 1.20: A cross-section of a TLA-SynRM with retaining sleeve (orange) [5] (edited).

Moreover, in the past 9 years, when the sleeve was being examined, it was found that it significantly reduces torque ripple of the given SynRM, which results in achieving higher power density and lower total losses, hence higher efficiency of the motor [5].

1.3.7 Bridges from low relative permeability materials

Recently, the possibility of replacing the bridges of TLA rotors with bridges made of materials with low relative permeability μ_r (e.g. Ti – titanium) has begun to be tested. This would result in a high reluctance of these bridges compared with the electrical steel, leading to an increase in ξ.
However, the manufacturing process of such TLA rotors would be much more complicated than that of the 'conventional' TLA rotors [5].

Chapter 2
Working principle

Generally, in order to discuss the working principle (torque production respectively) of any electric motor, it is necessary first to understand the construction of the motor and then second, the powering of the motor. As the construction has already been clarified, the explanation on how SynRM is powered is going to be provided in first of the two following subchapters, followed by an analysis on how the torque in SynRM is produced in the second of the subchapters.

2.1 Powering

Since stator of SynRM typically features a 3-phase winding, SynRM is usually powered by a 3-phase power source. At the ends of each winding, alternating voltages are applied, all sharing the same frequency, amplitude, and being electrically phase-shifted by $2\pi/3$ rad (120° respectively) relative to each other. Combined with the sinusoidally distributed winding around the stator circumference (as described in *subchapter 1.1*), a rotating circular magnetic field in the air gap is created. The field then rotates at the so-called synchronous speed and the creation of the field is one of the fundamental conditions for functioning of SynRM [1], [14].

Essentially, there are two available sources of the alternating voltages:

- 3-phase power grid,
- inverter (VFD respectively).

Powering from a 3-phase power grid – and thus, in most cases, DOL starting – can only be considered for SynRM that have squirrel cage implemented in their rotor. However, according to *subchapter 1.3.1*, this method of powering cannot be considered nowadays almost for any SynRM [5], [19]. Thus, and for other reasons listed in the forementioned subchapter, this method of powering will not be further considered.
Powering from an inverter[1], or from a VFD respectively (as inverter is a part of most VFD) is much more relevant today, because modern VFD allow very easy, smooth, precise and reliable speed control of AC (Alternating Current) motors [1], [15].

[1] **Voltage Source Inverter (VSI)** rather than **Current Source Inverter (CSI)** is used in the vast majority of cases [1], [15].

A power circuit diagram depicting the discussed situation can be seen in the figure below (for the inverter part only):

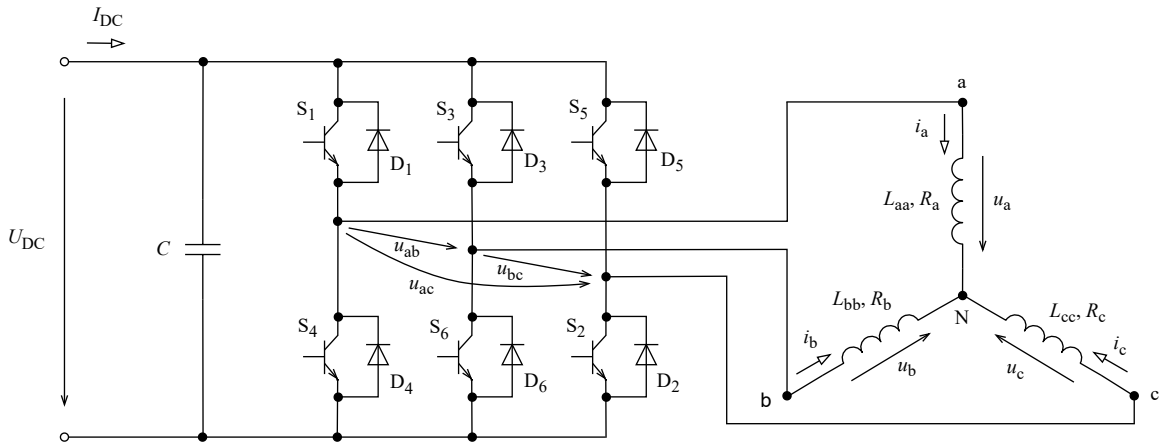

Figure 2.1: A simple power circuit diagram of a SynRM connected to a power supply [1], [15],

where U_{DC} is the voltage in the DC (Direct Current) link, I_{DC} is the current in the DC link, C is the capacitance of the input capacitor, u_{ab}, u_{ac}, u_{bc} are the line voltages between each of the stator phases, u_a, u_b, u_c are the phase voltages across each stator phase, i_a, i_b, i_c are the phase currents flowing through each stator phase, and L_{aa}, L_{bb}, L_{cc} and R_a, R_b, R_c are the self-inductances and resistances of each stator phase. For clarity, the stator windings are represented by coils, which also include the resistances of the respective phases in themselves, as indicated in the diagram. The transistors are labeled S (switch), because they are used as electronic switches in this circuit [1]. The windings can obviously also be connected in delta configuration [13] – however, star configuration without neutral (N) conductor was chosen for the diagram.

The conclusion reached is that the choice of power supply for SynRM is generally determined by evaluating the following main criteria:

- type of rotor,
- application,
- financial budget.

Regarding the type of rotor, then for example ALA-SynRM can only be powered almost exclusively by a VFD due to the reasons given in *subchapter 1.3.1* [19].

However, regardless of the evaluation of any criteria, it is observed that, due to all the facts presented so far, SynRM is generally almost always powered by a VFD nowadays. Furthermore, other, let alone better options are not currently available [1], [15].

Finally, comparing the method of powering SynRM with the method of powering IM, it is noted that, due to having the same stator which is wound in the same way, the methods would be identical. Similarly, the stator windings of the IM could also be connected in delta configuration, and the power circuit diagram when powered by an inverter (by a VFD respectively) would also be the same as in the case of SynRM.

However, when powering IM using DOL method, for which IM is inherently designed (having a squirrel cage in its rotor), the power source section of the diagram would obviously look different. IM is in applications where speed control is not required, unlike SynRM, often run DOL. This allows the owner of the drive system to save money on a VFD, which is not required in this case [1], [13], [15], [19].

2.2 Torque production

The principle of torque production in SynRM is now going to be clarified. Firstly, for simplicity and clarity, the torque production is going to be described for the case of a homogeneous and static magnetic field. Subsequently, the case of a real SynRM, where the magnetic field is rotating and circular [13], [15] is going to be discussed.

2.2.1 Homogeneous static magnetic field

Let us consider a body made of magnetic material, which is magnetically anisotropic in the d and q axes – meaning it has different reluctance (permeance, inductance, reactance respectively) in these axes.
If the body was to be placed in a homogeneous static magnetic field, it would always seek a position in which the energy of the magnetic circuit is maximized, that is the one that minimizes the reluctance of the magnetic circuit (the d-axis would then be parallel to the magnetic field lines) [3].
If its capability of free rotational motion was ensured before the insertion into the field (e.g. by attaching the body to a shaft mounted in bearings), tangential forces $\boldsymbol{F}_\mathrm{t}$ would begin to act on the body[2], and since they would act on an arm with respect to the axis of rotation, torque would be produced, that would align the body to the sought position. This torque, due to its origin, is called **reluctance torque** [1], [5].
The discussed situation is depicted in the case a) of the following figure, where the magnetic field is represented by the magnetic field lines of the magnetic flux linkage Ψ [3], [5]:

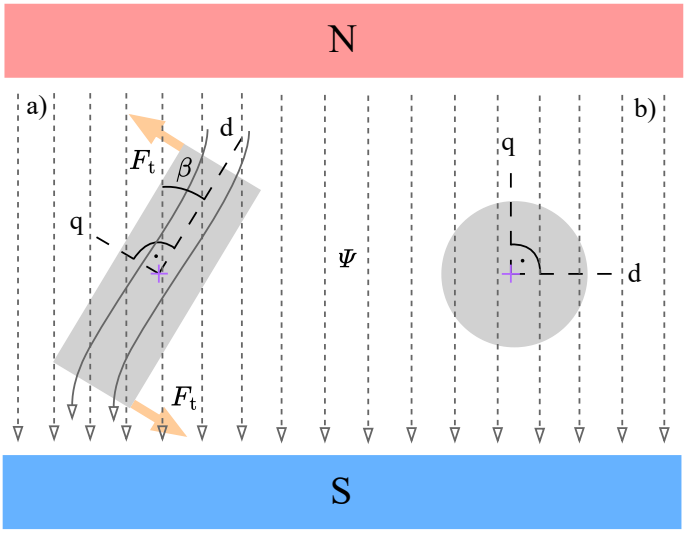

Figure 2.2: Reluctance torque production – a) a magnetically anisotropic body, b) a magnetically isotropic body [3].

[2] Throughout the thesis, vector quantities (and also matrices) are going to be distinguished from scalar quantities by making the vector quantities (or matrices) in bold.

Obivously, if the mentioned body attached to a shaft mounted in bearings was already inserted into the field in the sought position, no reluctance torque would be produced. Similarly, it would not be produced even if the body was positioned so that the d-axis was perpendicular to the magnetic field lines, as is going to be proven by the mathematical formula for reluctance torque in later explanations. Put in words, the tangential forces would cancel out, and the body would be in a labile position [5]. Paradoxically, it might seem to be the position where the maximum torque is achieved. However, placing the rotor so that the d-axis is exactly perpendicular to the magnetic field lines cannot be achieved.
Finally, torque would also not be produced in case b) of *Figure 2.2*, as production of reluctance torque is conditioned by the existence of magnetic anisotropy in the d and q axes, and this body is magnetically isotropic in these axes, meaning it has the same reluctance (permeance, inductance, reactance respectively) in their direction [1].

2.2.2 Rotating circular magnetic field

First, let us consider how the placement of various rotors made of magnetic material would appear in a real stator of SynRM in terms of magnetic field lines, though with the stator's magnetic field still being homogeneous and static:

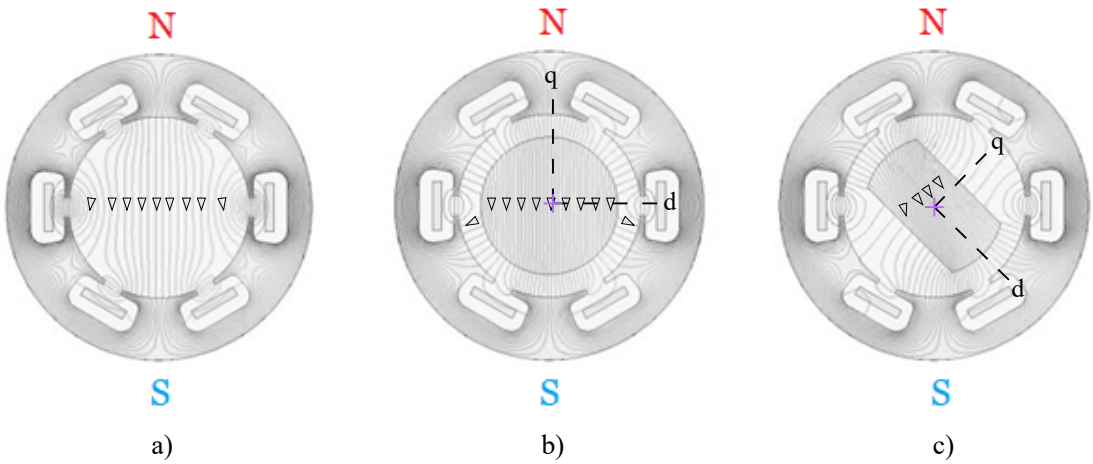

Figure 2.3: Magnetic field lines of a homogeneous static stator magnetic field in various cases [43] (edited).

Case a) depicts the magnetic field lines when the rotor is absent. In case b), the rotor is now present but magnetically isotropic, thus the field lines remain unaffected. In case c), the rotor is present and magnetically anisotropic, which causes the field lines to deform in a way that maximizes the number of the field lines running in the direction of the d-axis, where the reluctance of the rotor is the lowest[3] [43].
The system will thus attempt to suppress this deformation by aligning the rotor to a position where the deformation is minimized, which corresponds to the position where the energy of the magnetic circuit is maximized [1], [5].

[3] The deformation of the field lines is also indicated in *Figure 2.2*, although not commented upon, serving more as an initial conceptual model.

However, as has been already stated, the construction and powering of the stator will not cause the magnetic field in the air gap to be homogeneous and static, but heterogeneous and dynamic – more specifically, it will be a rotating circular magnetic field, and its direction will therefore be constantly changing.
Consequently, the reluctance torque acting on the rotor will also be constantly changing. If this is happening too quickly, the rotor will only 'tremble' in place at most, but in the end, nothing will actually happen to it, let alone to start rotating [3].
Therefore, the motor will only start when there is enough time for magnetic coupling between the field and the rotor to develop, so the rotor will then be pulled into synchronism by the field (the field will start 'drifting' the rotor – or in other words, the field will start rotating the rotor). Once pulled into synchronism, the torque acting on the rotor will be constant (ideally – because in reality there is still some torque ripple as was already being mentioned throughout the previous chapters).
Hence, it is necessary to start rotating the field at an appropriate speed, and only after the rotor is pulled into synchronism, gradually increase the speed of the field if necessary. As has been already said, this is done using a VFD [1]. It is now clear why cageless SynRM cannot be started DOL [19].

The rotor is now rotating in synchronism with the rotating circular magnetic field of the stator. The presence of a load, or rather a load torque on the shaft, causes the d-axis to deviate from the direction of the flux lines of Ψ by the so-called **load angle** β (which could already have been seen in *Figure 2.2*), whose magnitude depends on the magnitude of the load. The load torque always acts against the direction of the reluctance torque [1].
In real motors, some load torque is always present, even when the motor is running in no-load operation. It stems from the loss torques of the motor itself, caused by mechanical friction in the bearings and by ventilation. However, in an ideal case, these would not be present, and the magnetic flux lines would run parallel to the d-axis [1], [13].

By a suitable control of the stator current space vector $\boldsymbol{I}_\mathrm{s}$ using for example the control method that is going to be outlined in *chapter 4*, the speed of the rotating magnetic field can be influenced while maintaining β at a desired value – which, as is now going to be shown mathematically, allows to influence the magnitude of the produced reluctance torque, which in the final consequence also means affecting the speed of the motor [3].

When deducing the mathematical formula for the produced torque of a SynRM, the following procedure is going to be followed. First, it is declared that mechanical angular velocities will be denoted as uppercase Ω and electrical angular velocities as lowercase ω in this thesis, with the following equation defining their relationship:

$$\Omega_x = \frac{\omega_x}{p_\mathrm{p}} = \frac{2\pi f_x}{p_\mathrm{p}}, \tag{2.1}$$

where p_p is the number of pole pairs of the motor, f is the frequency, and the subscript x can be substituted by either 's' – stator (or synchronous respectively) – relating to the rotating magnetic field, 'r' – rotor – relating to the rotation of the rotor, or '2' – relating to quantities in the rotor (e.g. rotor current).

The electrical angular velocity of quantities in the rotor would then be calculated as:

$$\omega_2 = \omega_\mathrm{s} - \omega_\mathrm{r} \tag{2.2}$$

or

$$f_2 = f_\mathrm{s} - f_\mathrm{r} \tag{2.3}$$

for frequencies respectively [13].
Then starting from the universal equation for the static torque (torque in **steady state (ss)**) of a synchronous machine:

$$T = T_\mathrm{s} + T_\mathrm{rel} = \frac{3}{\Omega_\mathrm{s}} \left(\frac{U_\mathrm{p} \cdot U_\mathrm{iep}}{X_\mathrm{d}} \sin\beta \right) + \frac{3}{\Omega_\mathrm{s}} \left(\frac{U_\mathrm{p}^2}{2} \left(\frac{1}{X_\mathrm{q}} - \frac{1}{X_\mathrm{d}} \right) \sin 2\beta \right), \tag{2.4}$$

where T_s is the synchronous torque, T_rel is the reluctance torque, U_p is the RMS (Root Mean Square) value of the stator phase voltage, U_iep is the RMS value of a stator phase **back electromotive force (back EMF)** produced by the rotating excited rotor and X_d and X_q are the reactances in the d and q axes of the rotor.
In the vast majority of cases, SynRM does not possess any source of T_s (as SynRM does not have any excitation winding, PM only in some cases), therefore the universal equation for its static torque is going to be:

$$T_\mathrm{rel} = \frac{3}{\Omega_\mathrm{s}} \left(\frac{U_\mathrm{p}^2}{2} \left(\frac{1}{X_\mathrm{q}} - \frac{1}{X_\mathrm{d}} \right) \sin 2\beta \right), \tag{2.5}$$

which means that SynRM indeed produces only reluctance torque, and that is why its torque is referred to as such [15], [43].
Therefore, it can be observed that the magnitude of the torque produced by SynRM is going to be influenced not only by Ω_s and U_p, but also by β and by the difference of the reciprocals of X_q and X_d, as was being pointed out over the course of *subchapter 1.2* and now verified mathematically.
The torque of a SynRM can be formulated in many ways [1], [3], [19] and more of them are going to be presented in *chapter 3*, along with their deductions and a clearer depiction of the used variables.

Finally, if the cause for the torque production in SynRM had to be compared with the cause for the torque production in IM, there would be a significant difference, primarily due to the construction of their rotors. In SynRM, there is no back EMF in its rotor as in a rotor of an IM, because there is nowhere for it to be produced. In IM, torque is produced as a result of the interaction of rotor conductors carrying current caused by the back EMF, with the magnetic field of the stator.
According to the principles of electromagnetism, this results in tangential forces acting on the conductors, and as the forces act on an arm with respect to the axis of rotation, torque is produced.
Also, SynRM inherently lacks slip [44], as evident from its categorization described in the *Introduction* section.

Chapter 3
Mathematical model

Generally, mathematical model of a SynRM varies by the absence or presence of squirrel cage and PM [19]. Furthermore, it also varies based on the desired level of accuracy of the model that is to be achieved. As greater accuracy increases the complexity of the model, the choice of the level of accuracy depends on the intended purpose of the model.
In this chapter, a simple model of the most basic SynRM with no squirrel cage, with no PM and with many simplifications is going to be introduced. The model is based on the mathematical model of a conventional synchronous machine with salient poles, from which the excitation and damper windings were removed [19].
Additionally, an outline of how nonlinearities would affect the model if they were included is going to be given, as they would need to be included in an accurate and thus more reality-corresponding model [3].
Lastly, only the model itself is going to be presented and explained. The principles of the means used to create it, such as the Park's transformation, space vector etc., are not going to be discussed in any detail.

3.1 Assumptions and simplifications

In order to start creating the defined model, several assumptions and simplifications need to be adopted, on which the model is going to be based – they are listed below.

1. The power system is 3-phase and symmetrical.
2. All voltages are harmonic.
3. The windings of each stator phase are sinusoidally distributed in the stator slots along the air gap.
4. For the resistances of each stator phase applies:

$$R_{\mathrm{a}} = R_{\mathrm{b}} = R_{\mathrm{c}} = R_{\mathrm{s}} = const. \tag{3.1}$$

5. The following is neglected:
   - stator slotting – thus, for the air gap width δ now applies:

$$\delta = const., \tag{3.2}$$

   - magnetic saturation,
   - cross-coupling,
   - iron losses ΔP_{Fe},
   - mechanical friction.

Points 1, 2, 3 together imply that the waveform of magnetic induction in the air gap is sinusoidal [45]. Point 4 implies, that R_{s} is now the resistance of a stator phase [1].

3.2 Model in the abc system

The model is going to be first described in the abc system. A conceptual model of a SynRM with stator phases a, b, c, from which is going to be further proceeded, is as follows:

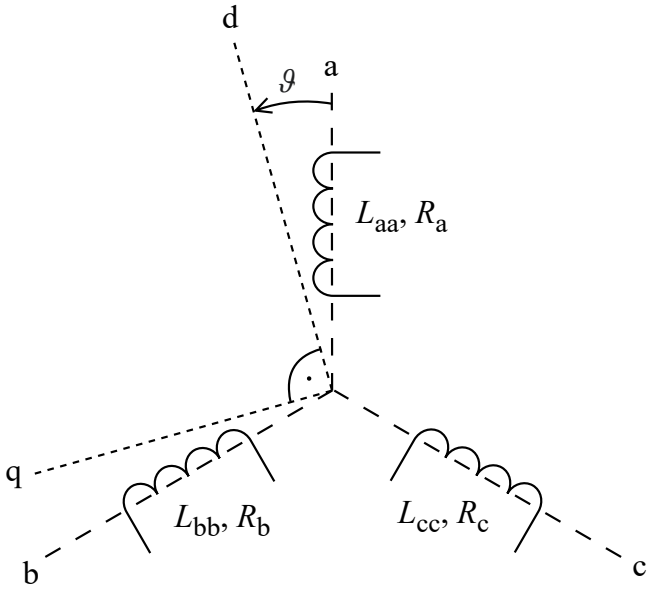

Figure 3.1: A conceptual model of a SynRM in the abc system [45].

According to *Figure 3.1*, the voltage equations are written as:

$$u_a = R_s i_a + \frac{d\psi_a}{dt}, \tag{3.3}$$

$$u_b = R_s i_b + \frac{d\psi_b}{dt}, \tag{3.4}$$

$$u_c = R_s i_c + \frac{d\psi_c}{dt}, \tag{3.5}$$

where u_a, u_b, u_c are the phase voltages across each stator phase, i_a, i_b, i_c are the phase currents flowing through each stator phase and ψ_a, ψ_b, ψ_c are the stator magnetic flux linkages caused by the currents.
For the magnetic flux linkages, the following flux equations apply:

$$\psi_a = L_{aa} i_a + L_{ab} i_b + L_{ac} i_c, \tag{3.6}$$

$$\psi_b = L_{ab} i_a + L_{bb} i_b + L_{bc} i_c, \tag{3.7}$$

$$\psi_c = L_{ac} i_a + L_{bc} i_b + L_{cc} i_c. \tag{3.8}$$

L_{aa}, L_{bb}, L_{cc} are the self-inductances of each stator phase:

$$L_{aa} = L_{s\sigma} + L_h + L_0 \cos 2\vartheta, \tag{3.9}$$

$$L_{bb} = L_{s\sigma} + L_h + L_0 \cos\left(2\vartheta - \frac{2\pi}{3}\right), \tag{3.10}$$

$$L_{cc} = L_{s\sigma} + L_h + L_0 \cos\left(2\vartheta + \frac{2\pi}{3}\right), \tag{3.11}$$

and L_{ab}, L_{ac}, L_{bc} are the mutual inductances between each of the stator phases:

$$L_{ab} = L_{ba} = -\frac{1}{2}L_h + L_0 \cos\left(2\vartheta - \frac{2\pi}{3}\right), \tag{3.12}$$

$$L_{ac} = L_{ca} = -\frac{1}{2}L_h + L_0 \cos\left(2\vartheta + \frac{2\pi}{3}\right), \tag{3.13}$$

$$L_{bc} = L_{cb} = -\frac{1}{2}L_h + L_0 \cos 2\vartheta, \tag{3.14}$$

where

$$\vartheta = \omega_r t \tag{3.15}$$

is the electrical angle of the turning of the rotor relatively to the stator, t is the time variable, $L_{s\sigma}$ is the leakage inductance of the stator winding, L_h is the magnetizing inductance component independent of ϑ and L_0 is the magnetizing inductance component caused by the anisotropy of the rotor [19], [45].

3.3 Model in the dq system

The model is now going to be described in the dq system. A conceptual model of a SynRM in the dq system is as follows:

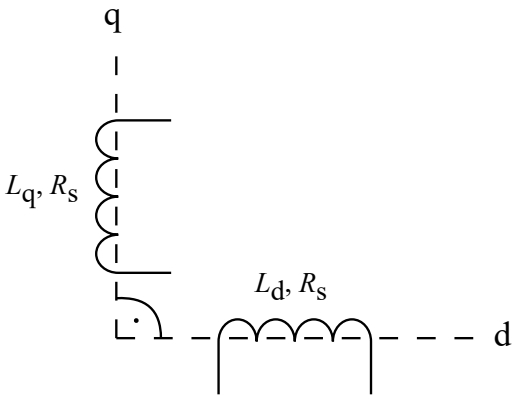

Figure 3.2: A conceptual model of a SynRM in the dq system [1].

If the system of differential *equations (3.3)–(3.5).* had to be solved, it would be challenging due to the presence of the variable ϑ – and thus, the use of a numerical method would likely be necessary. However, this obstruction can be overcome by employing the Park's transformation of all quantities from the abc coordinate system to the dq coordinate system, which is rotating with a general electrical angular velocity ω_k.

The formula for the Park's transformation is generally given by the following transformation matrix:

$$\boldsymbol{P} = K \cdot \begin{pmatrix} \cos\omega_k t & \cos\left(\omega_k t - \frac{2\pi}{3}\right) & \cos\left(\omega_k t + \frac{2\pi}{3}\right) \\ -\sin\omega_k t & -\sin\left(\omega_k t - \frac{2\pi}{3}\right) & -\sin\left(\omega_k t + \frac{2\pi}{3}\right) \end{pmatrix}, \tag{3.16}$$

where K is the Park's transformation coefficient. The values $\omega_k = \omega_\mathrm{r}$ and $K = 2/3$ are chosen for further procedure. This value of K ensures that the amplitude of the 3-phase waveform of a given quantity in the abc system will be equal to the magnitude of the space vector of this quantity in the dq system.

After applying the transformation to *equations (3.3)–(3.5)*, the voltage equations in the dq system are obtained:

$$u_\mathrm{d} = R_\mathrm{s} i_\mathrm{d} + \frac{\mathrm{d}\psi_\mathrm{d}}{\mathrm{d}t} - \omega_\mathrm{r}\psi_\mathrm{q}, \tag{3.17}$$

$$u_\mathrm{q} = R_\mathrm{s} i_\mathrm{q} + \frac{\mathrm{d}\psi_\mathrm{q}}{\mathrm{d}t} + \omega_\mathrm{r}\psi_\mathrm{d}, \tag{3.18}$$

where u_d, u_q are the components of the stator voltage space vector $\boldsymbol{U}_\mathrm{s}$ in the d and q axes, i_d, i_q are the components of $\boldsymbol{I}_\mathrm{s}$ in the d and q axes, ψ_d, ψ_q are the components of the stator magnetic flux linkage space vector $\boldsymbol{\Psi}_\mathrm{s}$ in the d and q axes, the terms $\mathrm{d}\psi_\mathrm{d}/\mathrm{d}t$ and $\mathrm{d}\psi_\mathrm{q}/\mathrm{d}t$ are the components of the so-called **transformational back EMF** and the terms $\omega_\mathrm{r}\psi_\mathrm{d}$ and $\omega_\mathrm{r}\psi_\mathrm{q}$ are the components of the so-called **rotational back EMF**.

For flux equations is going to apply [46]:

$$\psi_\mathrm{d} = L_\mathrm{d} i_\mathrm{d}, \tag{3.19}$$

$$\psi_\mathrm{q} = L_\mathrm{q} i_\mathrm{q}, \tag{3.20}$$

and for inductances in the d and q axes applies:

$$L_\mathrm{d} = L_{\mathrm{s}\sigma} + L_\mathrm{md}, \tag{3.21}$$

$$L_\mathrm{q} = L_{\mathrm{s}\sigma} + L_\mathrm{mq}, \tag{3.22}$$

where L_md and L_mq are the magnetizing inductances in the d and q axes. From *equations (3.17)–(3.22)*, an equivalent circuit of a SynRM can be constructed, which will itself consist of two circuits, each for one of the axes. The circuits are interconnected via back EMFs generated by the magnetic flux linkage from the other of the axes [1]:

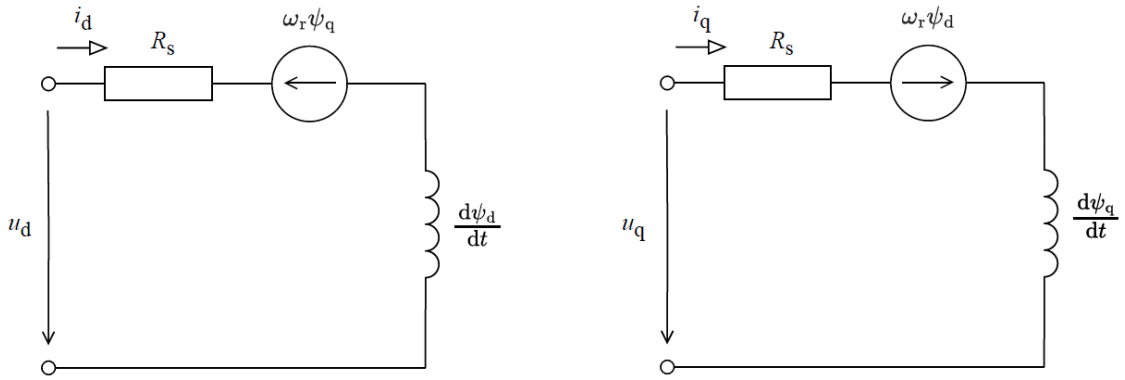

Figure 3.3: An equivalent circuit of a SynRM – the d-axis part on the left-hand side, the q-axis part on the right-hand side [19].

For the model to be complete, it is necessary to provide two more equations, the first of which is the relationship for the **electromagnetic torque** (also known as the **internal torque**) of the SynRM.
Starting from the most common form of the equation for the electromagnetic torque of a synchronous machine in the dq system [1]:

$$T = \frac{3}{2} p_\mathrm{p} \left(\psi_\mathrm{d} i_\mathrm{q} - \psi_\mathrm{q} i_\mathrm{d} \right), \tag{3.23}$$

on which a rearrangement is going to be performed to explicitly display the vital inductances of a SynRM [19]:

$$T = \frac{3}{2} p_\mathrm{p} \left(L_\mathrm{d} - L_\mathrm{q} \right) i_\mathrm{d} i_\mathrm{q}. \tag{3.24}$$

The second equation is **the equation of motion of an electric drive system**:

$$T - T_\mathrm{L} = J \frac{\mathrm{d}\Omega_\mathrm{r}}{\mathrm{d}t}, \tag{3.25}$$

where T is the driving torque of the motor, T_L is the load torque acting on the motor shaft, J is the moment of inertia of the rotating parts of the entire mechanism with respect to the axis of rotation and Ω_r is the mechanical angular velocity of the rotor. If the loss torques of the motor itself are included into T_L, then T in *equation (3.25)* will become the electromagnetic torque [1].

3.4 Unaccounted nonlinearities

If an almost complete, and thus an almost accurate model of a SynRM is to be obtained, it is necessary to include these unaccounted nonlinearities in it (the word 'almost' is used due to the fact that, besides other, most of the assumptions and simplifications from *subchapter 3.1* would still be in effect) [19], [45].

3.4.1 Magnetic saturation

Generally, magnetic saturation refers to the relationship between magnetic flux linkage, inductance and current $\psi = L \cdot i$. In the presented model, the complete behavior of this relationship is not implemented and the relationship is considered linear at all times, thus $L = const$. However, the stator and rotor sheets of a SynRM are made of ferromagnetic material, for which in reality, the relationship becomes nonlinear after surpassing the so-called **saturation limit**. Beyond this limit, ψ further increases only slightly. The reason for this is that after surpassing a certain value of i that defines this limit, L begins to decrease.

Therefore if magnetic saturation was considered, *equations (3.19), (3.20)* would also need to be rewitten into their complete form, further adding that the inductances in the d and q axes are dependent on both of the components of $\boldsymbol{I}_\mathrm{s}$ in the dq system:

$$\psi_\mathrm{d} = L_\mathrm{d} \left(i_\mathrm{d}, i_\mathrm{q} \right) \cdot i_\mathrm{d}, \tag{3.26}$$

$$\psi_\mathrm{q} = L_\mathrm{q} \left(i_\mathrm{d}, i_\mathrm{q} \right) \cdot i_\mathrm{q}. \tag{3.27}$$

Generally in SynRM, ψ_d saturates much earlier with increasing i_d and constant i_q than ψ_q with increasing i_q and constant i_d, where the growth is almost linear. This is due to the much smaller reluctance in the d-axis compared with the q-axis.
For ALA-SynRM, magnetic saturation generally occurs only in the d-axis, hence i_d would play a significant role for L_d, and L_q would not change with i_q almost at all (it would only change at very high magnitudes of i_q) [3].

3.4.2 Cross-coupling

This nonlinearity would cause ψ_d to decrease with increasing i_q, with the decrease being more significant for lower i_d. Analogically, this also applies to ψ_q in the case of increasing i_d, which can have negative effects, for example in the FW operating range of the motor [10], [11].

3.5 Steady state

In ss, in addition to the assumptions and simplifications given in *subchapter 3.1*, the below statements apply.

1. $\Omega_r = \Omega_s$, or $\omega_r = \omega_s$ respectively.
2. Stator voltages and currents are symmetrical and sinusoidal.
3. All derivatives are zero [1].

Voltage equations in the abc system are thus written as:

$$u_a = \sqrt{2}\, U_p \cos\vartheta, \tag{3.28}$$

$$u_b = \sqrt{2}\, U_p \cos\left(\vartheta - \frac{2\pi}{3}\right), \tag{3.29}$$

$$u_c = \sqrt{2}\, U_p \cos\left(\vartheta + \frac{2\pi}{3}\right), \tag{3.30}$$

where u_a, u_b, u_c are the phase voltages across each stator phase and U_p is the RMS value of a stator phase voltage.

The voltage equations in the dq system are obtained by first substituting [46]

$$\omega_k t = \omega_r t - \vartheta_0 \tag{3.31}$$

into *(3.16)*, where (for motor mode):

$$\vartheta_0 = \frac{\pi}{2} + \beta \tag{3.32}$$

is the angle by which $\boldsymbol{U}_s$ 'leads' the d-axis and β is the already mentioned load angle, by which $\boldsymbol{U}_s$ 'leads' the q-axis.

The resulting transformation matrix is then applied to *equations (3.28)–(3.30)*, yielding:

$$U_\mathrm{d} = \sqrt{2}\, U_\mathrm{p} \cos \vartheta_0, \tag{3.33}$$

$$U_\mathrm{q} = \sqrt{2}\, U_\mathrm{p} \sin \vartheta_0, \tag{3.34}$$

where U_d, U_q are the components of $\boldsymbol{U}_\mathrm{s}$ in the d and q axes in ss.

The equations could also be obtained, just in a different form, by omitting the derivatives from *equations (3.17), (3.18)*, according to the statements for ss given at the beginning of this subchapter:

$$U_\mathrm{d} = R_\mathrm{s} I_\mathrm{d} - \omega_\mathrm{r} \Psi_\mathrm{q}, \tag{3.35}$$

$$U_\mathrm{q} = R_\mathrm{s} I_\mathrm{q} + \omega_\mathrm{r} \Psi_\mathrm{d}, \tag{3.36}$$

where I_d, I_q are the components of $\boldsymbol{I}_\mathrm{s}$ in the d and q axes in ss and Ψ_d, Ψ_q are the components of $\boldsymbol{\Psi}_\mathrm{s}$ in the d and q axes in ss.

Current equations in the dq system will be identically structured as *equations (3.33), (3.34)*, except that the lagging of $\boldsymbol{I}_\mathrm{s}$ behind $\boldsymbol{U}_\mathrm{s}$ by the angle φ needs to be incroporated:

$$I_\mathrm{d} = \sqrt{2}\, I_\mathrm{p} \cos\left(\vartheta_0 - \varphi\right), \tag{3.37}$$

$$I_\mathrm{q} = \sqrt{2}\, I_\mathrm{p} \sin\left(\vartheta_0 - \varphi\right), \tag{3.38}$$

where I_p is the RMS value of a stator phase current.

Due to U_d, U_q being DC quantities in ss together with the statements given at the beginning of this subchapter being in effect, I_d, I_q, Ψ_d, Ψ_q will also be DC quantities [3], [19].

Now, sufficient information has been obtained for the construction of a phasor diagram of a SynRM in ss, where all space vectors and the dq coordiante system itself is rotating with the electrical angular velocity ω_r:

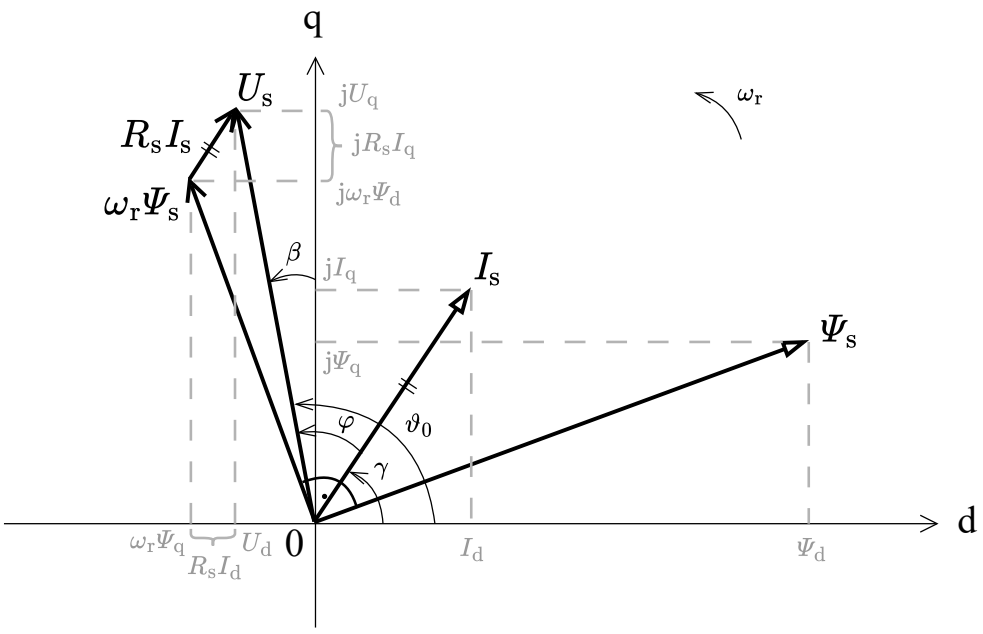

Figure 3.4: A phasor diagram of a SynRM in steady state [19].

For the model of a SynRM in ss to be complete, it is yet necessary to provide it with the relationship for torque, which is going to be deduced using the phasor diagram in *Figure 3.4*. The introduction of the equation of motion, whose general formula remains the same, into the model of a SynRM in ss is not meaningful, as T and T_L are equal in ss and the derivative on the right-hand side of the equation is zero, thus $0 = 0$.

Using β, the components of $\boldsymbol{U}_\mathrm{s}$ in the d and q axes in ss are first going to be formulated:

$$U_\mathrm{d} = \sqrt{2}\, U_\mathrm{p} \sin\beta, \tag{3.39}$$

$$U_\mathrm{q} = \sqrt{2}\, U_\mathrm{p} \cos\beta. \tag{3.40}$$

In further deduction it is going to be assumed that in *equations (3.35), (3.36)*, the voltage drop due to R_s compared with the rotational back EMF is negligible (in reality, this is true for higher motor speeds). Yelding:

$$U_\mathrm{d} = -\omega_\mathrm{r}\, \Psi_\mathrm{q}, \tag{3.41}$$

$$U_\mathrm{q} = \omega_\mathrm{r}\, \Psi_\mathrm{d}. \tag{3.42}$$

Now, from *equations (3.41), (3.42)*, Ψ_d, Ψ_q is going to be expressed, as well as i_d, i_q from *equations (3.19), (3.20)*. The obtained relationships are then going to be substituted into *equation (3.23)*, yielding:

$$T = \frac{3\, p_\mathrm{p}}{4\, \omega_\mathrm{r}} \left(\frac{1}{X_\mathrm{q}} - \frac{1}{X_\mathrm{d}} \right) U_\mathrm{d}\, U_\mathrm{q}, \tag{3.43}$$

where:

$$X_\mathrm{d} = \omega_\mathrm{r} L_\mathrm{d}, \tag{3.44}$$

$$X_\mathrm{q} = \omega_\mathrm{r} L_\mathrm{q}. \tag{3.45}$$

Equations (3.39), (3.40) are then substituted into *equation (3.43)*, and after a few rearrangements, the final form of the equation for the torque of a SynRM in ss is obtained:

$$T = \frac{3\, p_\mathrm{p}}{2\, \omega_\mathrm{r}} \left(\frac{1}{X_\mathrm{q}} - \frac{1}{X_\mathrm{d}} \right) U_\mathrm{p}^2 \sin 2\beta. \tag{3.46}$$

Under the conditions $U_\mathrm{p} = const.$ and $\omega_\mathrm{r} = const.$, the maximum torque is achieved at $\beta = \pi/4$. Conversely, at values of 0 or $\pi/2$, the output torque is zero.

The torque of a SynRM in ss can also be formulated using the angle γ, by which $\boldsymbol{I}_\mathrm{s}$ 'leads' the d-axis. First, the components of $\boldsymbol{I}_\mathrm{s}$ in the d and q axes in ss are going to be formulated using this angle:

$$I_\mathrm{d} = \sqrt{2}\, I_\mathrm{p} \cos\gamma, \tag{3.47}$$

$$I_\mathrm{q} = \sqrt{2}\, I_\mathrm{p} \sin\gamma, \tag{3.48}$$

which is going to be substituted into *(3.24)*, yielding [3], [19]:

$$T = \frac{3}{2}\, p_\mathrm{p} \left(L_\mathrm{d} - L_\mathrm{q} \right) I_\mathrm{p}^2 \sin 2\gamma. \tag{3.49}$$

The maximum torque, under the condition $I_\mathrm{p} = const.$, is achieved at $\gamma = \pi/4$. However, this is valid only under the statements presented at the beginning of this subchapter together with the assumptions and simplifications stated in *subchapter 3.1* – because in reality, increasing the value of I_p also causes the optimal γ to increase [3], [19].

Chapter 4
Control method – FOC

Firstly, speed control of SynRM considers cagless rotors exclusively (as stated in *sub-chapter 1.3.1*) [19]. Furthermore, it has been also already mentioned that SynRM is powered by an inverter (or VFD) in the vast majority of cases, thus the motor speed is controlled by varying the frequency of the supply voltage. This method of control is therefore called frequency speed control, which can be classified into categories:

- Scalar Control (V/f control, V/Hz control, U/f control),
- Vector Control,
  - Field-Oriented Control (FOC),
  - Direct Torque Control (DTC).

When scalar control is discussed, it is also possible to encounter the abbreviation SC, whereas when vector control is discussed, it is possible to encounter the abbreviation VC. However, generally, when the term vector control is used, it is commonly referred to FOC. Therefore, to avoid confusion, this transferred meaning will not be used in this thesis and each of the terms from the list above will be referred to by only one abbreviation – that is V/f, VC, FOC, and DTC, according to the sequence in which the terms were presented.

When comparing V/f and VC – the two main branches of speed control methods of electric motors, V/f is limited only to the frequency and magnitude of the space vector of the given motor quantity (such as current, magnetic flux or voltage). On the contrary, when VC is used, also the position of these vectors can be controlled. VC is generally more modern and technologically advanced, which results in greater precision of the speed control (as VC controls to an exact speed setpoint unlike V/f that controls to a supply voltage frequency setpoint), better dynamics, and a smaller occurrence of uncontrolled transients. However, VC requires much larger computational capacity of the microprocessor used than is required for V/f, as the control algorithm is more complex than the control algorithm of V/f [1], [47].

VC is commonly divided according to the method used to control the space vectors, as can be seen from the categorization above. However, it can also be divided in other ways, such as by the controllers used, etc. [47].

Out of the presented control methods, only FOC is going to be briefly outlined in this thesis, as it is a modern and the most commonly used method for controlling SynRM and generally all AC motors among all the methods presented [1]. Therefore, V/f or DTC are not going to be further addressed in this thesis.

The control processes of FOC take place in the dq system, in which the components of the particular space vectors are DC quantities, which makes their control much easier.

The principle of FOC then builds upon the fact that in the dq system, $\boldsymbol{I}_\mathrm{s}$ can be broken down into two components – each for one of the axes of the dq system. These components are also frequently referred to as:

- i_d – the field-producing component of the stator current,
- i_q – the torque-producing component of the stator current,

where the field-producing component is tied with the magnetic flux linkage of the motor and the torque-producing component is tied with the torque of the motor.

The control of the components is carried out using two controllers – one for each of the components, thus closely resembling the control of a separately excited DC motor. Simply put, as a result, the flux linkage determining the degree of 'excitation' of the motor readily available during its operation is chosen, as well as the speed setpoint, which eventually collaborates with the controller of the torque-producing component to accelerate or decelerate the motor to achieve the setpoint.
However, there is an issue that in a real motor, there is only one stator current, and its breakdown into components is therefore merely an imaginary concept. This results in the control of one component in the imaginary conceptual control system affecting the control of the other. Nevertheless, nowadays the technology of FOC is advanced enough to sufficiently mitigate this issue [1].
A simple block diagram of FOC of a SynRM, from which the principle of function of this control method is evident, is depicted in the figure below:

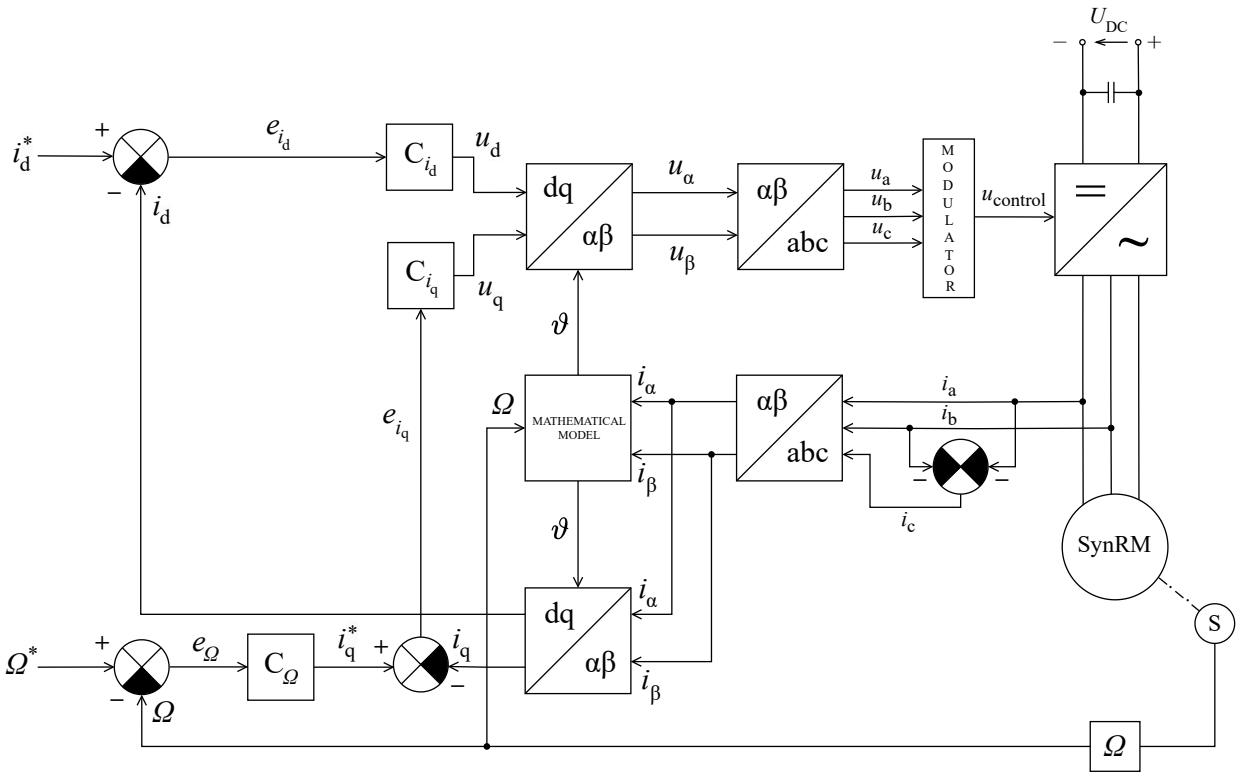

Figure 4.1: A simple block diagram of FOC of a SynRM [1].

The blocks and other components of the diagram as well as their placement within the diagram may vary, leading to different variants of FOC [1].

For example, in practice, for rotor position detection and for its speed determination, sensors such as incremental rotary encoders, absolute rotary encoders, etc. (denoted as S in *Figure 4.1*) are commonly used. However, in applications that do not require precise speed control (e.g., pumps, fans, and compressors), money can be saved on the sensor and its cabling by using a less accurate option – the mathematical model of the given SynRM. Unlike when a sensor is used, the model determines the position and speed directly from the equation of motion of the drive system. Moreover, if the model is accurate enough, a relatively fairly precise control is still achievable [48].

4.1 Control strategies for FOC

Control strategies for FOC generally assist in optimizing the motor control by providing the optimal pair of values of i_d and i_q, thus the optimal γ from *subchapter 3.5*, which needs to be achieved through the control in order to ensure that the power supplied to the motor is utilized as efficiently as possible relative to the goal of the strategy. The strategy is then usually named according to its objective.

If any control strategy is to be used, it is necessary, as SynRM is powered by an inverter (by a VFD respectively), for $|\boldsymbol{U}_\mathrm{s}|$ and $|\boldsymbol{I}_\mathrm{s}|$ to always satisfy:

$$|\boldsymbol{U}_\mathrm{s}| = \sqrt{u_\mathrm{d}^2 + u_\mathrm{q}^2} \leq |\boldsymbol{U}_\mathrm{s}|_\mathrm{max}\,, \tag{4.1}$$

$$|\boldsymbol{I}_\mathrm{s}| = \sqrt{i_\mathrm{d}^2 + i_\mathrm{q}^2} \leq |\boldsymbol{I}_\mathrm{s}|_\mathrm{max}\,, \tag{4.2}$$

where $|\boldsymbol{U}_\mathrm{s}|_\mathrm{max}$ is the maximum voltage that the given inverter is capable of supplying[1] and $|\boldsymbol{I}_\mathrm{s}|_\mathrm{max}$ is the maximum current for which the inverter and motor are designed [49].

The most commonly used control strategies for FOC of a SynRM [50] are now going to be described.

4.1.1 MTPA

Maximum Torque Per Ampere (MTPA) is a strategy that identifies such a γ_MTPA at which the maximum possible output torque is achieved for a given magnitude of stator current. The main advantage of this strategy is the reduction in Joule losses in the motor, because the desired torque is produced using the minimum possible current. Sometimes, this method can also be referred to as Maximum Efficiency (ME), due to the reduction in these losses.

One of the analytical methods to find the γ_MTPA (which can similarly be used for other strategies that are going to be mentioned) involves searching for constrained extrema – for example, using Lagrange multipliers.
The procedure involves taking the formula for the torque of a SynRM and solving an optimization problem. From all of the presented versions of formulas for the torque of a SynRM, *equation (3.24)* is going to be used. The problem is formulated differently depending on whether the output of the speed controller is the torque setpoint T^* or the torque-producing component setpoint i_q^*. However, both formulations of the problem lead to the same result.

[1] Its magnitude depends on the modulation method used and on the value of U_DC – i.e. for Space Vector Pulse Width Modulation (SVPWM) $|\boldsymbol{U}_\mathrm{s}|_\mathrm{max} = U_\mathrm{DC}/\sqrt{3}$.

If it is T^*, the optimization problem is formulated as:

```
find min(i_d,i_q) for |I_s(i_d,i_q)| so that
sqrt{i^2_d+i^2_q} less or equal than |I_s(i_d,i_q)|_max while
T(i_d,i_q)=T^*(i_d,i_q).
```

If it is i_q^*, the optimization problem is formulated as:

```
find max(i_d,i_q) for T(i_d,i_q) so that
sqrt{i^2_d+i^2_q} less or equal than |I_s(i_d,i_q)|_max while
i_q=i^*_q.
```

As a result, the currents $i_{\mathrm{d,MTPA}}$ and $i_{\mathrm{q,MTPA}}$ corresponding to the specified requirements will be obtained.
The sought angle is then determined as:

$$\gamma_{\mathrm{MTPA}} = \operatorname{arctg}\left(\frac{i_{\mathrm{q,MTPA}}}{i_{\mathrm{d,MTPA}}}\right). \tag{4.3}$$

For SynRM, under the conditions stated in *subchapter 3.5*, applies $\gamma_{\mathrm{MTPA}} = \pi/4$, thus $i_{\mathrm{d,MTPA}} = i_{\mathrm{q,MTPA}}$, which has already been mentioned in that subchapter.

However, if magnetic saturation was considered, the search for γ_{MTPA} would be much more complicated. In most cases, due to computational complexity, the MTPA trajectory is not determined analytically, but rather by other means (similarly applies to trajectories of other strategies that are going to be mentioned) [49].

4.1.2 MTPV

Maximum Torque Per Volt (MTPV) is a strategy that identifies such a γ_{MTPV} at which the maximum possible output torque is achieved for a given magnitude of stator voltage. MTPV is used, for instance, during FW with stator current limiting, when the objective is to achieve high motor speeds while maximizing torque simultaneously.

Nevertheless, the search for the extrema follows the same rules and procedures as MTPA, only with the exception that the criteria for the search are altered.

After solving the optimization problem and also after neglecting the voltage drop due to the stator winding resistance, the sought angle is determined as [49]:

$$\gamma_{\mathrm{MTPV}} = \operatorname{arctg}\left(\frac{L_\mathrm{d}}{L_\mathrm{q}}\right) = \operatorname{arctg}\xi. \tag{4.4}$$

4.1.3 MTPF

Maximum Torque Per Flux (MTPF) is a strategy that identifies such a γ_{MTPF} at which the maximum possible output torque is achieved for a given magnitude of motor magnetic flux. At high speeds, MTPF minimizes iron losses.

Sometimes, this method is referred to as MTPV – however, this substitution is not always correct and can lead to erroneous results because MTPV generally addresses a different optimization problem than MTPF.

Only when the voltage drop due to the stator winding resistance is neglected or when its magnitude is very small and motor speeds are high, the trajectories of MTPV and MTPF overlap. The search for the extrema also follows the same rules and procedures as MTPA, only with the exception that the criteria for the search are, again, altered.

After solving the optimization problem and also after neglecting the voltage drop due to the stator winding resistance, the sought angle is determined the same way as in the case of MTPV [49], [51]:

$$\gamma_{\mathrm{MTPF}} = \operatorname{arctg}\left(\frac{L_{\mathrm{d}}}{L_{\mathrm{q}}}\right) = \operatorname{arctg}\xi. \tag{4.5}$$

4.1.4 MPFC (MTPkVA)

Maximum Power Factor Control (MPFC), or sometimes also referred to as Maximum Torque Per kilovolt-ampere (MTPkVA), utilizes the dependency of power factor $\cos\varphi$ on γ given by *function (5.2)*. It identifies such a γ_{MPFC} at which the maximum possible power factor is achieved for a given speed, magnitude of stator current, etc.

After solving the optimization problem, the sought angle is determined as [49], [51]:

$$\gamma_{\mathrm{MPFC}} = \operatorname{arctg}\left(\sqrt{\frac{L_{\mathrm{d}}}{L_{\mathrm{q}}}}\right) = \operatorname{arctg}\xi. \tag{4.6}$$

4.2 Selection of the control strategy based on the motor speed

The optimal choice of the control strategy based on the desired speed at which the SynRM is to be rotating while, of course, maintaining the requirements for $|\boldsymbol{U}_{\mathrm{s}}|$ and $|\boldsymbol{I}_{\mathrm{s}}|$ from *equations (4.1) and (4.2)* is now going to be discussed.

Starting with the introduction of the ideal course of RMS values of output torque (T), output power (P), stator voltage (U), and stator current (I) of a SynRM vs. its mechanical angular velocity Ω:

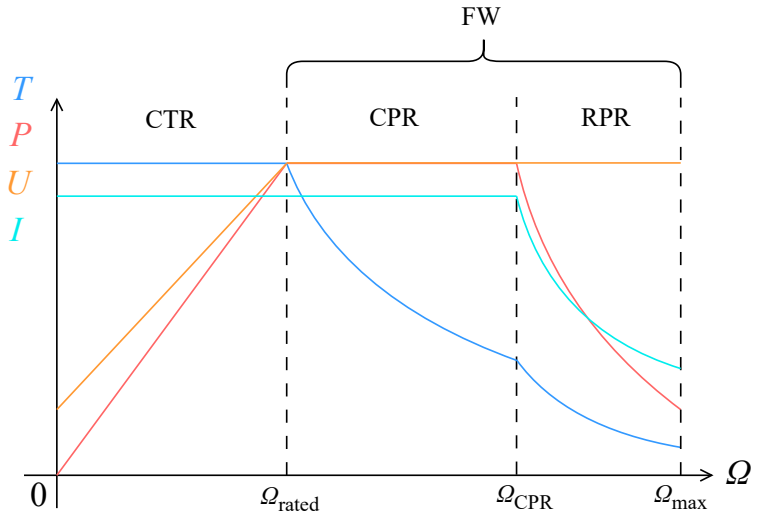

Figure 4.2: The ideal course of RMS values of T, P, U, I of a SynRM vs. its Ω [50].

As can be seen, the course is divided into 3 ranges, which are:

- Constant Torque Range (CTR),
- Constant Power Range (CPR),
- Reduced Power Range (RPR),

whereby in each of them, the optimal control strategy of a SynRM is different [49], [50].

For further procedure, the mathematical relationship for the upper speed limit of the CTR, or for the rated speed respectively is going to be introduced:

$$\Omega_{\text{rated}} = \frac{1}{p_{\text{p}}} \cdot \frac{|\boldsymbol{U}_{\text{s}}|_{\text{max}} - R_{\text{s}}\sqrt{i_{\text{d}}^2 + i_{\text{q}}^2}}{\sqrt{L_{\text{d}} i_{\text{d}} + L_{\text{q}} i_{\text{q}}}}. \tag{4.7}$$

Now, the limits that are necessary to fulfill when increasing speed can be graphically deduced. In the deduction, the voltage drops due to the stator winding resistance are neglected. Then, *(4.7)* is substituted into *(4.1)* and after a few rearrangements, the following is obtained:

$$\frac{i_{\text{d}}^2}{\left(\frac{|\boldsymbol{U}_{\text{s}}|_{\text{max}}}{\omega_{\text{r}} L_{\text{d}}}\right)^2} + \frac{i_{\text{q}}^2}{\left(\frac{|\boldsymbol{U}_{\text{s}}|_{\text{max}}}{\omega_{\text{r}} L_{\text{q}}}\right)^2} \leq 1. \tag{4.8}$$

From this relationship, it can be seen that $|\boldsymbol{U}_{\text{s}}|_{\text{max}}$ represents an ellipse in the Cartesian coordinate system, where i_{d} is identified with the x-axis and i_{q} with the y-axis. With increasing speed, this ellipse is shrinking to the point (0, 0). To maintain the condition defined by *(4.1)*, the motor's operating point in this Cartesian coordinate system must be located inside or on the edge of the given ellipse. At the same time, the operating point must also be located inside or on the edge of the circle given by the condition defined by *(4.2)*. The graphical description of the situation is in the figure below:

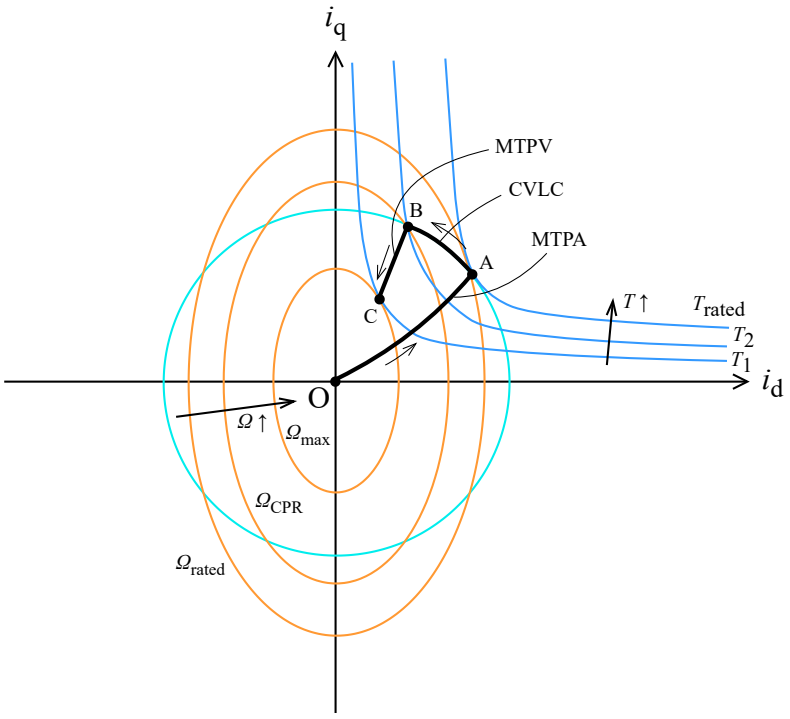

Figure 4.3: Voltage ellipses (orange), current circle (turquoise) and torque hyperbolas (blue) vs. MTPA, CVLC and MTPV trajectories [50].

Now, it is possible to provide a more detailed description of each range and its corresponding optimal control strategy [49], [50].

CTR

The name of this range derives from the fact that the speed of the motor is controlled at constant torque in it. Since utilizing the maximum of the power offered by the motor is aimed for, operating with $|\boldsymbol{I}_\mathrm{s}|_\mathrm{max}$ within this range is going to be considered. In CTR, MTPA strategy should be chosen as it reduces Joule losses in the stator winding, which represent the majority in the total losses in a SynRM in this range.

According to *equations (3.35), (3.36)* and from the phasor diagram in *Figure 3.4*, it is evident that the stator voltage increases with increasing speed. Once this voltage reaches the value of $|\boldsymbol{U}_\mathrm{s}|_\mathrm{max}$, or when Ω_rated from *equation (4.7)* is reached respectively, the voltage ellipse intersects the current circle in the MTPA point (see *Figure 4.3* – point A), where the motor also achieves its maximum power.

For further speed increase, it is necessary to begin FW, as otherwise, with increasing speed, the operating point A would not satisfy condition defined by *(4.8)*. FW generally extends the range of operating speeds of the motor – however, any increase in speed should always be subject to the maximum permissible speed that the motor is designed for while it is also necessary to change the control strategy [49], [50].

CPR

The name of this range derives from the fact that the power of the motor is constant in it – thus, the speed control of the motor continues at the maximum value of the motor's power. This is ensured by maintaining constant voltage and current using the Current-Voltage Limit Control (CVLC) strategy. The principle of function of this strategy is not going to be explained. FW of the motor is commenced at the beginning of CPR [49], [50]. In *Figure 4.3*, CPR is depicted by the curve between points A and B.

RPR

The name of this range derives from the fact that the power of the motor decreases in it while FW still staking place.
The motor will be operating in RPR when a certain speed is reached, at which the respective voltage ellipse and current circle intersect - in *Figure 4.3*, it is the point B. At this moment, the control strategy should be switched to MTPV, with its advantage over CVLC used in the previous range being that it enables achieving higher operating speeds [1], [49], [50]. A section of the MTPV trajectory is depicted in *Figure 4.3* between the points B and C.

Chapter 5
Comparison of qualitative parameters with IM

Qualitative parameters of an electric motor typically refer to properties that describe its performance and operational features.
These parameters are primarily of interest in terms of the practical use of the motor. Many of them are therefore found in datasheets and often serve as the basis for an electric motor company's promotional and marketing plans for the given series of motors.
In this chapter, qualitative parameters of SynRM and IM that are considered most relevant and attractive for this thesis and current practice in terms of their optimization [11] are going to be discussed and compared. A brief summary of this comparison is then going to be provided at the end of this chapter.
Mathematical formulas – without their deduction, for some of these SynRM parameters are also going to be presented. This is going to confirm the earlier suggestions that ξ often has a significant influence on their magnitude.
It must be mentioned that for both motors, it is not possible to optimize all the parameters to the best values in one design. Therefore, some of these parameters must be prioritized in the design (depending on what is required from the motor). This means that the design will, once again, be based on trade-offs.
Finally, a property of SynRM, which is not quite a qualitative parameter, is that due to its working principle, unlike in IM, its speed does not change with load, which is positive in many respects [11].

5.1 Losses

Generally, losses in an electric motor depend on its construction and the physical phenomena acting on it during its operation [13].
It has been already mentioned that the only constructional difference between SynRM and IM lies in their rotors and, moreover, the rotor sheets can be considered the same for the purpose of assessing losses. Therefore, the only remaining difference is that there are no conductors (winding/cage) in the rotor of SynRM [15]. This naturally results in Joule losses in the rotor of SynRM being zero, unlike in the rotor of IM [5].

The following figure clearly illustrates the comparison of the total losses in these two motors:

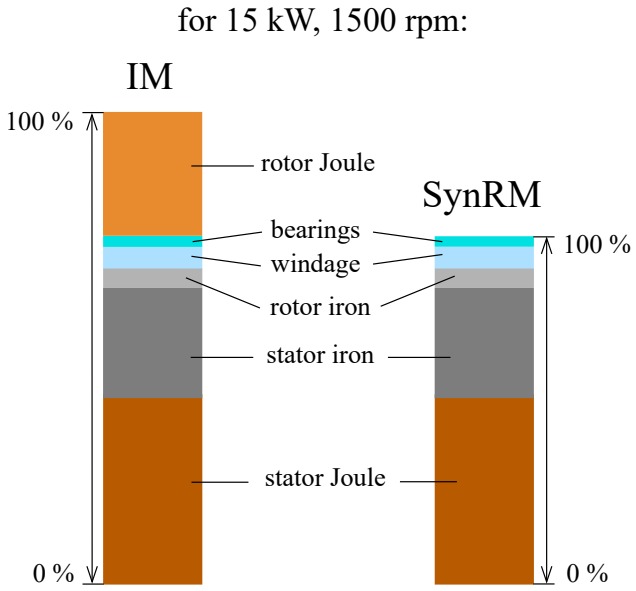

Figure 5.1: An illustration of approximate theoretical comparison of total losses in SynRM and IM for a given output power and speed [48].

Thus, SynRM generally have smaller total losses than IM of the same rated power [14], [48], by up to 40 % [52].

Moreover, for both motor types, there is an option for further reduction in the total losses by reducing the thickness of the stator and/or rotor sheets, which leads to a reduction in iron losses in stator and/or rotor. However, thinner sheets (< 0.2 mm) make the production of the stacks difficult for many reasons, such as:

- handling of the sheets,
- increase in the wear of the sheet punching tool (if this manufacturing technology is used),
- special attention to the respective production processes to avoid the need for additional machining of the stack must be paid.

The increase in the wear is due to the fact that more sheets per motor are needed. Furthermore, the attention must be paid because otherwise both motor types would face problems as they are highly sensitive towards geometric errors (deviations) that can, apart from the initial design stage, also happen during manufacturing and assembly [9].

5.2 Operating temperature

Operating temperature of SynRM is lower than that of IM due to the absence of rotor Joule losses, as has just been described [9]. SynRM is therefore sometimes called a **'cool motor'** [48].

Thus, external cooling is generally not necessary in SynRM, the lifespan of the stator winding insulation is extended [9], [48] and the thermal load on the bearings is reduced [9]. In general, the motor has a greater overall thermal reserve compared with IM.
At the same operating temperature, SynRM achieves higher power than IM by 5-15 % [5].

5.3 Efficiency

Efficiency is arguably the most attractive feature SynRM offers and is also the reason why commercial interest in these motors has been revived in the last 10-15 years. Efficiency is a highly debated topic today due to reasons such as carbon footprint, electricity price per kWh, and sustainability in general – thus, an emphasis on efficiency is placed as well in the electric motor industry [14], [44].

The efficiency of a SynRM can be approximated – if out of its total losses only Joule losses in the stator winding are considered – by the following formula:

$$\eta \approx \left(1 + \frac{1}{\frac{\Omega_\mathrm{r}}{3\,R_\mathrm{s}} \cdot \frac{T}{I_\mathrm{p}^2}} \right)^{-1}, \tag{5.1}$$

where Ω_r is the mechanical angular velocity of the rotor, R_s is the resistance of a stator phase, T is the electromagnetic torque of the motor and I_p is the RMS value of a stator phase current.
Thus, for maximizing efficiency, it is aimed to maximize the ratio T/I_p^2 [21]. Also, the efficiency of a SynRM is found to be very sensitive to any increase in the width of the air gap between the stator and the rotor due to geometric errors or due to the use of a rotor retaining sleeve [9].

SynRM achieves efficiencies of up to 95 % due to the forementioned almost absent rotor losses [9], which is about 5–8 % higher than the efficiency of an IM, whose efficiency essentially cannot be further increased through its construction, while other ways also not providing significant improvements [22].
Thus, the efficiency classes (which are going to be further discussed in *chapter 7*) that SynRM usually achieve are IE4–IE5, while for IM it is IE1–IE3 (though being true that some manufacturers also offer IM that achieve IE4).

Finally, when comparing their efficiency, it is crucial to distinguish which operating point is being referred to, as the difference in efficiency of these motors is not constant throughout their entire operating ranges – for example, in the partial load range and at the rated operating point, the difference in efficiency of these motors will be considerably different [33], [53].

The comparison of their efficiency curves vs. the torque of the motor for a given operating speed (for a given supply voltage frequency respectively) is **approximately** as follows:

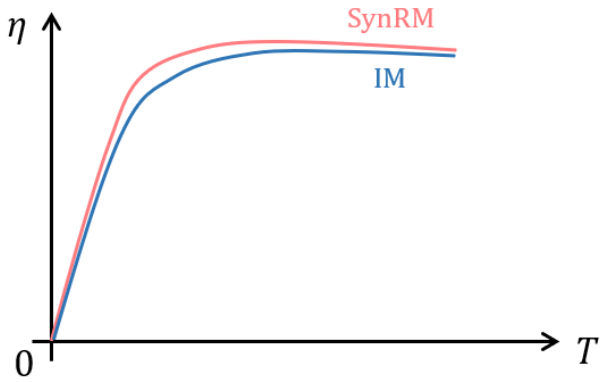

Figure 5.2: An illustration of the approximate theoretical comparison of efficiency curves of SynRM and IM for a given operating speed (frequency respectively) [53].

5.4 Power factor

If the voltage drop due to the resistance of the stator winding and iron losses are neglected and subsequently a more complex deduction using the phasor diagram from *Figure 3.4* is performed, the following formula for the power factor of SynRM is obtained [34]:

$$\cos\varphi = \frac{\xi - 1}{\sqrt{\xi^2 \frac{1}{\sin^2\gamma} + \frac{1}{\cos^2\gamma}}}, \tag{5.2}$$

where φ indeed corresponds to the respective angle from the phasor diagram in *Figure 3.4*. Plotting the *function (5.2)* gives the following graph:

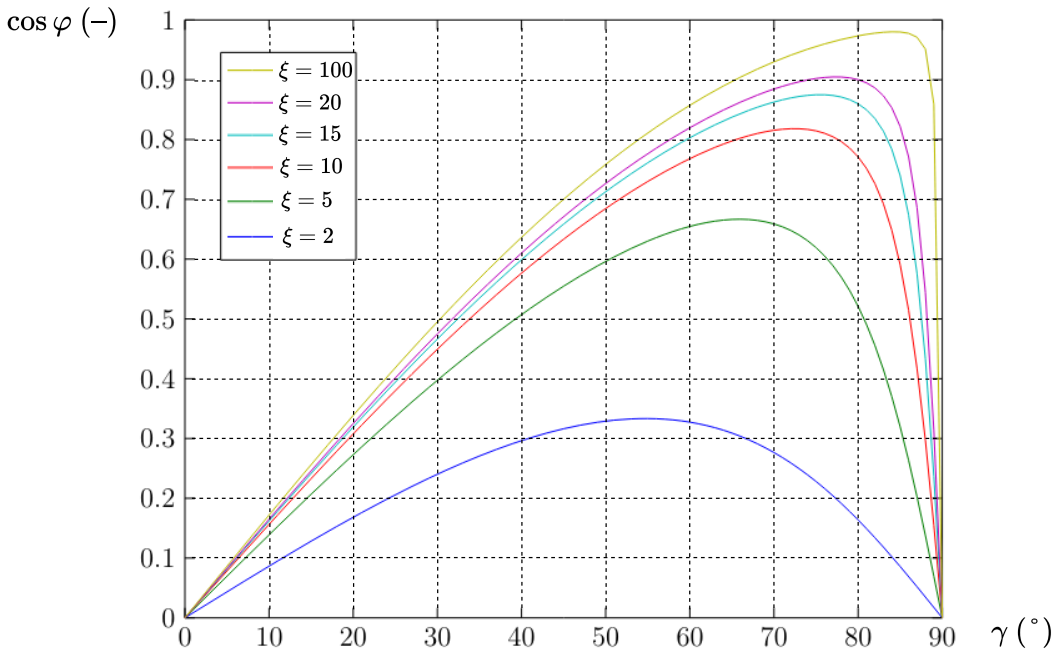

Figure 5.3: The dependence of $\cos\varphi$ on γ for various values of ξ [34] (edited).

The maximum power factor of the given SynRM is then obtained by seeking the maximum of the *function (5.2)* [34]:

$$(\cos\varphi)_{\max} = \frac{\xi - 1}{\xi + 1}, \tag{5.3}$$

while for achieving a power factor of at least 0.9 it is necessary for the ξ of the motor to be at least 20, which can be challenging even for ALA rotors, which generally achieve the best ξ among all SynRM rotors [27].
Therefore, SynRM achieve relatively low power factors, the cause of which is now apparent. The power factor of SynRM is thus generally lower than that of IM.
The power factor of both SynRM and IM, similar to efficiency, also depends on the operating point at which the given motor operates [34].

For electric motors that possess power factor, its lower magnitude generally leads to a lower ratio of the motor torque to the supplied stator current [3] – and since SynRM has a lower power factor than IM, this ratio will thus be lower for SynRM than for IM. In other words, SynRM will require more input power to achieve the same output power as IM [14]. Therefore, SynRM will need a more powerful VFD (one that has a higher volt-ampere (VA) rating – or in other words, higher rated apparent power) [5].
However, if a PMa-SynRM had to achieve the same output power as an IM, the VA rating of its VFD could remain the same as the VA rating of the IM's VFD – or the VA rating of the PMa-SynRM's VFD could even be lower than that of the IM's VFD (it would be up to an individual assesment of the particular case) [20].

Improvement of power factor is generally more beneficial with increasing speed [20].

5.5 Torque ripple

As has already been mentioned many times throughout this thesis, all SynRM suffer from torque ripple, which is a periodic deviation of the instantaneous value of torque over time from the constant value of torque that should act on the synchronously rotating rotor of SynRM in steady state, and to which the instantaneous value of torque should, under the condition of steady state, always be equal [32].
Torque ripple is undesirable because it exerts increased mechanical stress on the motor (concerning the rotor primarily) and increases motor vibrations and thus noise, which are also dependent on the speed and mechanical balancing of the rotor [9]. Therefore, there is an effort to reduce torque ripple as much as possible – however, complete smoothing of the torque waveform can never be achieved [5].
SynRM have higher torque ripple and consequently vibrate more and are therefore noisier than IM [3]. However, in this subchapter, only the torque ripple of SynRM is going to be further addressed.

Torque ripple in SynRM is caused by the so-called **slotting effect** [2], [19]. It states that the reluctance of the magnetic paths between the stator and the rotor in the d and q axes, or the inductances L_d and L_q respectively, are due to the stator slotting[1] dependent on the mechanical position of the rotor relative to the stator [2].

[1] Or, described in greater detail, due to the fact that the magnetic flux path from the stator to the rotor passing through the stator teeth has lower reluctance (higher inductance respectively) than the path passing through the slots.

Therefore, in an ideal scenario, where the stator would be slotless, torque ripple would not occur. In reality, this is not feasible as there would be nowhere to place the stator winding.
However, if the rotor structure (or the rotor barriers) was designed to compensate for the slotting effect, then the torque ripple would be minimal ('only' minimal as there would still be some really small geometric deviations causing some tiny torque ripple) [2]. Additionally, another explanation (which is also more concise) which can be encountered is that torque ripple occurs due to the interaction of higher space harmonics of magnetomotive force (MMF), which are generally caused by stator slotting, with the anisotropy of the rotor. Both formulations of the cause of torque ripple are equivalent [20], [32].

The magnitude of torque ripple of a SynRM is usually given as a percentage according to the following relationship:

$$T_{\text{ripple}} = \frac{T_{\text{max}} - T_{\text{min}}}{T_{\text{avg}}} \cdot 100, \tag{5.4}$$

where T_{max} and T_{min} are the maximum and minimum values of torque within one period of its deviation and T_{avg} is the average value of torque within one period of this deviation [5].
Increasing T_{avg} and generally, decreasing T_{ripple} has a major impact on the rotor iron losses [21] and on significant amount of other properties of the motor, as was being mentioned throughout the previous chapters.

Thus, expanding the list of already known aspects affecting torque ripple of SynRM and expanding the list of already proposed options for its reduction, if a SynRM with no modifications is considered, it is the following rotor design parameters that are regarded as having the biggest positive effect on torque ripple reduction of the motor:

- optimal number of the flux carriers and the flux barriers with respect to the ratio $number\ of\ stator\ slots/p_{\text{p}}$ [12], [32],
- constant ratio $length\ of\ a\ flux\ carrier/width\ of\ a\ flux\ carrier$ for all of the flux carriers [21],
- optimal width of the flux barriers [41],
- optimal shape of the flux barriers,
- wider tangential and radial bridges [12].

The $length\ of\ a\ flux\ carrier$ in the second listed is measured in a 'circumferential manner', while the $width\ of\ a\ flux\ carrier$ is measured in 'from the center of the rotor sheet onwards to its edge' manner, as was already mentioned in previous chapters.
The second listed then ensures a constant reluctance of the flux carriers that minimizes the interaction of the forementioned higher space harmonics of MMF with the anisotropy of the rotor [21].
To conclude, another commonly used method for torque ripple reduction is called **stator winding chording**, referring to the shortening of the coil pitch of the stator winding. This leads to a reduction of the content of low-order higher space harmonics of MMF, resulting in the wanted decrease in torque ripple [5].

Generally nowadays, there are many methods by which torque ripple in SynRM can be reduced, with many of them reducing it substantially. Therefore, torque ripple is far from being as significant drawback of SynRM as it appeared to be 10 years ago [5].

5.6 Dynamics

Dynamics of an electric motor, that is how quickly in reality the motor responds to the instructions given to it by its control (e.g. acceleration or deceleration to a certain speed), are primarily determined by its:

- time constant τ,
- moment of inertia J of its rotor with respect to the axis of rotation.

The time constant is given for both SynRM and IM as:

$$\tau = \frac{L_{\mathrm{q}}}{3\,R_{\mathrm{s}}} \tag{5.5}$$

where R_{s} is the resistance of a stator phase. From this formula, it can be seen that the time constant of both motors depends solely on the magnitude of the torque-producing component of the stator current i_{q}, which is readily available.

Moment of inertia of an electric motor's rotor depends on its weight and on the distribution of its mass around the axis of rotation.
If rotors of a SynRM and an IM, which belong to the identical motor shaft height (SH) (also referred to as frame size (FS)) were compared, the rotor of the SynRM would have a lower moment of inertia because it does not contain winding/squirrel cage and, moreover, cointains flux barriers that are filled with air.

Thus, in general, it can be stated that precisely because of the lower moment of inertia, SynRM have better dynamics than IM [5], [7].

5.7 Weight

Weight of an electric motor obviously depends on the material from which its frame is made of (cast iron or Al). However, if a SynRM and an IM, whose frames are both made of the same material and are the same size are considered, then the SynRM would be lighter. Again, this is due to the absence of winding/squirrel cage in the rotor and the presence of flux barriers [7], [44].

5.8 Evaluation

For additional clarity, the evaluation of the conducted comparison of qualitative parameters of SynRM and IM is now going to be performed in tabular form along with a score assignment, similar to *Table 1.1*:

Qualitative parameter	SynRM	IM
Losses	[5], [14], [15], [48], [52]	[5], [14], [15], [48], [52]
Operating temperature	[5], [9], [48]	[5], [9], [48]
Efficiency	[9], [21], [22], [33], [53]	[22], [33], [53]
Power factor	[5], [14], [27], [34]	[5], [14], [34]
Torque ripple	[3]	[3]
Dynamics	[5], [7]	[5], [7]
Weight	[7], [44]	[7], [44]
KEY		
EXCELLENT		
GOOD		
SATISFACTORY		
BAD		

Table 5.1: A comparison of qualitative parameters of SynRM and IM.

Chapter 6
Applications

In the following two subchapters, the use of SynRM in industry and as a traction motor is going to be discussed.

SynRM are generally manufactured with power ratings ranging from tenths to hundreds of kW, indicating that they are considered for higher power applications as well, although they are primarily used in applications requiring lower tens of kW of power.

Generally, it could be stated that over the past 10-15 years, SynRM have started to be used in most applications where IM are used, with IM still remaining the most used type of electric motor in the world. They remain so despite the reasons why SynRM have begun to be implemented in practice in the first place, which are:

- today's demands for higher overall sustainability,
- today's demands for reduction of CO_2 footprint,
- marketing-promoted reduction of operating costs of the drive system if SynRM is used.

SynRM meet these points accurately due to their higher efficiency compared with IM (further details are going to be presented in *chapter 7*) [5].

6.1 Industries

SynRM are used in many industries (sometimes also referred to as **vertical markets**, or **verticals** in short) around the world, such as:

- chemicals,
- food & beverage,
- oil & gas,
- water & wastewater,
- pulp & paper,
- cement,
- metals,
- commercial buildings[1],
- pharmaceutical,
- battery,
- hydrogen,
- transportation.

[1] Primarily Heating, Ventilation and Air Conditioning (HVAC).

In every industry, there are then specific application examples, which, however, can be (and often are) common to multiple industries. Instances of the most common application examples for SynRM are:

- pumps [34], [53],
- fans,
- compressors,
- conveyors,
- mixers,
- extruders,
- winches [5], [14].

Traction motors fall under the transportation industry – however, the following brief subchapter is going to be dedicated to them separately, because in the field of electric drive systems, traction motors are generally a greatly important topic [20], [36].

6.2 Traction motors

In many research studies, the 'conventional' SynRM is also discussed as a suitable choice for traction motors due to its relatively favorable cost and satisfactory range of operating speeds. However, currently, 'conventional' SynRM are not widely used as traction motors due to slightly lower efficiency, low power factor, and lower torque and power density compared with **Permanent Magnet Synchronous Motor (PMSM)**, which, conversely, is as traction motor used very often.

Another reason is likely the fact that IM and PMSM have been more verified and tested in practice in the field of traction motors, as these motors have been used in this field longer and, moreover, have achieved very good results.

Therefore, although it has been proven that the torque density of 'conventional' SynRM is sufficient for its use as a traction motor, it remains a question whether 'conventional' SynRM will evolve and establish themselves enough in the future to be implemented in this field to a greater extent [5], [20].

However, the situation is different for PMa-SynRM, which have such better power factor, torque and power density and efficiency compared with 'conventional' SynRM that they have attracted many commercial companies and are starting to compete with PMSM, especially in the electric vehicle (EV) sector – for example, the car company Tesla often uses these motors in their vehicles.

There is generally consideration for the use of PMa-SynRM in railway traction as well [5], [36].

Chapter 7
Future of SynRM

The completion to *subchapter 5.3* is now going to be initiated. In the subchapter it has been outlined that electric motors are assigned an efficiency class that belongs to the particular motor according to certain criteria. Efficiency classes of electric motors for the whole world, except for North America, are managed according to the Standard 60034-1 from the International Electrotechnical Commission (IEC). For North America, efficiency classes are managed according to the book MG 1 from the National Electrical Manufacturers Association (NEMA), which has its equivalent names established for the IEC classes:

IEC	NEMA
IE1	Standard Efficiency
IE2	High Efficiency
IE3	Premium Efficiency
IE4	Super Premium Efficiency
IE5	Ultra Premium Efficiency

Table 7.1: The efficiency classes of electric motors according to IEC and NEMA [54],

where IE stands for International Efficiency and each class signifying a 10 % reduction in total losses in the motor compared with the previous class [54].

In the Czech Republic (CR), the legislative regulations concerning the efficiency of electric motors are given by IEC standards, technical standards and regulations of the European Union (EU) – as CR is a part of it, and of course, Czech technical standards (ČSN).

As of May 2024, when this thesis is completed and published, the following legislative regulations issued by the mentioned entities concerning the efficiency of electric motors are in effect within the territory of the CR:

- IEC,
  - IEC 60034-2-1,
  - IEC 60034-2-3,
  - IEC 60034-30-1,
  - IEC 61800-9-2,
- EU,
  - Commission Regulation 2019/1781 [55],
- CR,
  - ČSN EN 60034-1 ED.2,
  - ČSN EN 60034-2-1 ED.2,
  - ČSN EN 60034-30-1,
  - ČSN EN 61800-9-2,
  - ČSN EN IEC 60034-2-3,
  - ČSN CLC IEC/TS 60034-30-2 [56], [57].

Briefly, it is for now sufficient to know, that these regulations together mandate that every electric motor must have an efficiency class stamped on its rating plate for its sale and operation within the territory of the CR (EU respectively) to even be considered.

And because electric motors account for 40-45 % of the total world's electrical energy consumption, and for about 70 % of the total industrial electrical energy consumption [14], [44], [58], their operation leaves a significant carbon footprint behind. Many governments of various countries around the world strive to generally reduce carbon footprint, including the carbon footprint of the electric motor sector [53].
Therefore, on July 1st, 2023, the so-called **Minimum Energy Performance Standard (MEPS)** introduced by the EU came into effect. This standard specifies the minimum required efficiency classes of electric motors according to their area of use, rated output power, number of poles, etc. As a result, most motors used in the EU today are required to have at least IE3 [55].

It is therefore very likely that the EU will aim to further increase its requirements for electric motors' efficiency classes in the upcoming years. This could lead to some IM (e.g. lower rated powers, that is < 30 kW) no longer being able to meet these requirements.
And it is precisely for these reasons that the most significant opportunity that arises for SynRM is the replacement of IM in the future [24], [44], [53].

The replacement could also have a positive financial impact on the owner of the drive system in the long run, as manufacturers of SynRM claim nowadays that energy savings in operating SynRM compared with IM can reach up to 10 % [3], while the market prices of SynRM and IM of the same SH being comparable[1] [14], [53]. Furthermore, the price of a SynRM drive system, as already stated in the preamble of *chapter 4*, can in some applications be reduced by the price of the rotor position/speed sensor and its cabling. Though, if the IM that is being replaced was operated DOL (or if a VFD with higher VA rating is now needed due to the lower power factor of the SynRM), it is necessary to include the purchase of a VFD into the financial calculation of the retrofit [48].

[1] The exact energy savings can be calculated online with the help of online tools from the manufacturers – for example, Siemens offers SinaSave [59].

However, as much as SynRM can seem promising, they also possess many drawbacks [15], the majority of which has already been presented. Therefore, SynRM nowadays appear to be a more advantageous choice only for certain applications. Thus, majority of IM will very likely remain in their place [3] until when the owners of the drive systems are due to the efficiency legislative regulations compelled to replace them.
Hence, if it is claimed somewhere that SynRM have already begun to replace IM in general, it is not true [14], [24], [44].

Finally, from a technological point of view, room for improvement in SynRM can be anticipated especially in the optimization of its rotor and coil pitch of the stator winding [3], while IM cannot be really further optimized in terms of their construction – at most, there is the possibility of further improvement of control strategies, which, however, are already at a relatively high technological level [1], [13], [50].

Chapter 8
SynRM drive system measurements

In this chapter, practical measurements are going to be performed on a SynRM drive system. The workplace with the drive system is going to be described, along with the necessary resources, the measurement procedure, and the acquired and processed data, which are eventually going to be evaluated.

8.1 Workplace description

The workplace is located in the faculty's laboratory T2:H1-26 in Prague 6 – Dejvice. It was constructed using Siemens products by a colleague John Francis Horabin as the topic of his bachelor's thesis from May 2023. A detailed description of the setup, including the connection of communication interfaces and all necessary settings, can be found in his thesis [7], so it is unnecessary to paraphrase it here. In [7], the method of programming the workplace through the so-called **Totally Integrated Automation (TIA) Portal** from Siemens is also described. TIA Portal is a software (SW) and tools package that aims to integrate multiple development tools for automation devices through unification and remodelling of preexisting SW such as SIMATIC STEP 7, SIMATIC Windows Control Center (WinCC), and SINAMICS STARTER, which are responsible for programming, configuring, and commissioning drive systems built using Siemens equipment [60].

Thus, for the purpose of understanding this measurement, it is sufficient to provide only a list of the components used, a photograph of the workplace, and a basic block diagram of the setup.

Starting with the components used – they are listed in the following table:

Number	Component	Siemens article number
1	SITOP Power Supply SU200M	6EP1333-3BA10
2	SINAMICS Control Unit CU320-2 PN	6SL3040-1MA01-0AA0
3	SIMATIC S7-1500T, CPU 1511T-1 PN (PLC and CPU)	6ES7511-1TK01-0AB0
4	SINAMICS S120 Active Line Module	6SL3130-7TE23-6AA3
5	SINAMICS S120 Active Interface Module	6SL3100-0BE23-6AB0
6	SINAMICS S120 Single Motor Module	6SL3120-1TE24-5AC0
7	SINAMICS SMC30 Sensor Module	6SL3055-0AA00-5CA2
8	SINAMICS S120 Basic Operator Panel BOP20	6SL3055-0AA00-4BA0
9	SIMATIC HMI MTP1500 Panel	6AV2128-3QB06-0AX1
10	SINAMICS S120 CompactFlash card	6SL3054-0FB10-1BA0
11	SINAMICS Terminal Board TB30	6SL3055-0AA00-2TA0
12	SINAMICS DRIVE-CLiQ Cable 0.31 m	6SL3060-4AK00-0AA0
13	SINAMICS DRIVE-CLiQ Cable 0.6 m	6SL3060-4AU00-0AA0
14	SINAMICS DRIVE-CLiQ Cable 1.2 m	6SL3060-4AW00-0AA0
15	Signal cable	6FX5002-2CA12-1BF0
16	Power cable	6FX5008-1BB41-1BF0
17	SIMOTICS Synchronous reluctance motor	1FP1014-1DB42-1AK4–Z
18	Sendix HTL 5020 Rotary incremental encoder	–
19	Dynamometer (DM)	–
20	Torque scale	–
21	Personal Computer (PC)	–

Table 8.1: The components of the workplace [7], [61], [62],

where PLC stands for Programmable Logic Controller, CPU stands for Central Processing Unit, and HMI stands for Human-Machine Interface. A dynamometer is a DC machine, which is often used as a variable load for the tested motor. Generally, it can also be equipped with a torque scale, which is used to measure the load torque applied to the tested motor, as was the case in this setup – however, torque scale is considered somewhat old-fashioned nowadays. A more detailed description of the components used can be found in [7].

The workplace looks as follows:

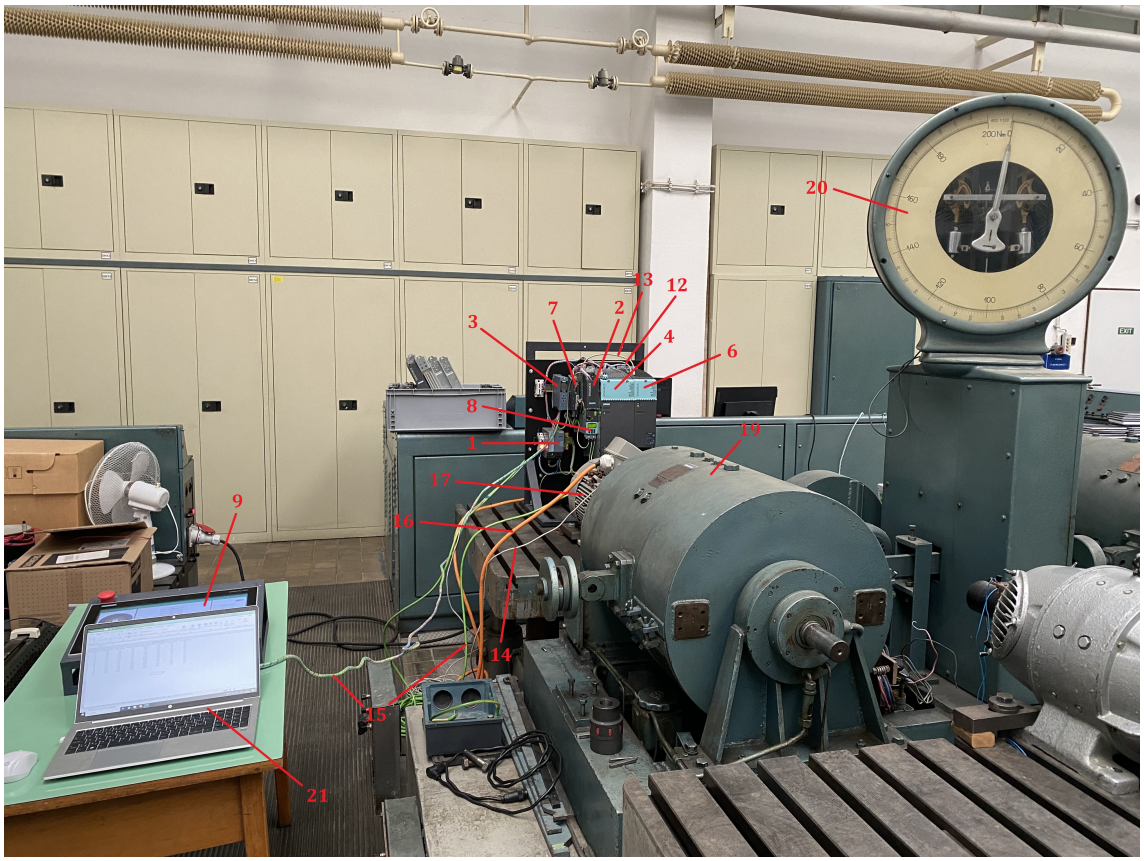

Figure 8.1: The workplace in reality.

Unfortunately, components 5, 10, 11, 18 cannot be seen in the photograph.

A block diagram of the setup is as follows:

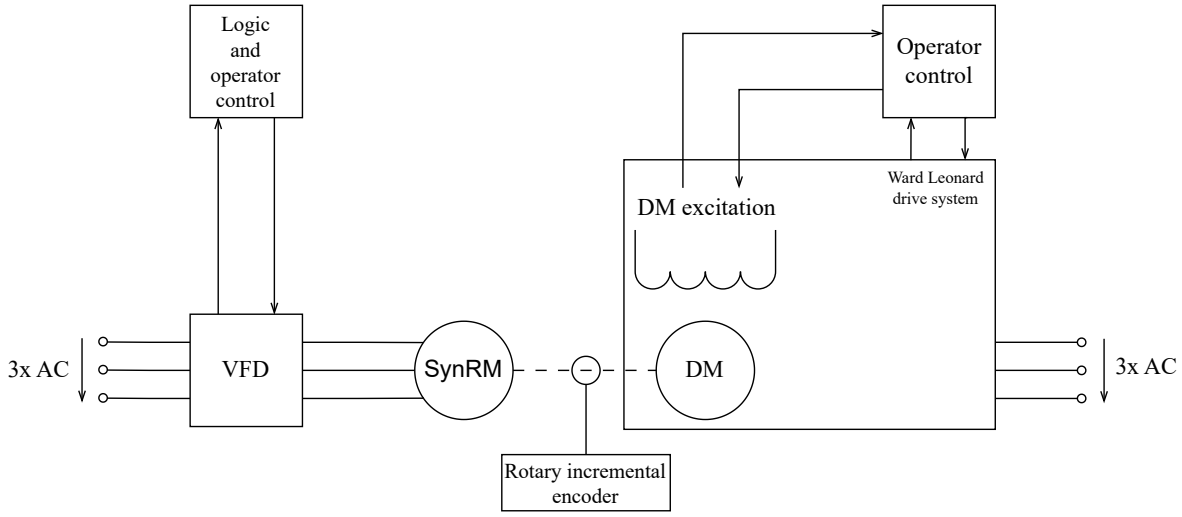

Figure 8.2: A block diagram of the workplace [7].

The touchscreen of the control HMI panel of the workplace looks as follows:

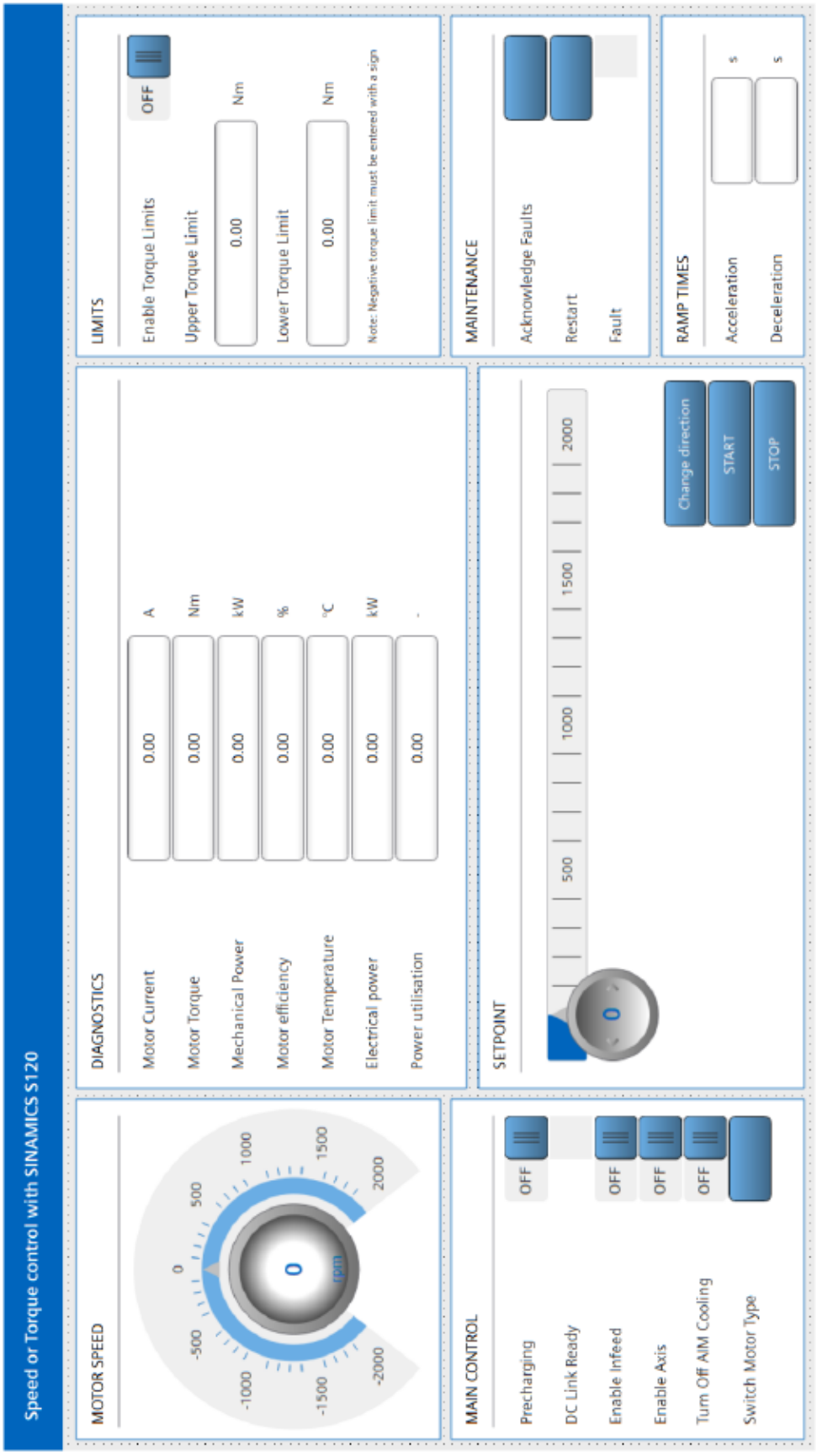

Figure 8.3: The touchscreen of the control HMI panel of the workplace [7],

where AIM stands for Active Interface Module. A more detailed description of what can be controlled and how it can be controlled via this screen is, again, available in [7]. For this measurement, the most important windows were 'SETPOINT' and 'DIAGNOSTICS'. The 'SETPOINT' window was used to accelerate the SynRM to the desired speed, and the 'DIAGNOSTICS' window was used for reading values of almost all of the measured quantities. All the OFF/ON sliding bars, except for 'Turn Off AIM Cooling', were in the right-hand side positions during the measurement (so for most, 'OFF' was visible on the left-hand sides of the sliding bars). Additionally, the 'DC Link Ready' indicator was lit green.

The rating plates of the electrical machines used are shown below:

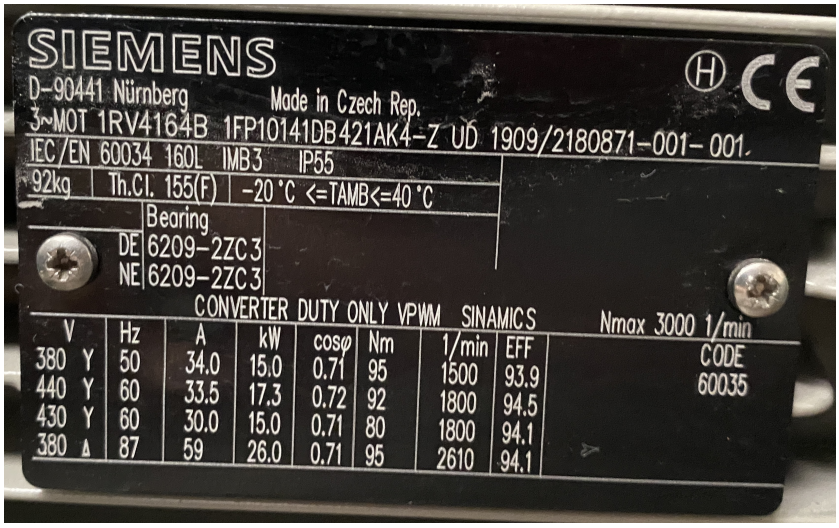

Figure 8.4: The rating plate of the used SynRM.

Figure 8.5: The rating plate of the used DM.

8.2 Procedure

1. The workplace is arranged and prepared for the measurement and its powering is switched on.
2. The speed of the SynRM is set to a given setpoint.
3. The DM is excited.
4. The armature voltage of the Ward Leonard drive system's DC generator (dynamo) is set to equal the armature voltage of the driven DM.
5. The armature circuits of the dynamo and the DM are connected together in parallel.
6. The desired load torque of the DM is set by changing the excitation current of the dynamo.
7. The values of the measured quantities are read.
8. Steps 6–7 are repeated for different values of the load torque.
9. The load torque produced by the DM is set to zero.
10. The armature voltage of the Ward Leonard drive system's dynamo is set to equal the armature voltage of the driven DM.
11. The armature circuits of the dynamo and the DM are disconnected from each other.
12. The DM is unexcited.
13. Steps 2–12 are repeated for different speeds of the SynRM.
14. After obtaining the very last value needed, steps 9–12 are performed, the SynRM is stopped and the powering of the workplace is switched off.

8.3 Acquired and processed data

The following 2 subchapters are going to be dedicated to the acquired and processed data from the measurement performed on May 6, 2024, 10:00 A.M.–12:30 P.M.

8.3.1 Tables

For the sake of orderliness, all data tables are going to be provided as *appendix D* at the very end of the thesis. The following quantities were measured:

- n_{M} (rpm) – speed (also referred to as revolutions) of the SynRM,
- T_{DM} (Nm) – dynamometer torque (load torque of the SynRM),
- I_{M} (A) – motor current (line current of the SynRM – per one line),
- T_{M} (Nm) – motor torque,
- P_{M} (kW) – mechanical output power on the shaft,
- η_{M} (%) – motor efficiency,
- $TEMP_{\mathrm{M}}$ (°C) – motor temperature,
- $P_{\mathrm{P,M}}$ (kW) – electrical input power (active input power),
- PUT_{M} (–) – motor power utilization.

Measured quantities that possess the subscript 'M' were provided by the SINAMICS S120 drive and were read from the HMI panel's display. What leads to the quantities being displayed on the HMI panel is described in [7] – it, besides other, involves the use of so-called **telegrams**, which is a data format used by the SINAMICS S120 drive, in which various data of the drive system are communicated between its components [7].

However, some values displayed on the HMI panel seem not to correspond to reality. Therefore, out of all the read values of the measured quantities, it is only the values of these quantities that can be considered as **corresponding to reality**:

- n_{M} (rpm) – obtained directly from the encoder,
- T_{DM} (Nm) – provided by the mechanical torque scale, which has been reliably functioning in the laboratory for decades,
- I_{M} (A) – the method by which S120 measures this current is quite accurate,
- $TEMP_{\mathrm{M}}$ (°C) – measured directly by the temperature sensor,
- $P_{\mathrm{P,M}}$ (kW) – only the product of multiplication between square root of 3, I_{M}, stator line voltage measured by S120 also quite accurately and power factor, also accurately determined by S120 [7].

This inconsistency with reality or sometimes outright nonsense can be clearly seen in the tables in *appendix D*, for example, in some values of η_{M}, which sometimes reached 100 % or more, which is obviously not possible. A commentary on the possible reason for incorrect values of η_{M} is going to be provided in *subchapter 8.4.2*
Therefore, attention will be paid only to the values of quantities that have been just listed as corresponding to reality. Values of the quantity PUT_{M}, which is also displayed by the HMI but not corresponding to reality, is not going to be evaluated at all – this quantity is included here only for the completeness of the measurement. More about its meaning can be found in [7].

Thus, generally, in order to make any meaningful evaluation of the data possible, it is necessary to calculate the reality-corresponding (or **real** in short) values of some of the 'suspected' quantities. However, in this thesis, only the real values of motor efficiency are going to be determined. The formula is as follows:

$$\eta_{\mathrm{M,real}} = \frac{T_{\mathrm{DM}} \cdot \frac{\pi\, n_{\mathrm{M}}}{30}}{P_{\mathrm{P,M}}} \cdot 100, \tag{8.1}$$

where the numerator represents the real mechanical output power on the shaft (**attention:** do not confuse this with real (active) electrical power that is a part of apparent electrical power, because the word 'real' is used in a different meaning in this part of the thesis).

The motor and dynamometer torque difference given as:

$$T_{\mathrm{diff}} = T_{\mathrm{M}} - T_{\mathrm{DM}} \tag{8.2}$$

is also going to be listed in the tables, as it is among the outputs of this measurement which are intended to be evaluated.

8.3.2 Heatmaps

The quantities primarily discussed so far and the ones that are according to the thesis assignment aimed to be evaluated are:

- $\eta_{\mathrm{M,real}}$,
- T_{diff},
- I_{M}.

From the data in the tables in *appendix D*, heatmaps of these quantities are now going to be constructed:

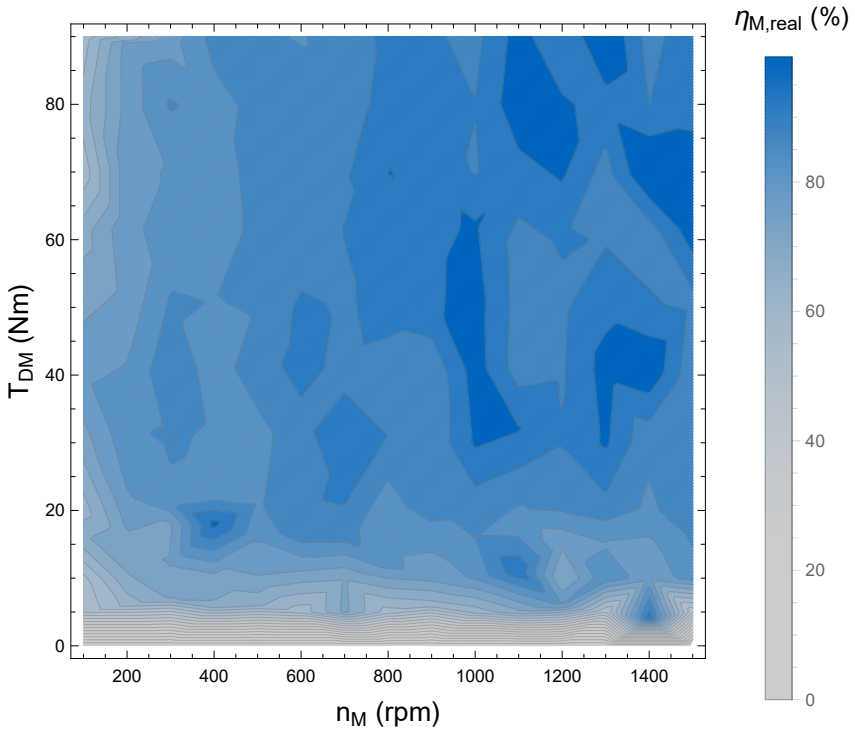

Figure 8.6: The efficiency map of the SynRM drive system,

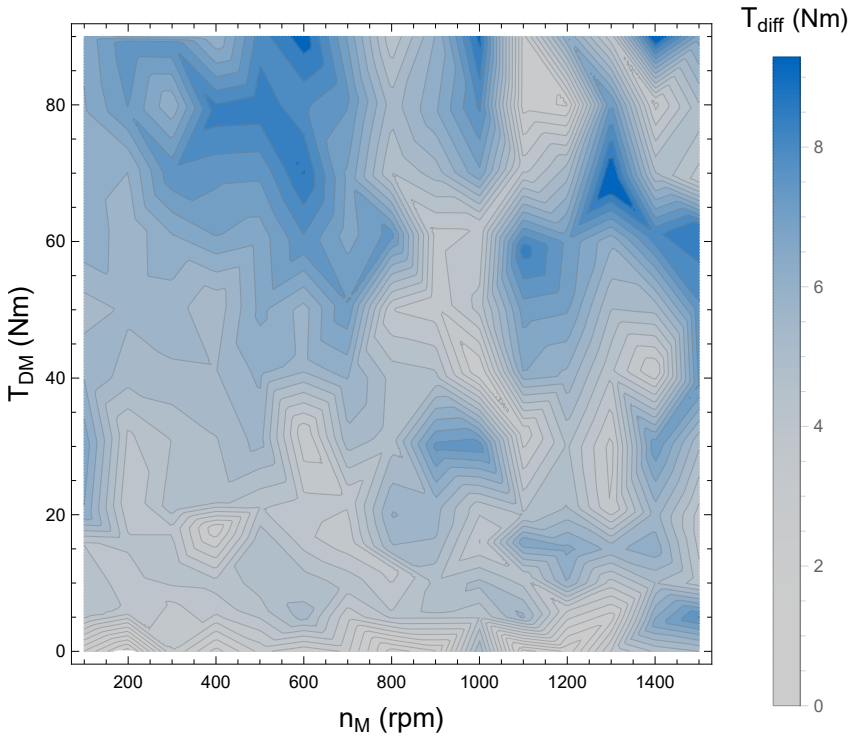

Figure 8.7: A heatmap of the motor and dynamometer torque difference,

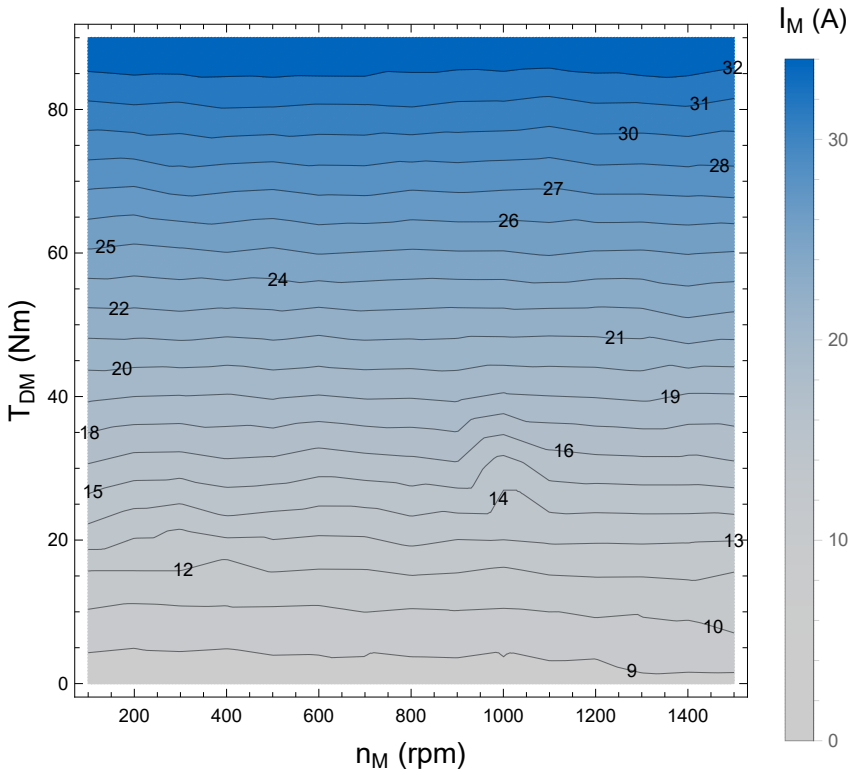

Figure 8.8: A heatmap of the motor current.

The heatmaps have been constructed in the software Wolfram Mathematica using the function ListContourPlot.

8.4 Discussion

In the following 5 subchapters, a constructive discussion of the main outputs of the measurement is going to be conducted.

8.4.1 Efficiency

For the reasons stated in *subchapter 8.3.1*, only the efficiency $\eta_{\mathrm{M,real}}$ is going to be assessed. As can be seen from the efficiency map in *Figure 8.6*, the claim from *subchapter 5.3* that SynRM achieves high efficiency of up to 95 % has indeed been confirmed. The highest efficiency was determined to be 99.35 % at values of $n_{\mathrm{M}} = 1400$ rpm and $T_{\mathrm{DM}} = 70$ Nm. However, this value is, of course, very likely somewhat exaggerated, which is probably due to the significant error factor of inaccurate reading of values in some operating points, accompanying the entire measurement.

Furthermore, *Figure 8.6* shows that at rated speed (which is 1500 rpm in this measurement), there is a relatively wide range ($T_{\mathrm{DM}} = 60 \div 75$ Nm) where the motor reaches its maximum efficiency values, i.e. above 90 %, which is truly very favorable.

Unfortunately, there is no IM with the same or very similar rated power available in the laboratory with which the efficiency of this SynRM could be relevantly and reasonably compared.

8.4.2 Motor and dynamometer torque difference

From the heatmap in *Figure 8.7*, it can be seen that the motor and dynamometer torque difference T_{diff} always ranges approximately between 2–6 Nm – there are only 3 very small areas where T_{diff} is higher (approximately 9 Nm). However, considering that T_{diff} is more or less constant and evenly distributed in the rest of the heatmap, and that these extreme areas are very small, their existence can again be attributed to inaccurate readings at the operating points where these extremes occurred.

Since values of T_{DM} can be considered as corresponding to reality for the reason mentioned in *subchapter 8.3.1*, values of T_{M} are then offset from reality by the already mentioned difference T_{diff}. In this measurement setup, unlike in [7], no torque sensor was present (as seen in *Figure 8.2*) – therefore, T_{M} displayed on the HMI panel was calculated by the S120 drive itself.
In the search for the origin of T_{diff}, various sources were thoroughly sought through and many manuals of the SINAMICS S120 drive were consulted to determine the complete origin of T_{M}, which apparently causes T_{diff}. The most 'promising' manuals, where these information could be listed, seemed to be SINAMICS S120/S150 – List Manual ed. 2023-11 [63] and SINAMICS S120 – Function Manual ed. 2020-06 [64]. However, even these did not contain any information clearly stating the complete origin of T_{M} – in [63], only diagrams were found that deduced the torque from other quantities, whose complete origin is again unknown.
In these diagrams and generally in both manuals, these quantities appeared through the so-called **parameters**, which already contained the 'ready-made' information about the values of the given quantities. For example, the information about the instantaneous value of the motor torque is encoded in the manuals as parameter 'r0080 – Torque actual value', or alternatively as a deduced parameter 'r0031 – Actual torque smoothed'. Then, generally, these and many other parameters are processed by the drive in some way (e.g. in motor speed control), as can be seen from various function diagrams in [63].
As a last resort, Siemens technical support was contacted, who also did not exactly know but suggested that the S120 most likely calculates it using a mathematical model of the controlled motor, which is though further a subject to the internal know-how of the Siemens company.

Therefore, it can be stated that assuming there is no torque sensor in the setup to provide data about the motor torque in some form, T_{M} is very likely obtained in the manner described by Siemens technical support. Generally, more detailed information on such matters is typically not accessible because it is a part of Siemens' internal know-how, and thus it is then not possible to assess whether T_{M} could be determined in a better, more accurate way and so on. The exact cause of T_{diff} is therefore going to remain unknown.

T_{diff} likely also subsequently causes the motor efficiency η_{M} determined by the drive not to correspond to reality and sometimes even to be outright nonsensical. The proof for this claim lies in *equation (8.1)*, according to which the drive calculates the motor efficiency – though, obviously, the drive considers P_{M} as the numerator [7]. Since it has been proven in the past that the values of electrical input power $P_{\text{P,M}}$ are provided reliably by the drive, examining how P_{M} is obtained is the only way to go from here.

According to [7], the drive calculates P_M as follows:

$$P_M = \frac{\pi n_M}{30} \cdot T_M. \tag{8.3}$$

As has already been stated in *subchapter 8.3.1*, the values of n_M can also be considered reliable. Therefore, the discrepancy of efficiency η_M from reality can only be attributed to incorrect T_M values, or to the existence of T_{diff} respectively.

8.4.3 Operating temperature

During operation, the SynRM remained relatively cool to the touch throughout the entire measurement, which lasted just under 3 hours, confirming the claim from *subchapter 5.2* regarding the relatively low operating temperatures of SynRM across their entire operating ranges.

8.4.4 Motor current

It seems that, in general, current measurements by the converter correspond to reality, which was further verified before the actual measurement by an oscilloscope with a current probe. However, this took place only one time before the measurement itself – just for verification. Thus, before the measurement begun, the oscilloscope with the current probe had been removed, so the current values were determined solely by the S120 drive throughout the entire measurement.

The fact that I_M in the heatmap in *Figure 8.8* exhibits a 'tooth' approximately at $n_M = 1000$ rpm and $T_M = 25 \div 38$ Nm is most likely again due to inaccurate readings at these operating points, as there are no other significant anomalies in the rest of the map.

8.4.5 Options available for the implementation of closed-loop torque control into the drive system

Implementing closed-loop torque control of the SynRM using the SINAMICS S120 drive into the drive system at the workplace enables fulfilling the overall purpose of the workplace, that is the SynRM serving as a variable load for the given tested motor – or conversely, as a motor whose output torque could be set to a setpoint to rotate the tested load at this torque [7].

However, due to time reasons, in Horabin's thesis [7], this was not implemented entirely – thus, options available for the implementation are now going to be analyzed.

8.4.5.1 Motor current is used for the control

The first recommended option regarding the implementation is that for the reasons mentioned in *subchapter 8.4.2* and *8.4.4*, motor current I_M, which closely relates to the motor torque T_M could be used for the control rather than directly controlling T_M itself. Moreover, according to the map in *Figure 8.8* it is possible to say that for each current value there is exactly one torque value (due to the lines in the mentioned map being nearly horizontally straight), which is very favorable regarding the just described recommended control principle.

8.4.5.2 Resolving the issue with incorrect motor torque values

The second recommended option is to use directly T_{M} for the control, though only after resolving the issue with its incorrect values – e.g. through some form of calibration. This option may seem more labor-intensive than the first one – however – as the aforementioned problem with T_{M} will be eliminated at the same time, another subsequent issues such as erroneous reporting of values of important operating quantities of the SynRM will be eliminated as well – thus more is achieved in one go.

Conclusion

In the first 7 chapters, SynRM has been theoretically analyzed from various perspectives, continuously highlighting its differences compared with IM, which is currently the most used type of electric motor.
A discussion regarding their potential replacement with SynRM also took place, although I personally do not think this will happen anytime soon (within the next 10-15 years) – or at least not to a significant extent. Moreover, it is not entirely certain that SynRM would be the alternative the owners of the drive systems would go for if IM started being replaced by another type of motor. However, there will definitely be ongoing pressure to improve efficiency, reduce carbon footprint, lower operating costs and enhance overall sustainability of electric motors.
Thus, in general, the first 7 chapters aimed to provide the reader with an overview of the technical fundamentals of SynRM while outlining the place of these motors in today's world. These chapters should therefore further serve as an educational material, offering a unified basic overview regarding the topic of SynRM at one place for anyone interested in learning about these motors in a straightforward, accessible, yet relevant and information-rich way.

In the second part of the thesis, high efficiency and relatively low operating temperature of SynRM have been proven through a measurement on a real SynRM drive system.
Through the measurement, some primarily SW-related deficiencies of the faculty's workplace with the SynRM drive system were also pointed out and two different options that could lead to their elimination were proposed. The actual realization of these or entirely different proposals could be the topic for my master's thesis, or generally, a separate bachelor's or master's thesis of someone else.

Finally, I thoroughly enjoyed working on this bachelor's thesis. I gained a lot of new information, learned new skills and I plan to continue pursuing this topic and engaging in it in the future – though the form of this engagement is yet to be discovered.

References

[1] KOBRLE, Pavel a PAVELKA, Jiří. *Elektrické pohony a jejich řízení*. 3. přepracované vydání. Praha, nakladatelství ČVUT, 2016. ISBN 978-80-01-06007-0.

[2] MOGHADDAM, Reza Rajabi. *Synchronous Reluctance Machine (SynRM) Design*, Master's thesis [online]. Stockholm, Royal Institute of Technology, Department of Electrical Engineering, 2007 [cit. 2024-03-01]. Available at: `https://www.diva-portal.org/smash/get/diva2:753114/FULLTEXT01.pdf`

[3] HRIŇA, Róbert. *Řízení synchronního reluktančního motoru*, Diplomová práca [online]. České vysoké učení technické v Praze, Fakulta elektrotechnická, 2020 [cit. 2024-03-01]. Available at: `https://dspace.cvut.cz/handle/10467/87741`

[4] KOSTKO, J. K. Polyphase reaction synchronous motors [online]. In: *Journal of the American Institute of Electrical Engineers*. 1923. vol. 42, no. 2, p. 1162–1168 [cit. 2024-03-04]. Available at: `https://doi.org/10.1109/JoAIEE.1923.6591529`

[5] RYPAN, Jakub. *Reluktanční synchronní motor*, Bakalářská práce [online]. České vysoké učení technické v Praze, Fakulta elektrotechnická, 2021 [cit. 2024-03-04]. Available at: `https://dspace.cvut.cz/handle/10467/96679`

[6] WIKIPEDIA. Induction motor [online]. In: *Wikipedia: the free encyclopedia*. San Francisco (CA), Wikimedia Foundation, 2003, last edited in 2024 [cit. 2024-03-10]. Available at: `https://en.wikipedia.org/wiki/Induction_motor`

[7] HORABIN, John Francis. *Workplace with SynRM Drive Fed by S120*, Bachelor's thesis [online]. České vysoké učení technické v Praze, Fakulta elektrotechnická, 2023 [cit. 2024-03-10]. Available at: `https://dspace.cvut.cz/handle/10467/108707`

[8] JURCA, Florin-Nicolae and RUBA Mircea. Performance Analysis of an Integrated Starter-Alternator- Booster for Hybrid Electric Vehicles [online]. In: *Hybrid Electric Vehicles*. InTech, 2017 [cit. 2024-03-11]. ISBN 978-953-51-3297-4. Available at: `https://doi.org/10.5772/intechopen.68861`

[9] HAUSMANN, Ludwig et al. Review and Enhancements of Rotor Designs for High Speed Synchronous Reluctance Machines [online]. In: *2020 10th International Electric Drives Production Conference (EDPC)*. IEEE, 2020. p. 1–8 [cit. 2024-03-11]. ISBN 978-1-7281-8458-6. Available at: `https://doi.org/10.1109/EDPC51184.2020.9388205`

[10] CREDO, Andrea, FABRI, Giuseppe, VILLANI, Marco and POPESCU, Mircea. High Speed Synchronous Reluctance Motors for Electric Vehicles [online]. In: *2019 IEEE International Electric Machines & Drives Conference (IEMDC)*. IEEE, 2019. p. 165–171 [cit. 2024-03-12]. ISBN 978-1-5386-9350-6. Available at: `https://doi.org/10.1109/IEMDC.2019.8785083`

[11] OZDIL, Ali and UZUN, Yunus. Design and Analysis of a Rotor for a 22 kW Transversally Laminated Anisotropic Synchronous Reluctance Motor [online]. In: *Elektronika ir Elektrotechnika*. 2021. vol. 27, no. 6, p. 17–24 [cit. 2024-03-13]. ISSN 2029-5731. Available at: https://doi.org/10.5755/j02.eie.29046

[12] ORLOVA, Svetlana, PUGACHOV, Vladislav, RASSNLKIN, Anton, KALLASTE, Ants and VAIMANN, Toomas. Design of Rotors for Synchronous Reluctance Motor [online]. In: *2019 21st European Conference on Power Electronics and Applications (EPE '19 ECCE Europe)*. IEEE, 2019. p. 1–10 [cit. 2024-03-13]. ISBN 978-9-0758-1531-3. Available at: https://doi.org/10.23919/EPE.2019.8914760

[13] VOŽENÍLEK, Petr, NOVOTNÝ, Vladimír a MINDL, Pavel. *Elektromechanické měniče*. 2. vyd. Praha, nakladatelství ČVUT, 2011. ISBN 978-80-01-04875-7.

[14] OZCELIK, Nezih Gokhan, DOGRU, Ugur Emre, IMERYUZ, Murat and ERGENE, Lale T. Synchronous Reluctance Motor vs. Induction Motor at Low-Power Industrial Applications: Design and Comparison [online]. In: *Energies*. 2019. vol. 12, no. 11 [cit. 2024-03-15]. ISSN 1996-1073. Available at: https://doi.org/10.3390/en12112190

[15] BOLDEA, I. *Reluctance synchronous machines and drives*. Monographs in electrical and electronic engineering. Clarendon Press, 1996. ISBN 9780198593911.

[16] B2BMAP. Top Quality DC Traction Motor Parts Stator and Rotor Laminated Steel Sheet [online]. In: *B2BMAP*. [cit. 2024-03-17]. Available at: https://b2bmap.com/products/top-quality-dc-traction-motor-parts-stator-and-rotor-laminated-steel-sheet

[17] ALIBABA.COM. Lamination Silicon steel sheet stator [online]. In: *Alibaba.com*. © 1999–2024 [cit. 2024-03-23]. Available at: https://www.alibaba.com/product-detail/lamination-Silicon-steel-sheet-stator_62557874741.html

[18] BODINE ELECTRIC COMPANY. AC Induction Motors with Squirrel Cage Rotors – Bodine – Gearmotor Blog [online]. In: *Bodine Electric Company – Gearmotors – AC & DC Electric Gear Motors*. 2016 [cit. 2024-03-23]. Available at: https://www.bodine-electric.com/blog/ac-induction-gearmotors/

[19] HRABOVCOVÁ, Valéria, JANOUŠEK, Ladislav, RAFAJDUS, Pavol a LIČKO, Miroslav. *Moderné elektrické stroje*. Žilina, EDIS – vydavateľstvo ŽU, 2001. ISBN 80-7100-809-5.

[20] BAN, Branko, STIPETIC, Stjepan and KLANAC, Mario. Synchronous Reluctance Machines: Theory, Design and the Potential Use in Traction Applications [online]. In: *2019 International Conference on Electrical Drives & Power Electronics (EDPE)*. IEEE, 2019. p. 177–188 [cit. 2024-03-26]. ISBN 978-1-7281-0389-1. Available at: https://doi.org/10.1109/EDPE.2019.8883905

[21] BARTA, Jan and ONDRUSEK, Cestmir. ROTOR DESIGN AND OPTIMIZATION OF SYNCHRONOUS RELUCTANCE MACHINE [online]. In: *MM Science Journal*. 2015. vol. 1, no. 1, p. 555–559 [cit. 2024-03-28]. Available at: https://doi.org/10.17973/MMSJ.2015_03_201504

[22] TAHI, Slimane, IBTIOUEN, Rachid and BOUNEKHLA, Mhamed. DESIGN OPTIMIZATION OF TWO SYNCHRONOUS RELUCTANCE MACHINE STRUCTURES WITH MAXIMIZED TORQUE AND POWER FACTOR [online]. In: *Progress In Electromagnetics Research B*. 2011. vol. 35, p. 369–387 [cit. 2024-03-31]. Available at: https://doi.org/10.2528/PIERB11091101

[23] LAWRENSON, P. J. and AGU, L. A. A new unexcited synchronous machine [online]. In: *Proceedings of the Institution of Electrical Engineers*. 1963. vol. 110, no. 7 [cit. 2024-04-01]. Available at: https://doi.org/10.1049/piee.1963.0179

[24] DONAGHY-SPARGO, Christopher. Synchronous reluctance motor technology: industrial opportunities, challenges and future direction [online]. In: *Engineering & Technology Reference*. [cit. 2024-04-03]. Available at: https://doi.org/10.1049/etr.2015.0044

[25] WALLMARK, O., KHAN, K. and LEKSELL, M. Design aspects on magnet placement in permanent-magnet assisted synchronous reluctance machines [online]. In: *5th IET International Conference on Power Electronics, Machines and Drives (PEMD 2010)*. Institution of Engineering and Technology, 2010. p. 313–313 [cit. 2024-04-03]. ISBN 9781849192316. Available at: https://doi.org/10.1049/cp.2010.0203

[26] SALEHINIA, Seyed Reza, AFJEI, Ebrahim and HEKMATI, Arsalan. Analytical Method to Optimum design of Synchronous Reluctance Motor for Electric Scooter Application [online]. In: *Scientia Iranica*. 2021. [cit. 2024-04-04]. Available at: https://doi.org/10.24200/sci.2021.56496.4748

[27] VAGATI, A., CANOVA, A., CHIAMPI, M., PASTORELLI, M. and REPETTO, M. Design refinement of synchronous reluctance motors through finite-element analysis [online]. In: *IEEE Transactions on Industry Applications*. IEEE, 2000. vol. 36, no. 4, p. 1094–1102 [cit. 2024-04-05]. Available at: https://doi.org/10.1109/28.855965

[28] ELECTRICAL ENGINEERING MATERIALS. SynRM-Synchronous Reluctance Motor [online]. In: *Electrical Engineering Materials*. 2022 [cit. 2024-04-05]. Available at: https://electengmaterials.com/synrm-synchronous-reluctance-motor/

[29] KOLEHMAINEN, Jere. Synchronous Reluctance Motor With Form Blocked Rotor [online]. In: *IEEE Transactions on Energy Conversion*. IEEE, 2010. vol. 25, no. 2, p. 450–456 [cit. 2024-04-08]. Available at: https://doi.org/10.1109/TEC.2009.2038579

[30] BAO, Yuli, DEGANO, Michele, WANG, Shuo, CHUAN, Liu, ZHANG, He, XU, Zhuang and GERADA, Chris. A Novel Concept of Ribless Synchronous Reluctance Motor for Enhanced Torque Capability [online]. In: *IEEE Transactions on Industrial Electronics*. IEEE, 2020. vol. 67, no. 4, p. 2553–2563 [cit. 2024-04-10]. Available at: https://doi.org/10.1109/TIE.2019.2914616

[31] KOLEHMAINEN, Jere. *Dovetail rotor poles in synchronous permanent magnet and reluctance machines*, Doctoral dissertation [online]. Helsinki, Aalto University, School of Electrical Engineering, Department of Electrical Engineering, 2011 [cit. 2024-04-11]. Available at: http://lib.tkk.fi/Diss/2011/isbn9789526041957/isbn9789526041957.pdf

[32] BIANCHI, Nicola, BOLOGNANI, Silverio, BON, Diego and DAI PRE, Michele. Rotor Flux-Barrier Design for Torque Ripple Reduction in Synchronous Reluctance and PM-Assisted Synchronous Reluctance Motors [online]. In: *IEEE Transactions on Industry Applications*. IEEE, 2009, vol. 45, no. 3, p. 921–928 [cit. 2024-04-12]. Available at: https://doi.org/10.1109/TIA.2009.2018960

[33] GUNDOGDU, Tayfun and KOMURGOZ, Guven. The impact of the selection of permanent magnets on the design of permanent magnet machines – a case study: Permanent magnet synchronous machine design with high efficiency [online]. In: *PRZEGLĄD ELEKTROTECHNICZNY*. 2013. vol. 89, no. 3, p. 103–108 [cit. 2024-04-13]. Available at: https://www.researchgate.net/publication/286402395

[34] BRIGGNER, Viktor. *Design and comparison of PMaSynRM versus PMSM for pumping applications*, Master's thesis [online]. Stockholm, KTH Royal Institute of Technology, School of Electrical Engineering and Computer Science, 2018 [cit. 2024-04-13]. Available at: https://www.diva-portal.org/smash/get/diva2:1249540/FULLTEXT01.pdf

[35] HUYNH, Thanh Anh, HSIEH, Min-Fu, SHIH, Kai-Jung and KUO, Hsiu-Fu. An Investigation Into the Effect of PM Arrangements on PMa-SynRM Performance [online]. In: *IEEE Transactions on Industry Applications*. IEEE, 2018. vol. 54, no. 6, p. 5856–5868 [cit. 2024-04-14]. Available at: https://doi.org/10.1109/TIA.2018.2853042

[36] MOHAMMADI, Mohammad Hossain. *Rotor Design Optimization of Permanent Magnet–Assisted Synchronous Reluctance Machines for Traction Applications*, Master's thesis [online]. Montreal (Québec), McGill University, Faculty of Engineering, Department of Electrical and Computer Engineering, 2015 [cit. 2024-04-15]. Available at: https://escholarship.mcgill.ca/concern/theses/mg74qq03n

[37] FAN, Zheming, LIU, Guangwei, JIN, Shi, SONG, Zhihuan and WANG, Jianqiao. Comparative study on torque characteristics of permanent magnet synchronous reluctance motors with different axial hybrid rotors [online]. In: *Energy Reports*. 2022. vol. 8, p. 1349–1359 [cit. 2024-04-15]. Available at: https://doi.org/10.1016/j.egyr.2022.03.023

[38] TAP, Alper, XHELADINI, Liridon, ASAN, Tasdemir, IMERYUZ, Murat, YILMAZ, Murat and ERGENE, Lale T. Effects of the rotor design parameters on the torque production of a PMaSynRM for washing machine applications [online]. In: *2017 International Conference on Optimization of Electrical and Electronic Equipment (OPTIM) & 2017 Intl Aegean Conference on Electrical Machines and Power Electronics (ACEMP)*. IEEE, 2017. p. 370–375 [cit. 2024-04-16]. ISBN 978-1-5090-4489-4. Available at: https://doi.org/10.1109/OPTIM.2017.7974998

[39] TRADEINDIA. Crc Industrial Skewed Stator [online]. In: *TradeIndia*. © 1999–2024 [cit. 2024-04-17]. Available at: https://www.tradeindia.com/products/industrial-skewed-stator-c7799455.html

[40] ZHANG, Gan, TAO, Jinxin, LI, Yifan, HUA, Wei, XU, Xiaohan and CHEN, Zhihong. Magnetic Equivalent Circuit and Optimization Method of a Synchronous Reluctance Motor with Concentrated Windings [online]. In: *Energies*. 2022. vol. 15, no. 5 [cit. 2024-04-17]. Available at: https://doi.org/10.3390/en15051735

[41] MUTEBA, M., TWALA, B. and NICOLAE, D. V. Torque ripple minimization in synchronous reluctance motor using a sinusoidal rotor lamination shape [online]. In: *2016 XXII International Conference on Electrical Machines (ICEM)*. IEEE, 2016. p. 606–611 [cit. 2024-04-17]. ISBN 978-1-5090-2538-1. Available at: https://doi.org/10.1109/ICELMACH.2016.7732588

[42] DOORSAMY, W., MUTEBA, M., TWALA, B. and NICOLAE, D. V. Investigation into effects of a novel rotor cut-off design for synchronous reluctance machines [online]. In: *2017 IEEE 26th International Symposium on Industrial Electronics (ISIE)*. IEEE, 2017, p. 315–320 [cit. 2024-04-18]. ISBN 978-1-5090-1412-5. Available at: https://doi.org/10.1109/ISIE.2017.8001266

[43] YAMMINE, M. Samer. *Contribution to the Synchronous Reluctance Machine Performance Improvement by Design Optimization and Current Harmonics Injection*, Doctoral dissertation [online]. Toulouse, Université de Toulouse, 2015 [cit. 2024-04-19]. Available at: https://oatao.univ-toulouse.fr/14555/1/yammine.pdf

[44] KARKKAINEN, Hannu et al. Technology comparison of induction motor and synchronous reluctance motor [online]. In: *IECON 2017 - 43rd Annual Conference of the IEEE Industrial Electronics Society*. IEEE, 2017. p. 2207–2212 [cit. 2024-04-20]. ISBN 978-1-5386-1127-2. Available at: https://doi.org/10.1109/IECON.2017.8216371

[45] MATHWORKS. Synchronous Reluctance Machine [online]. In: *MathWorks*. 2017, last edited in 2024 [cit. 2024-04-21]. Available at: https://www.mathworks.com/help/sps/ref/synchronousreluctancemachine.html

[46] GRUNDEN, Joanne B. *Simulation and comparison of a permanent magnet DC brushless motor, induction motor, and variable reluctance motor*, Master's thesis [online]. Cambridge (MA), Massachusetts Institute of Technology, Department of Electrical Engineering and Computer Science, 1992 [cit. 2024-04-22]. Available at: https://dspace.mit.edu/handle/1721.1/152604

[47] FINIO, Benjamin. *Roll, Pitch and Yaw Torque Control for a Robotic Bee*, Doctoral dissertation [online]. Cambridge (MA), Harvard University, 2012 [cit. 2024-04-25]. Available at: https://dash.harvard.edu/handle/1/9920663

[48] MOGHADDAM, Reza Rajabi, LENDENMANN, Heinz, TAMMI, Ari and THAND, Lars-Erik. Motoring ahead: Synchronous motors controlled by variable-speed drives are bringing higher efficiencies to industrial applications [online]. In: *ABB review*. 2011. vol. 11, no. 1, p. 56–61 [cit. 2024-04-27]. Available at: https://library.e.abb.com/public/58b63ea623dddaf9c125786800278df5/56-61%201m103_ENG_72dpi.pdf

[49] JERIE, Michal. *Modely synchronních reluktančních motorů*, Bakalářská práce [online]. České vysoké učení technické v Praze, Fakulta elektrotechnická, 2023 [cit. 2024-04-30]. Available at: https://dspace.cvut.cz/handle/10467/108852

[50] CHEN, Shih-Gang, LIN, Faa-Jeng, LIANG, Chia-Hui and LIAO, Chen-Hao. Development of FW and MTPV Control for SynRM via Feedforward Voltage Angle Control [online]. In: *IEEE/ASME Transactions on Mechatronics*. IEEE, 2021. vol. 26, no. 6, p. 3254–3264 [cit. 2024-05-01]. Available at: https://doi.org/10.1109/TMECH.2021.3056745

[51] ELDEEB, Hisham, HACKL, Christoph M., HORLBECK, Lorenz and KULLICK, Julian. A unified theory for optimal feedforward torque control of anisotropic synchronous machines [online]. In: *International Journal of Control*. 2017. vol. 91, no. 10, p. 2273–2302 [cit. 2024-05-02]. Available at: https://doi.org/10.1080/00207179.2017.1338359

[52] MATYSKA, Pavel. Advantages of Synchronous Reluctance Motors [online]. In: *Transactions on Electrical Engineering*. 2014. vol. 3, no. 2, p. 44–47 [cit. 2024-05-03]. Available at: https://ojs.cvut.cz/ojs/index.php/TEE/article/view/6466

[53] GOMAN, Victor, PRAKHT, Vladimir, KAZAKBAEV, Vadim and DMITRIEVSKII, Vladimir. Comparative Study of Energy Consumption and CO2 Emissions of Variable-Speed Electric Drives with Induction and Synchronous Reluctance Motors in Pump Units [online]. In: *Mathematics*. 2021. vol. 9, no. 21 [cit. 2024-05-04]. ISSN 2227-7390. Available at: https://doi.org/10.3390/math9212679

[54] ABB GROUP. NEMA vs. IEC Efficiencies [online]. In: *ABB Group*. 2020 [cit. 2024-05-05]. Available at: https://new.abb.com/news/detail/70167/nema-vs-iec-efficiencies

[55] SIEMENS. Minimum Energy Performance Standard – European Union [online]. In: *Siemens*. © 1996–2024 [cit. 2024-05-07]. Available at: https://meps.siemens.com/en/country/eu

[56] TECHNOR – TECHNICKÉ NORMY ČSN. 3500 – Točivé elektrické stroje všeobecně [online]. In: *TECHNOR – Technické normy ČSN*. © 2020–2022 [cit. 2024-05-08]. Available at: https://www.technicke-normy-csn.cz/technicke-normy-csn/35-elektrotechnika/3500-tocive-elektricke-stroje-vseobecne/

[57] TECHNOR – TECHNICKÉ NORMY ČSN. 3517 – Tyristorové pohony [online]. In: *TECHNOR – Technické normy ČSN*. © 2020–2022 [cit. 2024-05-09]. Available at: https://www.technicke-normy-csn.cz/technicke-normy-csn/35-elektrotechnika/3517-tyristorove-pohony/

[58] NABIL, M. and SERGEANT, Peter. Synchronous reluctance machines [online]. In: *Universiteit Gent*. © 2024 [cit. 2024-05-10]. Available at: https://www.ugent.be/ea/emsme/en/research/eelab/drivesystems/synchronous_reluctance

[59] SIEMENS. SinaSave [online]. In: *Siemens*. © 1996–2024 [cit. 2024-05-11]. Available at: https://www.sinasave.siemens.com/en/

[60] SOLISPLC | ONLINE PLC AUTOMATION TRAINING. The Complete Practical Guide to Siemens Tia Portal Programming [online]. In: *SolisPLC | Online PLC Automation Training*. [cit. 2024-05-15]. Available at: https://www.solisplc.com/tutorials/a-practical-guide-to-siemens-tia-portal-programming

[61] *Catalog D 21.4 – SINAMICS S120 and SIMOTICS* [online]. Siemens, 2017 [cit. 2024-05-16]. Available at: https://assets.new.siemens.com/siemens/assets/api/uuid:529f0703-eac7-47cf-b8b0-1324bf7b2647/catalog-d21-4-sinamics-s120-simotics.pdf

[62] *Catalog D 81.1 – SIMOTICS GP, SD, XP, DP Low-Voltage Motors* [online]. Siemens, 2022-02 [cit. 2024-05-17]. Available at: https://cache.industry.siemens.com/dl/files/197/109749197/att_1094438/v1/Motors-D81-1-complete-English-12-2021-Update_2022-02.pdf

[63] *SINAMICS S120/S150 – List Manual* [online]. Siemens, 2023-11 [cit. 2024-05-18]. Available at: https://support.industry.siemens.com/cs/document/109827046/sinamics-s120-s150?dti=0&lc=en-CZ

[64] *SINAMICS S120 – Function Manual* [online]. Siemens, 2020-06 [cit. 2024-05-18]. Available at: https://support.industry.siemens.com/cs/document/109781535/sinamics-s120-function-manual-for-drive-functions?dti=0&lc=en-CZ

Appendix A
Index

The meanings to the abbreviations below are located on the pages on the right-hand sides of the abbreviations.

Appendix B
List of Notation

Quantity	Meaning (SI unit considered)
B	width of a barrier of a PMa-SynRM (the longest side of the rectangle representing the given barrier in a cross-sectional drawing of the rotor) (mm)
C	capacitance (F)
e	error of the controlled quantity, relating to the block diagram of FOC (SI unit thus depends on the given quantity)
$\boldsymbol{F}$	force (N)
f	frequency (Hz)
I	current – constant value in time (A)
$\boldsymbol{I}$	current space vector (A)
i	current – instantaneous value in time (A)
J	moment of inertia ($\mathrm{kg} \cdot \mathrm{m}^2$)
K	Park's transformation coefficient (–)
K_w	insulation ratio (–)
L	inductance (H)
$length\ of\ a\ flux\ carrier$	length of a flux carrier (mm)
M	width of the PM of a PMa-SynRM – in the same sense as for B (mm)
n	speed (also referred to as revolutions) (rpm)
$number\ of\ stator\ slots$	number of stator slots (–)
P	power (W)
PUT	power utilization (–)
ΔP	losses (W)
p_p	number of pole pairs (–)
R	resistance (Ω)
T	torque (Nm)
$TEMP$	temperature (°C)

t	time (s)
U	voltage – constant value in time (V)
$\boldsymbol{U}$	voltage space vector (V)
u	voltage – instantaneous value in time (V)
w_{bar}	total width of all the flux barriers (mm)
w_{car}	total witdth of all the flux carriers (also called flux guides) (mm)
width of a flux carrier	width of a flux carrier (mm)
X	reactance (Ω)
α	coefficient relating to the gradual decrease of the width of the PM of a PMa-SynRM towards the outermost barrier layer (–)
β	load angle (rad)
γ	angle by which $\boldsymbol{I}_{\mathrm{s}}$ 'leads' the d-axis (rad)
δ	width of air gap between stator and rotor (mm)
η	efficiency (%)
ϑ	electrical angle of the turning of the rotor relatively to the stator (rad)
μ	permeability ($\mathrm{H} \cdot \mathrm{m}^{-1}$)
ξ	saliency ratio (–)
τ	time constant (s)
φ	angle by which $\boldsymbol{I}_{\mathrm{s}}$ lags $\boldsymbol{U}_{\mathrm{s}}$ (rad)
$\cos\varphi$	power factor (–)
Ψ	magnetic flux linkage – constant value in time (Wb)
$\boldsymbol{\Psi}$	magnetic flux linkage space vector (Wb)
ψ	magnetic flux linkage – instantaneous value in time (Wb)
Ω	mechanical angular velocity (also referred to as speed as there is direct proportion between the two) ($\mathrm{rad} \cdot \mathrm{s}^{-1}$)
ω	electrical angular velocity ($\mathrm{rad} \cdot \mathrm{s}^{-1}$)
–	electricity consumption (kWh)

Subscript	Meaning
a	relating to phase a
aa	a self-value of phase a (e.g. inductance)
ab/ba	between phase a and b/b and a
ac/ca	between phase a and c/c and a
air	relating to air
avg	average – **if this subscript is not used and the quantity is scalar, periodic, not maximum or minimum and denoted by an uppercase, then it is a RMS value**
b	relating to phase b
bb	a self-value of phase b (e.g. inductance)
bc/cb	between phase b and c/c and b
CPR	relating to the CPR range (if used with Ω, it denotes the speed at which the CPR range ends)
c	relating to phase c
cc	a self-value of phase c (e.g. inductance)
control	relating to control voltage from the block diagram of FOC
DC	a DC value (in this thesis relating to the DC values of voltage and current in the DC link of an inverter)
DM	dynamometer
d	relating to the d-axis of the dq system (if used with i, it denotes the field-producing component of the stator current)
diff	difference
Fe	iron (e.g. losses)
h	relating to the magnetizing inductance component independent of ϑ
ie	given quantity is produced by the rotating excited rotor of a synchronous machine
k	substitutable by a subscript that denotes a particular electrical angular velocity of the rotating dq coordinate system (if used alone with ω, it denotes the general electrical angular velocity of the rotating dq coordinate system)
L	load
M	motor
MPFC	relating to the optimal value of γ (i_d and i_q respectively) for the MPFC (MTPkVA respectively) control strategy

MTPA	relating to the optimal value of γ (i_d and i_q respectively) for the MTPA control strategy
MTPF	relating to the optimal value of γ (i_d and i_q respectively) for the MTPF control strategy
MTPV	relating to the optimal value of γ (i_d and i_q respectively) for the MTPV control strategy
m	magnetizing
max	maximum – **if this subscript is not used and the quantity is scalar, periodic, not average or minimum and denoted by an uppercase, then it is a RMS value**
min	minimum – **if this subscript is not used and the quantity is scalar, periodic, not average or maximum and denoted by an uppercase, then it is a RMS value**
n	order of the given barrier layer of a barrier rotor, counted from the center of the rotor sheet onwards to its edge
P	used with P to denote input power
PM	relating to permanent magnets
p	phase
q	relating to the q-axis of the dq system (if used with i, it denotes the torque-producing component of the stator current)
r	1st meaning: relative, 2nd meaning: rotor – relating to the rotation of rotor (depends on the context)
rated	a rated value
real	a real value
rel	reluctance
ripple	used with T to denote torque ripple
s	stator (or synchronous respectively) – relating to the rotating magnetic field (if used with 'R', it denotes the resistance of a stator phase)
t	tangential
x	substituable by either 's', 'r' or '2' and is related to the definition of the relationship between mechanical and electrical angular velocities
α	relating to the α-axis of the $\alpha\beta$ system
β	relating to the β-axis of the $\alpha\beta$ system
σ	a leakage quantity

0	1st meaning: relating to the magnetizing inductance component caused by the anisotropy of the rotor, 2nd meaning: if used with ϑ, it denotes the angle by which $\boldsymbol{U}_\mathrm{s}$ 'leads' the d-axis (depends on the context)
2	relating to quantities in rotor (e.g. rotor current)

Superscript	Meaning
*	setpoint

Chemical element	Meaning
Al	aluminium
B	boron
C	carbon
Co	cobalt
Fe	iron
Nd	neodymium
Ni	nickel
O	oxygen
Sm	samarium
Ti	titanium

Other	Meaning
abc	the abc system
C	controller
D	diode
d	denotation of the d-axis of the dq system
dq	the dq system
f	denotation of frequency in the list of other possible names for scalar control
j	imaginary operator
N	1st meaning: neutral (conductor), 2nd meaning: north pole of a magnet (depends on the context)
$\boldsymbol{P}$	Park's transformation matrix

q	denotation of the q-axis of the dq system
S	1st meaning: switch (in this thesis an electronic one), 2nd meaning: south pole of a magnet, 3rd meaning: sensor (depends on the context)
U	denotation of voltage in the list of other possible names for scalar control
V	denotation of voltage in the list of other possible names for scalar control
$\alpha\beta$	the $\alpha\beta$ system
Ω	denotation of mechanical angular velocities (or speeds respectively, as there is direct proportion between the two)
ω	denotation of electrical angular velocities

Appendix C
Contents of the electronic attachments

All electronic attachments are located in the ZIP file '`F3-BT-2024-Tlamsa-Petr-electronic_attachments.zip`' available at ČVUT DSpace (electronic version of the thesis) or on the attached CD (paper version of the thesis).

The file contains:

- `data.xlsx` – an excel notebook with all the acquired (measured) data, processed data and data prepared for the Wolfram Mathematica notebook,
- `heatmaps.nb` – a Wolfram Mathematica notebook with a code that constructs the heatmaps from the prepared data and exports these maps to `.pdf`.

Appendix D
Data tables

n_{M} (rpm)	T_{DM} (Nm)	I_{M} (A)	T_{M} (Nm)	P_{M} (kW)	η_{M} (%)	$TEMP_{\mathrm{M}}$ (°C)	$P_{\mathrm{P,M}}$ (kW)	PUT_{M} (–)	$\eta_{\mathrm{M,real}}$ (%)	T_{diff} (Nm)
100	0	8.92	1.69	0.02	61.20	25.00	0.05	0.01	0.00	1.69
100	5	9.71	9.36	0.10	80.78	25.18	0.10	0.01	52.36	4.36
100	10	10.72	14.65	0.15	109.00	25.42	0.19	0.01	55.12	4.65
100	16	12.07	20.27	0.22	95.50	25.60	0.24	0.01	69.81	4.27
100	20	13.75	26.40	0.29	88.90	26.90	0.33	0.02	63.47	6.40
100	30	16.62	36.75	0.38	75.00	26.57	0.43	0.03	73.06	6.75
100	40	19.41	46.00	0.50	89.80	26.89	0.53	0.03	79.03	6.00
100	50	22.16	55.56	0.61	77.39	27.75	0.71	0.04	74.04	5.36
100	61	25.33	67.42	0.74	79.95	29.16	0.93	0.05	68.69	6.42
100	70	27.93	76.31	0.77	76.60	30.40	1.26	0.05	58.18	6.31
100	79	30.56	85.39	0.90	75.50	31.90	1.30	0.06	63.64	6.39
100	90	33.77	96.57	0.97	69.16	34.00	1.61	0.07	58.54	6.57
200	0	8.82	0.14	0.00	15.34	32.75	0.05	0.00	0.00	0.14
200	6	9.77	10.24	0.22	112.20	31.90	0.20	0.01	62.83	4.24
200	10	10.50	14.04	0.30	99.50	31.35	0.30	0.02	69.81	4.04
200	16	12.07	20.39	0.43	105.30	30.96	0.45	0.03	74.47	4.39
200	22	13.66	25.89	0.55	100.30	30.74	0.58	0.04	79.44	3.89
200	32	16.74	36.24	0.78	97.80	30.69	0.80	0.05	83.78	4.24
200	40	19.20	45.34	0.94	94.20	30.82	1.04	0.06	80.55	5.34
200	50	22.16	55.68	1.15	87.99	31.30	1.36	0.08	77.00	5.68
200	62	25.40	67.71	1.40	87.19	31.90	1.65	0.09	78.70	5.71
200	71	28.12	77.05	1.62	85.60	32.95	1.89	0.11	78.68	6.05
200	79	30.72	86.30	1.82	82.51	34.06	2.15	0.12	76.96	7.30
200	89	33.62	96.64	2.02	81.49	35.61	2.42	0.13	77.03	7.64

Table D.1: Data for $n_{\mathrm{M}} = 100$ rpm and $n_{\mathrm{M}} = 200$ rpm.

n_{M} (rpm)	T_{DM} (Nm)	I_{M} (A)	T_{M} (Nm)	P_{M} (kW)	η_{M} (%)	$TEMP_{\mathrm{M}}$ (°C)	$P_{\mathrm{P,M}}$ (kW)	PUT_{M} (–)	$\eta_{\mathrm{M,real}}$ (%)	T_{diff} (Nm)
300	0	9.02	3.45	0.11	108.70	35.14	0.11	0.01	0.00	3.45
300	7	9.93	10.83	0.35	114.85	34.34	0.31	0.02	70.94	3.83
300	12	11.07	16.73	0.52	106.22	33.70	0.50	0.03	75.40	4.73
300	18	12.57	22.22	0.70	105.14	33.21	0.76	0.05	74.41	4.22
300	21	13.02	25.97	0.82	102.50	32.90	0.79	0.06	83.51	4.97
300	31	16.40	35.75	1.12	96.59	32.89	1.14	0.07	85.43	4.75
300	41	19.45	46.55	1.48	92.93	33.00	1.46	0.10	88.22	5.55
300	50	22.29	55.75	1.76	95.33	33.37	1.84	0.12	85.37	5.75
300	61	25.28	67.44	2.12	94.49	33.97	2.34	0.14	81.90	6.44
300	70	28.23	77.64	2.45	87.15	34.04	2.74	0.16	80.26	7.64
300	80	30.89	86.09	2.67	87.90	36.10	2.95	0.18	85.20	6.09
300	89	33.65	96.67	3.05	86.97	37.49	3.58	0.20	78.10	7.67
400	0	8.96	1.96	0.11	77.02	37.04	0.09	0.01	0.00	1.96
400	6	9.75	10.05	0.42	109.60	34.20	0.36	0.03	69.81	4.05
400	10	10.64	14.46	0.61	112.50	35.59	0.57	0.04	73.49	4.46
400	18	12.13	20.19	0.87	109.15	35.29	0.79	0.06	95.44	2.19
400	22	13.98	26.90	1.13	101.90	34.99	1.11	0.08	83.02	4.90
400	31	16.71	36.13	1.57	103.20	34.86	1.55	0.10	83.78	5.13
400	41	19.38	46.57	1.97	98.57	34.88	2.09	0.13	82.17	5.57
400	51	22.41	56.29	2.35	97.17	35.19	2.53	0.16	84.44	5.29
400	61	25.48	67.91	2.87	90.88	35.09	3.14	0.19	81.37	6.91
400	70	28.04	77.44	3.25	92.04	36.43	3.61	0.22	81.22	7.44
400	79	30.87	87.40	3.65	89.50	37.40	4.01	0.24	82.52	8.40
400	90	33.88	96.04	4.01	89.18	38.50	4.37	0.27	86.27	6.04

Table D.2: Data for $n_{\mathrm{M}} = 300$ rpm and $n_{\mathrm{M}} = 400$ rpm.

n_{M} (rpm)	T_{DM} (Nm)	I_{M} (A)	T_{M} (Nm)	P_{M} (kW)	η_{M} (%)	$TEMP_{\mathrm{M}}$ (°C)	$P_{\mathrm{P,M}}$ (kW)	PUT_{M} (–)	$\eta_{\mathrm{M,real}}$ (%)	T_{diff} (Nm)
500	0	9.04	3.14	0.15	107.00	34.72	0.14	0.01	0.00	3.14
500	6	9.89	10.57	0.56	111.87	34.54	0.47	0.04	66.84	4.57
500	10	10.62	14.89	0.78	106.80	34.42	0.70	0.05	74.80	4.89
500	16	12.11	21.11	1.08	104.90	34.30	1.04	0.07	80.55	5.11
500	21	13.45	25.33	1.33	108.13	34.30	1.31	0.09	83.94	4.33
500	31	16.62	36.77	1.92	101.27	34.34	1.96	0.13	82.81	5.77
500	41	19.62	47.14	2.47	100.38	34.77	2.46	0.17	87.27	6.14
500	50	22.22	56.56	2.99	100.64	35.28	3.08	0.20	85.00	6.56
500	61	25.27	67.66	3.53	95.17	36.08	3.70	0.23	86.32	6.66
500	70	27.94	77.40	4.02	94.73	36.91	4.21	0.27	87.06	7.40
500	80	31.10	88.47	4.61	93.81	37.95	4.86	0.31	86.19	8.47
500	90	34.00	97.95	5.14	92.74	39.48	5.52	0.34	85.37	7.95
600	0	9.10	2.66	0.17	114.17	39.14	0.13	0.01	0.00	2.66
600	5	9.73	10.35	0.63	121.51	38.42	0.54	0.04	58.18	5.35
600	11	10.82	15.85	0.98	109.79	37.65	0.92	0.07	75.13	4.85
600	17	12.25	20.97	1.32	102.52	37.15	1.21	0.09	88.28	3.97
600	21	13.30	25.08	1.59	104.93	36.80	1.49	0.11	88.55	4.08
600	32	16.53	35.04	2.29	99.01	36.63	2.29	0.15	87.80	3.04
600	42	19.78	47.90	2.99	101.16	36.89	2.90	0.20	91.00	5.90
600	50	22.01	55.84	3.52	101.28	37.05	3.48	0.23	90.28	5.84
600	60	25.25	67.64	4.28	98.73	37.70	4.37	0.28	86.27	7.64
600	70	28.17	78.63	4.91	101.90	38.59	5.03	0.33	87.44	8.63
600	80	30.97	87.82	5.52	95.20	39.29	5.80	0.36	86.66	7.82
600	90	34.03	98.86	6.21	94.11	40.41	6.71	0.41	84.28	8.86

Table D.3: Data for $n_{\mathrm{M}} = 500$ rpm and $n_{\mathrm{M}} = 600$ rpm.

n_{M} (rpm)	T_{DM} (Nm)	I_{M} (A)	T_{M} (Nm)	P_{M} (kW)	η_{M} (%)	$TEMP_{\mathrm{M}}$ (°C)	$P_{\mathrm{P,M}}$ (kW)	PUT_{M} (–)	$\eta_{\mathrm{M,real}}$ (%)	T_{diff} (Nm)
700	0	9.26	3.09	0.24	127.74	39.91	0.11	0.01	0.00	3.09
700	5	9.71	8.55	0.62	119.00	39.08	0.51	0.05	71.87	3.55
700	10	10.81	14.60	1.13	114.05	38.50	1.03	0.07	71.17	4.60
700	16	12.02	19.57	1.44	107.09	37.89	1.36	0.10	86.24	3.57
700	22	13.60	25.94	1.85	105.58	37.61	1.79	0.13	90.09	3.94
700	31	16.45	36.45	2.50	102.50	37.50	2.44	0.17	93.13	5.45
700	40	19.31	46.07	3.41	101.63	37.59	3.34	0.23	87.79	6.07
700	51	22.52	58.32	4.28	99.79	37.90	4.22	0.28	88.59	7.32
700	61	25.44	67.68	4.95	96.83	38.34	5.00	0.33	89.43	6.68
700	69	27.91	75.78	5.52	96.18	39.10	5.70	0.37	88.74	6.78
700	81	31.29	88.39	6.49	95.21	40.23	6.90	0.43	86.05	7.39
700	90	34.04	96.81	7.28	94.96	41.75	7.61	0.47	86.69	6.81
800	0	8.86	1.03	0.08	90.30	40.85	0.08	0.00	0.00	1.03
800	5	9.85	9.38	0.88	123.41	39.79	0.71	0.05	59.00	4.38
800	12	11.07	15.65	1.35	114.74	39.29	1.23	0.09	81.73	3.65
800	15	11.98	20.53	1.79	118.41	38.90	1.54	0.11	81.60	5.53
800	20	13.45	26.07	2.19	109.32	38.59	2.06	0.15	81.34	6.07
800	31	16.60	35.94	3.03	102.82	39.39	2.91	0.20	89.25	4.94
800	40	19.27	45.02	3.79	101.88	38.42	3.86	0.25	86.81	5.02
800	50	22.17	53.86	4.54	100.93	38.70	4.59	0.31	91.26	3.86
800	61	25.34	68.48	5.45	97.55	39.18	5.60	0.38	91.26	7.48
800	70	27.96	74.71	6.49	97.21	39.97	6.23	0.41	94.13	4.71
800	80	31.11	85.35	7.12	95.51	40.97	7.31	0.49	91.68	5.35
800	90	33.61	94.36	8.01	95.77	42.11	8.33	0.53	90.51	4.36

Table D.4: Data for $n_{\mathrm{M}} = 700$ rpm and $n_{\mathrm{M}} = 800$ rpm.

n_{M} (rpm)	T_{DM} (Nm)	I_{M} (A)	T_{M} (Nm)	P_{M} (kW)	η_{M} (%)	$TEMP_{\mathrm{M}}$ (°C)	$P_{\mathrm{P,M}}$ (kW)	PUT_{M} (–)	$\eta_{\mathrm{M,real}}$ (%)	T_{diff} (Nm)
900	0	8.87	1.67	0.14	116.57	41.27	0.15	0.01	0.00	1.67
900	6	10.09	10.91	1.02	119.12	40.58	0.89	0.07	63.54	4.91
900	10	10.76	14.84	1.41	114.02	40.00	1.23	0.09	76.62	4.84
900	17	12.36	22.64	2.13	106.00	39.50	1.94	0.13	82.59	5.64
900	21	13.45	26.75	2.44	108.50	39.14	2.23	0.17	88.75	5.75
900	30	16.55	37.46	3.44	104.57	39.00	3.30	0.23	85.68	7.46
900	40	19.42	44.87	4.22	104.20	39.03	4.41	0.29	85.49	4.87
900	51	22.38	54.53	5.12	100.70	39.23	5.16	0.35	93.15	3.53
900	61	25.42	64.71	6.36	99.38	39.70	6.18	0.41	93.03	3.71
900	70	28.06	75.36	7.08	99.34	40.62	7.10	0.47	92.92	5.36
900	79	30.63	85.39	8.07	96.06	41.78	8.22	0.53	90.58	6.39
900	90	33.61	96.04	9.06	95.95	43.46	9.43	0.59	89.95	6.04
1000	0	9.31	5.53	0.60	126.55	43.21	0.25	0.04	0.00	5.53
1000	5	9.70	9.34	1.00	121.32	42.50	0.83	0.07	63.08	4.34
1000	10	10.70	15.28	1.69	115.63	41.66	1.30	0.10	80.55	5.28
1000	16	11.93	19.83	1.96	109.23	40.94	1.98	0.13	84.62	3.83
1000	21	13.50	25.43	2.72	108.81	40.50	2.52	0.19	87.27	4.43
1000	30	14.86	37.60	3.46	106.18	40.20	3.32	0.32	94.63	7.60
1000	41	19.39	43.55	4.60	104.50	40.12	4.46	0.30	96.27	2.55
1000	50	22.10	54.44	5.54	103.27	40.54	5.46	0.37	95.90	4.44
1000	62	25.71	65.90	6.90	100.93	41.09	6.87	0.48	94.51	3.90
1000	70	27.95	76.80	8.13	97.73	41.75	8.24	0.53	88.96	6.80
1000	80	30.87	87.85	9.20	97.64	42.66	9.37	0.61	89.41	7.85
1000	90	33.75	98.76	10.26	95.35	43.96	10.71	0.68	88.00	8.76

Table D.5: Data for $n_{\mathrm{M}} = 900$ rpm and $n_{\mathrm{M}} = 1000$ rpm.

n_{M} (rpm)	T_{DM} (Nm)	I_{M} (A)	T_{M} (Nm)	P_{M} (kW)	η_{M} (%)	$TEMP_{\mathrm{M}}$ (°C)	$P_{\mathrm{P,M}}$ (kW)	PUT_{M} (–)	$\eta_{\mathrm{M,real}}$ (%)	T_{diff} (Nm)
1100	0	8.88	0.65	0.01	105.48	43.08	0.07	0.01	0.00	0.65
1100	5	10.01	10.70	1.34	117.05	42.24	0.83	0.07	69.39	5.70
1100	11	10.96	15.41	1.56	110.28	41.69	1.36	0.12	93.17	4.41
1100	16	12.22	22.80	2.49	109.30	41.14	2.18	0.17	84.54	6.80
1100	20	13.35	24.75	2.78	104.09	40.91	2.74	0.18	84.08	4.75
1100	32	16.62	35.10	4.22	103.42	40.61	3.91	0.27	94.27	3.10
1100	41	19.49	47.48	5.40	101.25	40.62	5.42	0.36	87.14	6.48
1100	50	22.04	57.08	6.33	99.57	40.81	6.57	0.43	87.66	7.08
1100	59	25.03	67.40	7.57	100.14	41.28	7.78	0.51	87.36	8.40
1100	71	28.16	75.03	8.76	100.54	41.90	8.81	0.59	92.83	4.03
1100	80	30.65	82.79	9.49	101.16	42.85	9.48	0.65	97.21	2.79
1100	90	33.68	92.82	11.24	100.40	44.09	10.80	0.70	95.99	2.82
1200	0	8.87	1.39	0.17	92.62	43.17	0.11	0.01	0.00	1.39
1200	6	10.14	9.47	1.13	124.34	42.54	0.94	0.08	80.21	3.47
1200	10	10.97	16.02	2.04	114.26	41.88	1.80	0.14	69.81	6.02
1200	15	12.04	21.60	2.70	107.17	41.43	2.48	0.18	76.01	6.60
1200	21	13.57	26.19	3.29	108.11	41.08	3.05	0.22	86.52	5.19
1200	30	16.22	34.79	4.36	103.20	40.94	4.21	0.29	89.55	4.79
1200	40	19.25	45.88	5.74	101.13	40.81	5.66	0.38	88.81	5.88
1200	51	22.35	58.04	7.28	100.46	41.14	7.26	0.48	88.28	7.04
1200	60	25.11	67.20	8.48	100.27	41.60	8.39	0.57	89.87	7.20
1200	71	28.45	76.21	9.63	102.17	42.32	9.37	0.64	95.22	5.21
1200	80	30.95	82.51	10.46	97.70	43.30	10.61	0.69	94.75	2.51
1200	90	33.81	96.42	12.15	94.80	44.63	12.63	0.81	89.55	6.42

Table D.6: Data for $n_{\mathrm{M}} = 1100$ rpm and $n_{\mathrm{M}} = 1200$ rpm.

n_{M} (rpm)	T_{DM} (Nm)	I_{M} (A)	T_{M} (Nm)	P_{M} (kW)	η_{M} (%)	$TEMP_{\mathrm{M}}$ (°C)	$P_{\mathrm{P,M}}$ (kW)	PUT_{M} (–)	$\eta_{\mathrm{M,real}}$ (%)	T_{diff} (Nm)
1300	0	9.24	3.93	0.57	128.58	44.35	0.41	0.04	0.00	3.93
1300	5	10.45	7.33	1.29	121.29	43.41	1.31	0.09	51.96	2.33
1300	10	10.86	14.09	2.22	116.41	42.71	1.63	0.15	83.52	4.09
1300	15	12.03	20.89	2.70	107.29	42.13	2.57	0.19	79.46	5.89
1300	21	13.61	24.40	3.48	109.50	41.80	3.24	0.25	88.24	3.40
1300	30	16.29	33.26	4.50	102.68	41.40	4.31	0.30	94.76	3.26
1300	41	19.71	45.37	6.08	104.32	41.45	5.82	0.40	95.90	4.37
1300	50	22.12	55.15	7.41	98.15	41.86	7.35	0.49	92.61	5.15
1300	60	25.07	66.11	9.12	98.72	42.31	9.18	0.61	88.98	6.11
1300	69	27.84	78.29	10.65	98.20	43.06	10.80	0.71	86.98	9.29
1300	80	30.92	87.35	11.82	101.27	43.91	11.82	0.79	92.14	7.35
1300	90	34.05	94.00	12.74	100.96	45.06	12.37	0.84	99.05	4.00
1400	0	9.14	4.81	0.52	123.42	44.86	0.51	0.05	0.00	4.81
1400	4	10.30	10.67	1.31	110.11	44.05	0.63	0.08	93.08	6.67
1400	10	10.92	15.17	2.06	115.35	43.16	1.90	0.12	77.16	5.17
1400	15	12.13	21.31	2.84	109.27	42.61	2.79	0.20	78.82	6.31
1400	20	13.30	25.77	3.65	106.16	42.22	3.51	0.24	83.54	5.77
1400	30	16.29	37.21	5.37	105.10	41.94	5.13	0.36	85.74	7.21
1400	41	19.36	43.95	6.48	106.18	41.90	6.12	0.42	98.22	2.95
1400	50	22.53	55.28	8.38	99.45	42.17	8.13	0.54	90.16	5.28
1400	61	25.53	69.10	10.15	98.47	42.61	10.30	0.68	86.83	8.10
1400	70	28.23	75.16	11.05	103.46	43.20	10.33	0.74	99.35	5.16
1400	80	31.07	83.29	12.25	95.20	44.31	13.14	0.83	89.26	3.29
1400	90	33.90	99.28	14.54	96.40	45.51	15.13	0.95	87.21	9.28

Table D.7: Data for $n_{\mathrm{M}} = 1300$ rpm and $n_{\mathrm{M}} = 1400$ rpm.

n_{M} (rpm)	T_{DM} (Nm)	I_{M} (A)	T_{M} (Nm)	P_{M} (kW)	η_{M} (%)	$TEMP_{\mathrm{M}}$ (°C)	$P_{\mathrm{P,M}}$ (kW)	PUT_{M} (–)	$\eta_{\mathrm{M,real}}$ (%)	T_{diff} (Nm)
1500	0	9.18	5.16	0.79	125.68	45.72	0.64	0.05	0.00	5.16
1500	5	10.54	12.80	2.02	118.70	44.76	1.66	0.13	47.31	7.80
1500	10	11.17	14.50	2.29	120.00	43.89	1.92	0.15	81.81	4.50
1500	17	12.22	21.10	3.38	109.57	43.38	3.11	0.22	85.86	4.10
1500	20	13.24	24.12	3.78	105.91	42.90	3.57	0.25	88.00	4.12
1500	31	16.80	36.33	5.62	103.34	42.63	5.54	0.37	87.90	5.33
1500	39	18.77	46.35	7.27	102.15	42.66	7.16	0.48	85.56	7.35
1500	51	22.57	58.72	9.25	104.22	42.80	9.11	0.61	87.94	7.72
1500	62	25.71	70.55	11.06	104.80	43.32	10.00	0.74	97.39	8.55
1500	69	28.03	73.08	11.48	103.17	43.90	10.92	0.76	99.25	4.08
1500	80	30.63	84.54	13.82	97.59	44.87	13.66	0.88	91.42	5.04
1500	90	33.58	96.64	15.21	101.42	46.23	15.19	1.01	93.07	6.64

Table D.8: Data for $n_{\mathrm{M}} = 1500$ rpm.